Unsaturated Zone Hydrology for Scientists and Engineers

James A. Tindall, Ph.D.

United States Geological Survey, National Research Program
Department of Geography and Environmental Sciences, University of Colorado Denver

James R. Kunkel, Ph.D., P.E.

Knight Piésold, LLC, Denver, Colorado;
Department of Geology and Geological Engineering, Colorado School of Mines

with

Dean E. Anderson, Ph.D.

United States Geological Survey, National Research Program

PRENTICE HALL
Upper Saddle River, New Jersey 07458

13

Applied Soil Physics: Modeling Water, Solute, and Vapor Movement

INTRODUCTION: MODELING APPROACHES

Variably-saturated-zone mathematical models are useful tools for predicting the extent of subsurface contamination and conducting pre-monitoring studies for the placement of detection devices, in a format understood by field response personnel as well as regulatory entities. Modeling approaches range from simple analytical and semianalytical solutions, to complex numerical codes. The assumptions inherent in each type of model are a key element in understanding the uncertainties associated with each type of approach. The primary emphasis here is the use of simple formulas and comprehensive tables to create a practically oriented and readily usable guide to some of the basic unsaturated-flow problems commonly encountered. In general, three different levels of sophistication are presented in this chapter: **(1)** simple analytical solutions (based upon applicable differential equations) formed by simplifying idealizations of the soil and boundary conditions, and resulting in estimates of flow and contaminant transport; **(2)** semi-analytical methods based upon the concept of soil potential, which provides for both steady-state fluid flow and approximate transient-fluid flow of a contaminant, corresponding to an arbitrary number of contaminant sources; and **(3)** sophisticated numerical models that can account for nonhomogeneous soil, dispersion, diffusion, and chemical processes (e.g., sorption, precipitation, decay, ion exchange, and degradation).

As indicated above, the emphasis in this chapter is on analytical solutions that are readily used to solve problems in unsaturated-zone flow; these solutions are easily used on spreadsheets. It is felt that analytical solutions—in addition to their use as check solutions for numerical models—can provide solutions even when large quantities of unsaturated-zone data are not available. Analytical solutions also provide guidance on the sensitivity of a given solution to various unsaturated-zone properties, thus permitting guidance on where to collect more data or to concentrate data-collection efforts.

Analytical Models

Analytical and semianalytical models are comprised of formulas that represent simplified physical and/or chemical conditions of the real world, based on the complete partial differential equations used in the more sophisticated numerical models. Analytical and semianalytical model solutions are usually linearized versions of the nonlinear partial differential equations of flow in soil (e.g., Richards' equation). Generally, simplified boundary conditions

are required (i.e., infinite or semi-infinite areal extent of the soil, or linear-vertical or horizontal boundaries) in order to obtain analytical solutions. Also, the nonlinear partial differential equations are linearized, usually accomplished through the use of mathematical transforms.

Analytical solutions give exact answers for the geometries and soil physical limitations required for their use. They are also used as confirmation for the solutions of more sophisticated numerical models, under the same geometries and physical parameters. Because analytical solutions are less expensive to set up and run—and often require less data than numerical models—they are valuable in assessing simple problems or for use as prescreening models. Their use under well-defined uncertainty constraints (or in the face of small data sets) is important because often, decisions related to regulatory issues and contaminant-cleanup timing are based on use of analytical models. Regulators, as well as the general public, often find analytical solutions easier to understand than complex numerical solutions.

Nevertheless, very few analytical solutions are available for flow and transport in unsaturated soil. Solutions are available for selected flow and transport problems, such as: determination of water content, matric potential, and unsaturated-hydraulic conductivity in layered soils (López-Bakovic and Nieber 1989); one-dimensional redistribution of moisture (Charbeneau 1989); three-dimensional steady-state and time-dependent moisture distributions from point sources (Bumb et al. 1988; McKee and Bumb 1988); three-dimensional steady-state and time-dependent distribution of nonwetting fluids from point sources (Murphy, Bumb, and McKee 1987); and three-dimensional time-dependent vapor diffusion from an initial contaminant distribution (Lawrence Livermore National Laboratory (LLNL) 1990). The derivation and use of these analytical-model solutions are discussed in detail in this chapter.

These analytical models are chosen from available analytical solutions because they represent basic flow and soil properties that are commonly encountered in typical experiences related to unsaturated flow. It should be noted that both one-dimensional and three-dimensional solutions for vertically homogeneous and layered-flow systems are presented.

Numerical Models

One of the decisions that needs to be made is whether to use an analytical model or a numerical model, to solve a particular problem. Because of the many simplifying assumptions inherent in analytical solutions, there exists some doubt as to the tractability of the solution, and its defensibility in light of those assumptions and simplifications (Javendel, Doughty, and Tsang 1984).

Numerical models are much less burdened by simplifications and assumptions, and are therefore inherently capable of addressing more complicated problems; they require significantly more data, however, and their solutions are still only numerical approximations. Assumptions regarding homogeneity and isotropy are unnecessary in a numerical model, due to its ability to assign nodal or elemental values for many variables of interest. In addition, the capacity to incorporate complex boundary conditions does not require the infinite-areal-extent assumption often needed in analytical models. Other choices, such as the time-step, distance-step, and numerical-solution scheme are chosen by the model user; improper choices of these variables can render the results of the numerical model incorrect and useless.

Several types of numerical models (methods) are generally available for solving unsaturated-flow and transport problems; the two principal ones are the finite-difference method and the finite-element method (Istok 1989). An overview of the current numerical

models for solving variably saturated-soil problems is presented in the following sections. Listings of selected numerical models also are presented, but not detailed descriptions. The reader is referred to the references section for more details on individual numerical models.

13.1 ONE-DIMENSIONAL DETERMINISTIC LIQUID-FLOW MODELS

Analytical Models

Analytical solutions to the unsaturated water-flow equation (Richards' equation) are based upon homogeneous soil layers, power and/or exponential relation for unsaturated hydraulic conductivity and soil-moisture characteristic curves. Both one-dimensional solutions by López-Bakovic and Nieber (1989) and Charbeneau (1989) and a three-dimensional solution by McKee and Bumb (1988), are derived by assuming Darcian water flow in homogeneous, unsaturated soil by representing Darcy's equation as

$$q = -K\frac{\partial \psi_h}{\partial z} \tag{13.1}$$

where q is the Darcian flux rate, K is the hydraulic conductivity as a function of water content, ψ_h is the total hydraulic potential with respect to a datum, and z is the vertical distance component. We note that ψ_h is represented as the sum of the gravitational potential ψ_z, the matric potential ψ_m, and the pressure potential ψ_p. For unsaturated conditions, ψ_p is zero, while ψ_z is represented by the distance z from an arbitrary datum. Thus, equation 13.1 becomes

$$q = -K\frac{\partial \psi_m}{\partial z} - K \tag{13.2}$$

or

$$q = -K\left(1 + \frac{\partial \psi_m}{\partial z}\right) \tag{13.3}$$

A general analytical solution to equation 13.3 is not available, because both K and ψ_m are a function of volumetric water content θ, and often z; therefore, the equation is nonlinear. If K and ψ are linear functions of θ, then equation 13.3 is linear. Two possibilities exist for linearizing equation 13.3; these include both integral and nonintegral linearization. An analytical solution to equation 13.3 is obtained by simplification, using a Kirchhoff integral transformation (McKee and Bumb 1988):

$$K\frac{\partial \psi_m}{\partial z} = \frac{\partial H}{\partial z} \tag{13.4}$$

where H is defined as the matric-flux potential by Gardner (1958) and Warrick (1974), and is given by

$$H = \int_{-\infty}^{p} K\,dp \tag{13.5}$$

where p is a variable of integration.

López-Bakovic and Nieber (1989) assume an exponential law relating hydraulic conductivity and matric potential of the form

$$K = K_s \exp(\alpha \psi_m) \tag{13.6}$$

where K_s is saturated hydraulic conductivity, and α is a constant (fitting parameter) related to the moisture-characteristic curve for a given unsaturated soil. Using the exponential relation of equation 13.6, the matric flux potential becomes

$$H = \int_{-\infty}^{\psi} K_s \exp(\alpha p)\, dp = \frac{K_s}{\alpha} [\exp(\alpha p)]_{-\infty}^{\psi} \tag{13.7}$$

Evaluating equation 13.7 gives

$$H = \frac{1}{\alpha} K_s \exp(\alpha \psi_m) = \frac{K}{\alpha} \tag{13.8}$$

McKee and Bumb (1988) assume a power law relating hydraulic conductivity and matric potential of the form

$$K = K_s(S_e)^n \tag{13.9}$$

where S_e is the effective saturation and n is an exponent. S_e is given by Corey (1977) and Bumb (1987) as

$$S_e = \frac{\theta - \theta_r}{\theta_m - \theta_r} = \exp\left(-\frac{\psi_m - \psi_1}{\beta}\right) \tag{13.10}$$

where θ is the volumetric water content, θ_m is the maximum volumetric water content, θ_r is the residual (or irreducible) volumetric water content, and β and ψ_1 are fitting parameters to the moisture-characteristic curve. Using the power-law relation of equation 13.9, the matric flux potential becomes

$$H = \int_{\psi}^{\infty} K_s(S_e)^n\, dp = -\frac{\beta K_s}{n} [(S_e)^n]_{\psi}^{\infty} \tag{13.11}$$

and evaluating equation (13.11) gives

$$H = \frac{\beta}{n} K_s(S_e)^n = \frac{\beta}{n} K \tag{13.12}$$

Comparison of equation 13.8 with equation 13.12 indicates that $\alpha = n/\beta$. Therefore, using either the exponential law or the power law to relate hydraulic conductivity and water content results in essentially the same relation for matric flux potential H, used to linearize the differential equation of unsaturated flow. Substituting the result of H (equation 13.8) into equation 13.3 results in the following linear differential equation

$$q = -\frac{\partial H}{\partial z} - \alpha H \tag{13.13}$$

Solving the transformed equation 13.13 and using the exponential law proposed by López-Bakovic and Nieber (1989), we obtain the following relation:

$$-q \exp(\alpha z) = \frac{\partial [H \exp(\alpha z)]}{\partial z} = \exp(\alpha z) \frac{\partial H}{\partial z} + \exp(\alpha z) \alpha H \tag{13.14}$$

Integrating both sides of equation 13.14 gives

$$H \exp(\alpha z) = -\int^{z} q \exp(\alpha t)\, dt + c \tag{13.15}$$

and solving for matric flux potential H gives

$$H = -\exp(-\alpha z) \int^{z} q \exp(\alpha t)\, dt + c \exp(-\alpha z) \tag{13.16}$$

Because we assume the flow to be steady-state, the water-flux rate q is constant throughout the vertical profile; q can be moved outside the integral sign and equation 13.16 is written as

$$H = -q \exp(-\alpha z) \int^{z} \exp(\alpha t)\, dt + c \exp(-\alpha z) \tag{13.17}$$

Performing the integration in equation 13.17 gives

$$H = -q \exp(-\alpha z) \frac{\exp(\alpha z)}{\alpha} + c \exp(-\alpha z) \tag{13.18}$$

Simplifying equation 13.18 gives the final expression for matric-flux potential H, as a function of depth z, in the unsaturated-soil profile as

$$H(z) = -\frac{q}{\alpha} + c \exp(-\alpha z) \tag{13.19}$$

where c is the constant of integration, defined by the boundary conditions for the particular problem being solved.

Analytical solution for a homogeneous soil A typical unsaturated-soil problem involves computation of matric potential ψ_m, volumetric water content θ, and unsaturated hydraulic conductivity K—all as a function of depth, z. Using figure 13.1 for definition, we assume a homogeneous and isothermal soil having a water table; with z increasing upward from the water table, and the flux rate q upward from the water table, the constant of integration in equation 13.19 can be evaluated. At the water table, $\psi_m = 0$, and $z = 0$, so equation 13.8 becomes

$$H(z = 0) = H_0 = \frac{1}{\alpha} K_s \exp(\alpha 0) = \frac{K_s}{\alpha} \tag{13.20}$$

Substituting equation 13.20 into equation 13.19 at $z = 0$ gives

$$H_0 = \frac{K_s}{\alpha} = -\frac{q}{\alpha} + c \exp(-\alpha 0) \tag{13.21}$$

Solving equation 13.21 for c gives

$$c = \frac{q + K_s}{\alpha} \tag{13.22}$$

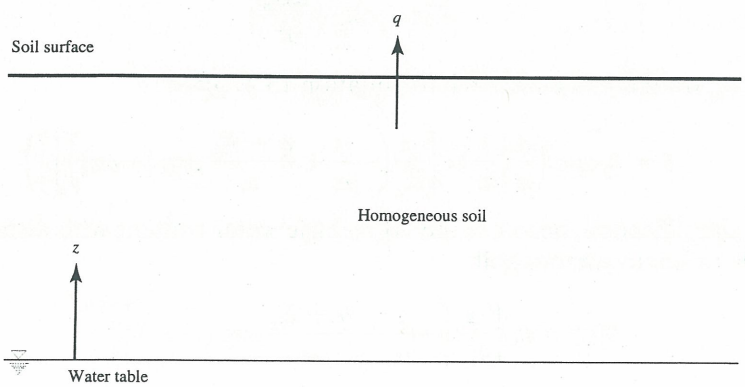

Figure 13.1 Definition of a homogeneous soil

Substitution of c into equation 13.19 gives the complete solution for matric-flux potential H for a homogeneous unsaturated soil, as defined by figure 13.1:

$$H(z) = -\frac{q}{\alpha} + \frac{q + K_s}{\alpha} \exp(-\alpha z) \tag{13.23}$$

López-Bakovic and Nieber (1989) derive analytical solutions (based on the above equations) for matric potential, volumetric water content, and unsaturated-hydraulic conductivity as a function of depth z, for the homogeneous soil described in figure 13.1. Their solution for matric potential ψ_m is derived by rearranging equation 13.8 and taking the natural logarithm of both sides:

$$\ln\left[\frac{\alpha H}{K_s}\right] = \ln[\exp(\alpha\psi_m)] = \alpha\psi_m \tag{13.24}$$

Solving for ψ gives the matric potential as a function of H

$$\psi_m = \frac{1}{\alpha} \ln\left[\frac{\alpha H}{K_s}\right] \tag{13.25}$$

Substituting equation 13.23 into equation 13.25 gives the matric potential as a function of depth z above the water table in a homogeneous soil

$$\psi_m(z) = \frac{1}{\alpha} \ln\left\{\frac{\alpha}{K_s}\left[-\frac{q}{\alpha} + \frac{q + K_s}{\alpha} \exp(-\alpha z)\right]\right\} \tag{13.26}$$

López-Bakovic and Nieber (1989) derive an expression for water content similar to the one for matric potential, using the following expression:

$$\frac{K}{K_s} = \left(\frac{\theta}{\theta_s}\right)^n \tag{13.27}$$

where θ is the unsaturated volumetric-water content, θ_s is the saturated volumetric-water content, and n is a dimensionless coefficient related to the pore-size distribution index, as defined by Brooks and Corey (1964). This n is the same as the exponent in equation 13.9. From equation 13.6, equation 13.27 is rewritten as

$$\frac{K}{K_s} = \exp(\alpha\psi_m) = \left(\frac{\theta}{\theta_s}\right)^n \tag{13.28}$$

and by taking the nth root of both sides of equation 13.28, gives

$$\theta = \theta_s \exp\left(\frac{\alpha\psi_m}{n}\right) \tag{13.29}$$

Substituting ψ_m from equation 13.26 into equation 13.29 gives

$$\theta = \theta_s \exp\left(\frac{\alpha}{n}\left\{\frac{1}{\alpha} \ln\left[\frac{\alpha}{K_s}\left(-\frac{q}{\alpha} + \frac{q + K_s}{\alpha} \exp[-\alpha z]\right)\right]\right\}\right) \tag{13.30}$$

which, upon simplification, becomes the volumetric water content with distance z above the water table for a homogeneous soil,

$$\theta(z) = \theta_s \left\{\frac{\alpha}{K_s}\left[-\frac{q}{\alpha} + \frac{q + K_s}{\alpha} \exp(-\alpha z)\right]\right\}^{1/n} \tag{13.31}$$

López-Bakovic and Nieber (1989) also present a solution for hydraulic conductivity by substituting the expression for ψ_m (equation 13.26) into equation 13.6, or

$$K = K_s \exp\left(\alpha\left\{\frac{1}{\alpha}\ln\left[\frac{\alpha}{K_s}\left(-\frac{q}{\alpha}+\frac{q+K_s}{\alpha}\exp\left[-\alpha z\right]\right)\right]\right\}\right) \tag{13.32}$$

which, upon simplification, becomes the hydraulic conductivity with distance z above the water table for a homogeneous soil,

$$K(z) = \alpha\left[-\frac{q}{\alpha}+\frac{q+K_s}{\alpha}\exp\left(-\alpha z\right)\right] \tag{13.33}$$

The above derivation presents equations for a homogeneous soil. These equations are now used to solve for matric potential, volumetric water content, and unsaturated hydraulic conductivity for a layered-soil profile.

Analytical solution for a layered soil Consider a soil profile comprised of discrete layers, where equation 13.3 applies within each layer [López-Bakovic and Nieber (1989)]. The solution, given by equation 13.19, also applies to each layer; however, the coefficient c in equation 13.19 is unique for each layer, and is determined by the conditions at each interlayer boundary. In addition, the matric potential must be continuous across each boundary.

Referring to figure 13.2, define i as the number of a layer, and $i + 1$ as the number of the layers above layer i. Then the matric-potential continuity across layer boundaries requires that ψ_i be equal to ψ_{i+1} at the boundary between layer i and layer $i + 1$. Therefore, using equations 13.18 and 13.25, it follows [López-Bakovic and Nieber (1989)] that

$$H_{i+1} = \frac{K_{si+1}}{\alpha_{i+1}}\exp\left(\alpha_{i+1}\,\psi_{i+1}\right) = \frac{K_{si+1}}{\alpha_{i+1}}\exp\left(\alpha_{i+1}\psi_i\right) \tag{13.34}$$

$$H_{i+1} = \frac{K_{si+1}}{\alpha_{i+1}}\exp\left\{\alpha_{i+1}\left[\frac{1}{\alpha_i}\ln\left(\frac{\alpha_i H_i}{K_{si}}\right)\right]\right\} \tag{13.35}$$

$$H_{i+1} = \frac{K_{si+1}}{\alpha_{i+1}}\left[\frac{\alpha_i H_i}{K_{si}}\right]^{\alpha_{i+1}/\alpha_i} \tag{13.36}$$

Again referring to figure 13.2, define L_i as the length from the water table to the boundary between the i and $i + 1$ layer. Using equation 13.35 and equation 13.19, the following

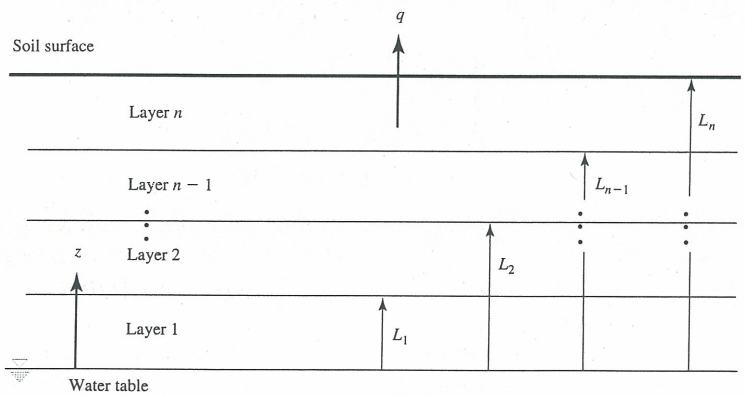

Figure 13.2 Definition of a layered soil (data from López-Bakovic and Nieber 1989)

equation results [López-Bakovic and Nieber (1989)]:

$$-\frac{q}{\alpha_{i+1}} + c_{i+1}\exp(-\alpha_{i+1}L_i) = \frac{K_{si+1}}{\alpha_{i+1}}\left\{\frac{\alpha_i}{K_{si}}\left[-\frac{q}{\alpha_i} + c_i\exp(-\alpha_i L_i)\right]\right\} \tag{13.37}$$

The relation between c_{i+1} and c_i is given by

$$\exp(\alpha_{i+1}L_i)\left\{\frac{q}{\alpha_{i+1}} + \frac{K_{si+1}}{\alpha_{i+1}}\left[\frac{\alpha_i}{K_{si}}\left(-\frac{q}{\alpha_i} + c_i\exp\{-\alpha_i L_i\}\right)\right]\right\}^{\alpha_{i+1}/\alpha_i} \tag{13.38}$$

knowing that

$$c_i = \frac{q + K_{si}}{\alpha_i} \tag{13.39}$$

In summary, as defined by figure 13.2, the resulting equations for a layered system are:

$$H_i(z) = -\frac{q}{\alpha_i} + c_i\exp(-\alpha_i z) \tag{13.40}$$

$$\psi_i(z) = \frac{1}{\alpha_i}\ln\left\{\frac{\alpha_i}{K_{si}}\left[-\frac{q}{\alpha_i} + c_i\exp(-\alpha_i z)\right]\right\} \tag{13.41}$$

$$\theta_i(z) = \theta_{si}\left\{\frac{\alpha_i}{K_{si}}\left[-\frac{q}{\alpha_i} + c_i\exp(-\alpha_i z)\right]\right\}^{1/n_i} \tag{13.42}$$

$$K_i(z) = \alpha_i\left[-\frac{q}{\alpha_i} + c_i\exp(-\alpha_i z)\right] \tag{13.43}$$

These equations apply to values of z between L_i and L_{i+1}. The coefficient c_i can be calculated for the appropriate layer from equations 13.38 and 13.39.

As an example of the application of the above equations, consider a soil with two layers, each 60-cm thick; a water table is located 1.2 meters below the soil surface. The properties of the layers are given as

Property	Top layer	Bottom layer
K_s	1×10^{-7} m/s	5×10^{-8} m/s
α	15/m	10/m
n	3	3
θ_s	0.50	0.60

Find the matric potential, volumetric water content, and hydraulic conductivity as a function of depth above the water table, if the following flux rates q are occurring:

$$q = 3.00 \times 10^{-14} \text{ m/s}$$
$$q = 0.0 \text{ m/s}$$
$$q = -3.00 \times 10^{-11} \text{ m/s}$$
$$q = -3.00 \times 10^{-8} \text{ m/s}$$

Note that negative flux rates mean infiltration is occurring; positive flux rates mean evaporation is occurring from the soil surface. The above flux rates were intentionally chosen to be less than the saturated hydraulic conductivities to avoid positive matric potentials, for which the solutions given are not valid.

Results of the example two-layer soil are presented in figure 13.3 for matric potential, figure 13.4 for volumetric water content, and figure 13.5 for hydraulic conductivity. The effect of the layering is clearly visible in figures 13.4 and 13.5, but only slightly visible in figure 13.3.

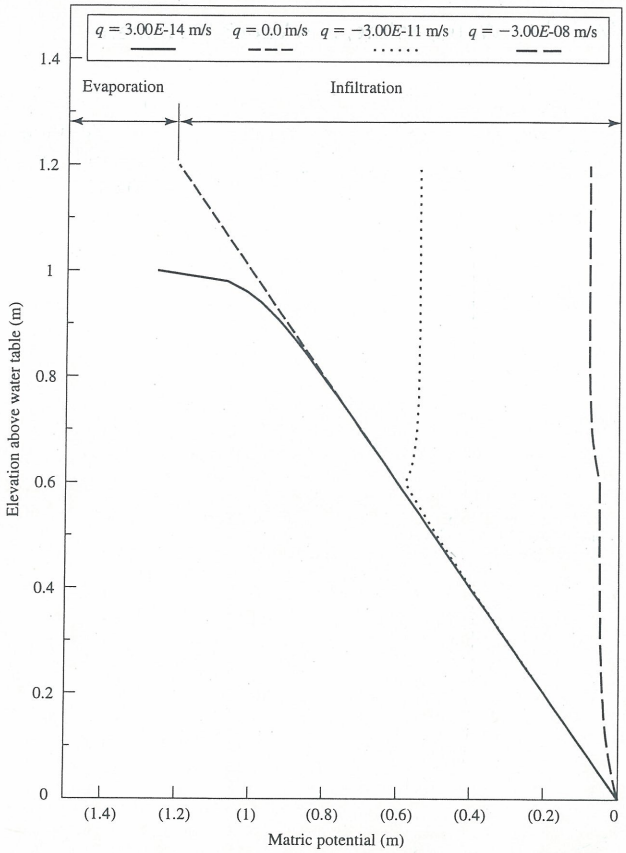

Figure 13.3 Matric potential versus elevation above the water table for a two-layer system with variable flux rates

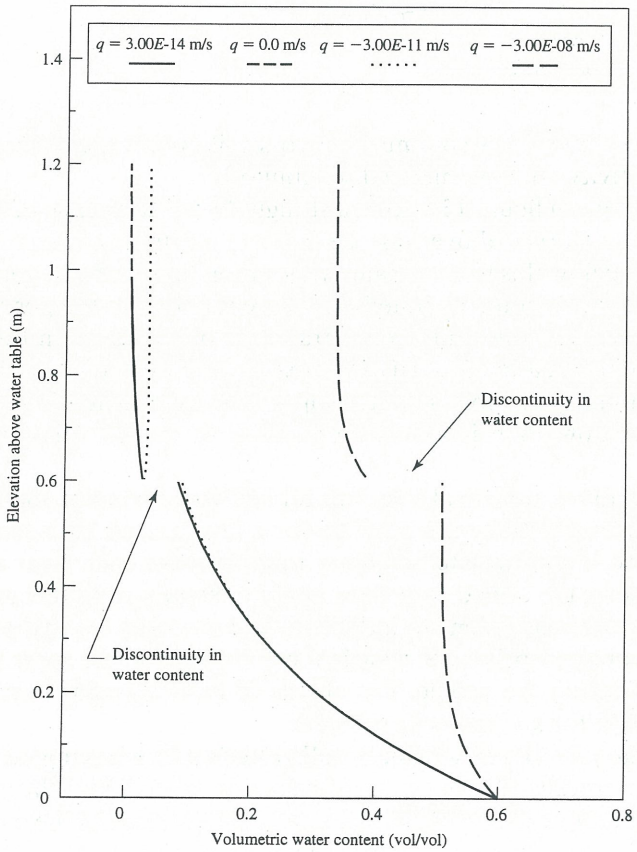

Figure 13.4 Volumetric water content versus elevation above the water table for a two-layer system with variable flux rates

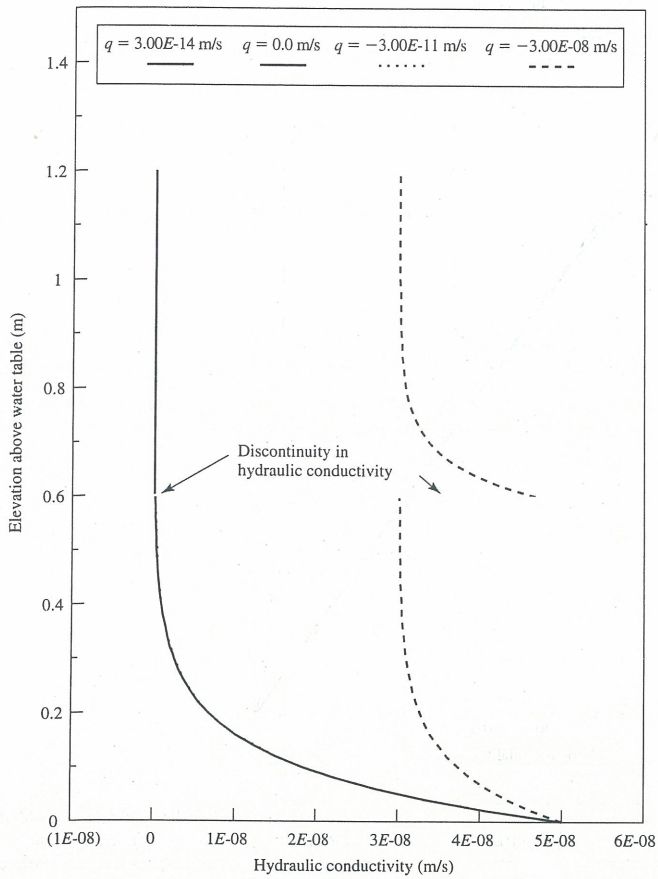

Figure 13.5 Hydraulic conductivity versus elevation above the water table for a two-layer system with variable flux rates

This is because matric potential is continuous across soil interfaces, whereas water content and hydraulic conductivity are both highly discontinuous.

The flux rate of zero in figure 13.3 gives a straight line with a slope of 1 between matric potential and elevation. Curves above this line indicate infiltration (negative or downward flux rates), and curves below this line indicate evaporation (exfiltration) associated with positive or upward flux rates. It should be noted that there is a limit to the positive flux rate that can be used. Mathematically, this limit to exfiltration is obtained when the matric flux potential H is set to zero in equation 13.40. Higher exfiltration rates require that H is less than zero, which is not physically possible. If water-vapor flow were included in the model in addition to liquid-water flow, then it would be possible to exceed this mathematical limit slightly.

In summary, the above analytical solutions for soil-water content, matric potential, and unsaturated hydraulic conductivity are possible for a layered soil between the water table and the ground surface, if appropriate boundary conditions for each layer are used. As with most analytical solutions, the above equations apply to steady-state flux rates with neither water extractions nor water additions to individual layers within the soil profile. Therefore, these equations are not appropriate for transient conditions and are most likely to apply to "average" conditions within the profile. The effects of layering using these equations can, however, be investigated for a variety of problems.

Analytical solution for liquid-moisture redistribution in a homogeneous soil Redistribution refers to the continued movement of water or other liquid through a soil profile after infiltration, irrigation, or other input has ceased at the surface of the soil (Jury, Gardner, and Gardner 1991). When surface storage of liquid is depleted, the movement of liquid

added to the soil does not immediately cease, but can continue for a long time as it redistributes within the profile. The major difference between redistribution and infiltration is that the wetting front continues to move as a result of water coming from the transmission zone, rather than from flux across the surface of the soil. At the same time, a significant amount of liquid is lost from the profile due to evaporation. According to Charbeneau (1989), a number of questions are directly related to redistribution processes. These include: **(1)** the length of time for the soil profile to drain; **(2)** the water content and matric potential near the surface of the soil; **(3)** the recharge (or flux) at depth; **(4)** the influence of evaporation on each wetting event; **(5)** the influence of multiple-wetting events; and **(6)** the effects of spatial variability in the physical parameters.

There have been relatively few analytical or semi-analytical solutions for liquid redistribution, compared to those for infiltration (Charbeneau 1989). Gardner, Hillel, and Benyamini (1970a) consider approximate solutions to the unsaturated-flow equation to describe the soil-water content above the initial wetting front, as a function of time. They also calculate the cumulative drainable water for a rectangular-redistribution profile. Gardner, Hillel, and Benyamini (1970b) show that redistribution reduces evaporation, and they develop expressions for obtaining an estimate of the amount of reduction in evaporation due to redistribution when the redistribution rate is known. Dagan and Bresler (1983) derive a rectangular-profile model for vertical redistribution of liquid in a homogeneous soil column. This approximate solution includes both the time distribution of soil-water content, and flux. Morel-Seytoux (1987) formulates a redistribution model using a kinematic approach, by assuming that the hydraulic conductivity function can be represented by a power function. Charbeneau (1989) summarizes two liquid-redistribution models—a rectangular and kinematic approach—with and without evaporation. These models are discussed in detail next.

For purposes of developing the analytical solution to one-dimensional (vertical) liquid-moisture redistribution, assume that a homogeneous soil lies in a horizontal plane x and y, with a vertical coordinate z, directed downward as shown in figure 13.6. Let the flux rate q be positive upward; let θ be the volumetric water content; ψ_m be the matric potential; and K the unsaturated hydraulic conductivity. Both ψ_m and K are functions of volumetric water content θ. The two basic equations are Darcy's equation (equation 13.3, above) and the continuity equation given by

$$\frac{\partial \theta}{\partial t} = -\frac{\partial q}{\partial z} \tag{13.44}$$

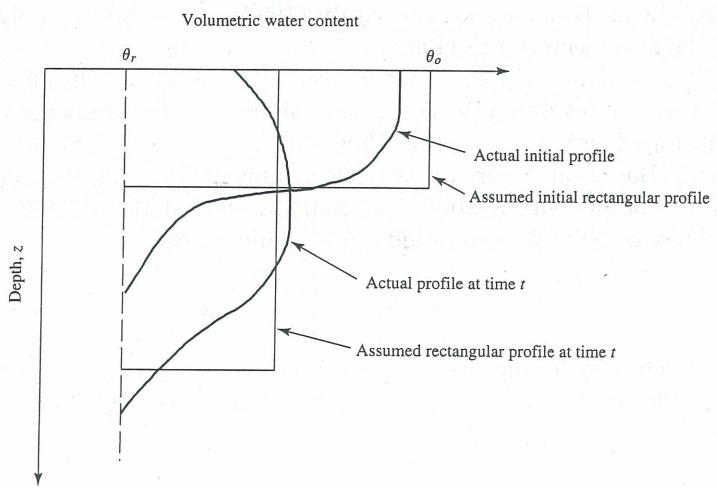

Figure 13.6 Actual and approximate rectangular moisture profile (data from Charbeneau 1989)

Substituting equation 13.3 into equation 13.44 gives

$$\frac{\partial \theta}{\partial t} = \frac{\partial}{\partial z}\left(K \frac{\partial \psi_m}{\partial z}\right) + \frac{\partial K}{\partial z} \tag{13.45}$$

Assuming smooth, single-valued functions of θ and ψ_m versus z, the chain rule gives

$$\frac{\partial \theta}{\partial t} = \frac{\partial}{\partial z}\left(K \frac{d\psi_m}{d\theta} \frac{\partial \theta}{\partial z}\right) + \frac{\partial K}{\partial z} \tag{13.46}$$

which is Richards' equation. We further recognize that the diffusivity D, also a function of volumetric water content, is given by

$$D = K \frac{d\psi_m}{d\theta} \tag{13.47}$$

Thus, Richards' equation can also be written in terms of diffusivity as

$$\frac{\partial \theta}{\partial t} + \frac{\partial}{\partial z}\left(D \frac{\partial \theta}{\partial z}\right) + \frac{\partial K}{\partial z} \tag{13.48}$$

For purposes of this analytical solution, a power law relating hydraulic conductivity and matric potential of the form used in equations 13.9 and 13.10 is used to give physically based parameters for the redistribution solution. These power equations can be written as

$$K = K_s(S_e)^n \tag{13.49}$$

and

$$S_e = \frac{\theta - \theta_r}{\theta_m - \theta_r} = \left(\frac{\psi_b}{\psi_m}\right)^{\lambda} \tag{13.50}$$

where: K is hydraulic conductivity as a function of volumetric-water content θ; K_s is saturated-hydraulic conductivity; n is an exponent; S_e is effective saturation; θ_r is residual or irreducible water content that occurs as K approaches zero; θ_m is the maximum volumetric water content that is close to the value of porosity, unless entrapped air reduces its value; ψ_m is matric potential; ψ_b is the air-entry (or bubbling) pressure, assumed to be the matric potential at which the largest pore in the soil begins to drain; and λ is an exponent. Brooks and Corey (1964) show that the exponent n in equation 13.49 is related to the pore-size distribution index λ, through $3 + 2/\lambda$. Small values of λ correspond to a wide range of pore sizes, while large values correspond to a narrow distribution. Bumb et al. (1988) present typical values of λ, along with typical values of porosity θ_r, and air-entry pressure ψ_b, for soil-texture data provided by Rawls, Brakensiek, and Sarabi (1982). These soil variables are treated in greater detail in later sections of this chapter.

During infiltration, the volumetric water content does not reach full saturation due to entrapped air. Brooks and Corey (1964) present values of θ_m (the maximum water content) as a result of entrapped air in various soils. These values are presented in a subsection of section 13.5, following. Based on empirical evidence, Bouwer (1966) suggests that the maximum effective-hydraulic conductivity is about one-half the saturated hydraulic conductivity for values of θ_m. This concept can be presented mathematically as

$$K_e = \frac{K_s}{2} \tag{13.51}$$

where K_e is the effective hydraulic conductivity. According to equation 13.49—assuming that K is equal to K_e—the corresponding effective saturation is given by

$$S_e = \left[\frac{1}{2}\right]^{1/n} \tag{13.52}$$

The analytical solutions presented here require that the antecedent volumetric-water content is known. For most unsaturated soil, the antecedent volumetric-water content is closely related to the average annual flux rate. The analytical solutions that follow assume that the antecedent water content of the soil is equal to the annual flux rate i_a, assuming uniform and steady infiltration. Rearranging equation 13.49 and assuming K is uniform, a steady infiltration rate of i_a gives

$$S_{ea} = \left[\frac{i_a}{K_s}\right]^{1/n} \tag{13.53}$$

where S_{ea} is the effective antecedent-water content. Because n usually has a value of 3 or greater (Brooks and Corey 1964; McKee and Bumb 1988), the value of S_{ea} is relatively insensitive to estimated values of i_a.

Charbeneau (1989) presents two approximate-profile models to simulate liquid-moisture redistribution in an unsaturated soil after infiltration has ceased. These simple profile solutions are the rectangular profile, taken from Gardner, Hillel, and Benyamini (1970a) and Dagan and Bresler (1983); and kinematic profiles (or Buckley–Leverett models), taken from Charbeneau (1984) and Morel-Seytoux (1987). These two approximate moisture-redistribution analytical solutions are discussed in detail next.

The rectangular profile The simplest shape of a soil-moisture redistribution profile is the rectangular profile, shown in figure 13.6. Using this profile, it is assumed that the initial soil-water content within the profile—prior to infiltration from the wetting event—corresponds to either residual saturation θ_r or effective antecedent saturation S_{ei}. The case of an initially dry soil θ_r is examined first.

The initial effective water content S_{ei} for the rectangular profile immediately behind the wetting front (after the wetting event) is found by comparing the average infiltration rate i during the wetting event, to the natural effective hydraulic conductivity K_e. If the average infiltration rate exceeds K_e, then the natural effective-saturation conditions occur, and S_{ei} is equal to S_e. Otherwise, for the average infiltration rate i equal to K, and using equation 13.49, gives

$$S_{ei} = \left[\frac{1}{2}\right]^{1/n}; \qquad i > K_e \tag{13.54}$$

or

$$S_{ei} = \left[\frac{i}{K_s}\right]^{1/n}; \qquad i < K_e \tag{13.55}$$

With S_{ei} known from either equation 13.54 or equation 13.55, the initial depth of the wetting front z_{fi} as a result of the wetting event, is given for the rectangular profile by

$$z_{fi} = \frac{I}{S_{ei}(\theta_m - \theta_r)} \tag{13.56}$$

where I is the cumulative infiltration depth associated with the wetting event.

As the wetting front moves deeper into the soil, the water content of the rectangular profile decreases with time. Neglecting evaporation and other losses, and letting S_{ea} equal zero, I is equal to $(\theta_m - \theta_r)S_e z_f$, with S_e and z_f both functions of time. Letting i be the rate of change in cumulative infiltration with respect to time, the derivative of I with respect to time is given by

$$i = \frac{dI}{dt} = S_e(\theta_m - \theta_r)\frac{dz_f}{dt} + z_f(\theta_m - \theta_r)\frac{dS_e}{dt} \tag{13.57}$$

Additionally, if the initial water content of the soil prior to wetting is assumed to be at residual, then

$$\frac{dz_f}{dt} = \frac{K(S_e)}{S_e(\theta_m - \theta_r)} \tag{13.58}$$

Using $z_f = I/S_e(\theta_m - \theta_r)$ the decrease in water content as the front moves deeper must satisfy

$$\frac{I}{S_e}\frac{dS_e}{dt} + K_s(S_e)^n = 0 \tag{13.59}$$

Integration of equation 13.59 and application of the initial condition $S_e = S_{ei}$ from either equation 13.54 or equation 13.55, gives the deterministic model to predict S_e as a function of time as

$$S_e = \frac{1}{\left[(S_{ei})^{-n} + \dfrac{nK_s t}{I}\right]^{1/n}} \tag{13.60}$$

A related relation includes the flux rate q (Darcian velocity) within the moisture-wetting front, which is numerically equal to equation 13.49, or $q = K_s(S_e)^n$. The Darcian flux, then, is given by

$$q = \frac{K_s}{(S_{ei})^{-n} + \dfrac{nK_s t}{I}} \tag{13.61}$$

Using $z_f = I/S_e(\theta_m - \theta_r)$, the deterministic model of the depth of the wetting front as a function of time is

$$z_f = \frac{I}{(\theta_m - \theta_r)}\left[(S_{ei})^{-n} + \frac{nK_s t}{I}\right]^{1/n} \tag{13.62}$$

Kinematic profiles Charbeneau (1984; 1989) has proposed using Buckley–Leverett models, or kinematic-wave models, to represent a second type of soil-moisture redistribution model. Figure 13.7 shows the progression of a soil-moisture wave moving downward. Figure 13.7(a) is the shape of the assumed wave immediately after the end of the wetting event. This wave consists of a rectangular wave similar to that shown in figure 13.6; as with the rectangular profile, a sharp wetting front is evident. After a short period of time, drainage within the profile causes increasing soil-water content with depth, resulting in a curved portion of the wave as shown in figure 13.7(b). Figure 13.7(b) also indicates that a constant soil-water content (plateau in the wave) still remains. This is because the draining part of the wave has not yet reached the wetting front, and is separated from the front by the plateau part of the wave. Figure 13.7(c) shows the wave at a later time after drainage has caught up with the wetting front. In this case, the plateau is no longer present.

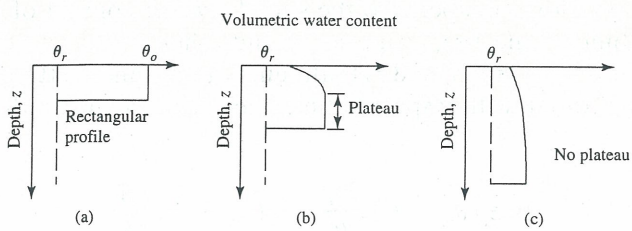

Figure 13.7 Kinematic wave moisture profiles (data from Charbeneau 1989)

The basic assumption in the application of kinematic models is that pressure gradients are negligibly small, and therefore, equation 13.3 (Darcy's equation) and equation 13.44 (continuity equation) become

$$(\theta_m - \theta_r)\frac{\partial S_e}{\partial t} + \frac{dK}{dS_e}\frac{\partial S_e}{\partial z} = 0 \tag{13.63}$$

Equation 13.63 can be solved using the method of characteristics (Sisson, Ferguson, and Van Genuchten 1980). According to the method of characteristics, S_e is constant along paths that satisfy

$$\frac{dz}{dt} = \frac{1}{(\theta_m - \theta_r)}\frac{dK}{dS_e} \tag{13.64}$$

Because dK/dS_e is only a function of S_e, and S_e is constant along each characteristic path (see figure 13.8), the images of these paths are straight lines in the z-t plane. Sisson, Ferguson, and Van Genuchten (1980) show that if the soil-water content changes abruptly at the wetting front (from $S_e = S_{ei}$ to $S_e = 0$) during redistribution, equation 13.64 is integrated and rearranged to determine the soil-water content as a function of z and t. Assuming the power law (equation 13.49), the integration of equation 13.64 gives

$$\frac{z}{t} = \int \frac{1}{\theta_m - \theta_r}\frac{dK}{dS_e} = \frac{nK_s(S_e)^{n-1}}{\theta_m - \theta_r} \tag{13.65}$$

Solving equation 13.65 for S_e (Sisson, Ferguson, and Van Genuchten 1980; Charbeneau 1984; 1989), gives the deterministic model to predict S_e versus time and depth for the kinematic model, as long as the profile remains continuous and no wetting front is encountered. This solution is given by

$$S_e = \left[\frac{(\theta_m - \theta_r)z}{nK_s t}\right]^{1/n-1} \tag{13.66}$$

where t is measured from the time at which the wetting event ends. As with the rectangular profile, the kinematic profile of Darcian flux is given by $q = K_s(S_e)^n$, or as a function of z and t by

$$q = \left[\frac{1}{K_s}\left(\frac{(\theta_m - \theta_r)z}{nt}\right)^n\right]^{1/n-1} \tag{13.67}$$

For the kinematic profile, the drainable water W in storage above any depth z is given by

$$W = (\theta_m - \theta_r)\int_0^z S_e\,dz = \frac{(n-1)z(\theta_m - \theta_r)}{n}S_{ez} \tag{13.68}$$

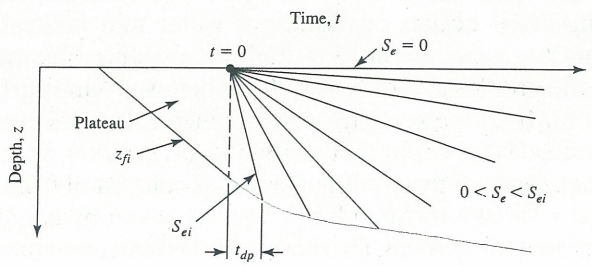

Figure 13.8 Characteristic plane of the kinematic model (data from Charbeneau 1989)

where S_{ez} is the effective water content above depth z in the soil. Equations 13.63 through 13.68 are appropriate as long as the kinematic profile remains continuous and no wetting fronts are encountered (Charbeneau 1989). At the wetting front, the water-content gradient becomes large (infinitely large in the kinematic profile), and therefore, equation 13.63 is no longer valid and the rate of change of the wetting front with respect to time becomes

$$(\theta_m - \theta_r)S_{ei}\frac{dz_f}{dt} = K_s(S_{ei})^n \tag{13.69}$$

Referring to figure 13.7, two separate cases describing the kinematic profile are identified. Figure 13.7(b) shows a plateau region between the draining upper part of the profile and the wetting front. This implies that S_{ei} is constant in equation 13.69, and the rate of movement of the wetting front also is constant. Therefore, the image of the wetting front in the z-t plane in figure 13.8 is a straight line; this is shown in figure 13.8 as the lower boundary of the plateau. At some time (designated t_{dp} in figure 13.8), the plateau has disappeared from the profile and only the wave behind the wetting front remains as shown in figure 13.7. In this case, the moisture arriving at the wetting front decreases with time, and the rate of movement of the wetting front also decreases (see figure 13.8). Combining equations 13.65 and 13.69 gives

$$\frac{dz_f}{dt} = \frac{K_s}{(\theta_m - \theta_r)}(S_e)^{n-1} = \frac{z_f}{nt} \tag{13.70}$$

Equation 13.70 can be integrated to give the following at the initial point (z_{fdp}, t_{dp}), which is the point where the plateau disappears

$$\frac{t}{t_{dp}} = \left(\frac{z_f}{z_{fdp}}\right)^{n-1} \tag{13.71}$$

The location of the initial point (z_{fdp}, t_{dp}) needs to be found in order to provide a method of calculating the time and location where the plateau disappears. Charbeneau (1989) shows that the initial point lies at the intersection of the wetting-front path originating from $z = z_{fi}$ at $t = 0$, and the characteristic with water content S_{ei} originating from the ground surface at $t = 0$ (see figure 13.8). These initial points are

$$z_{fdp} = \frac{n}{n-1}z_{fi} \tag{13.72}$$

$$t_{dp} = \frac{(\theta_m - \theta_t)z_{fi}}{(n-1)K_s(S_{ei})^{n-1}} \tag{13.73}$$

where z_{fi} remains as given by equation 13.56.

To demonstrate the use of the above equations, find the rectangular and kinematic profiles at times of 8, 48, and 240 hours, for a sandy loam as defined by Rawls, Brakensiek, and Saxton (1982). The sandy loam is assumed to have the following characteristics: $\theta_m = 0.453$; $\theta_r = 0.041$; $K_s = 2.59$ cm/hr; $\lambda = 0.378$; and $n = 3 + 2/\lambda = 8.29$ (Brooks and Corey 1964). Also assume that a wetting event occurs, consisting of water that infiltrates at a rate of 1.0 cm/ hr for 4 hours, giving $I = 4$ cm. We need to find the moisture flux rate q for each of the rectangular and kinematic profiles at a depth of 30 cm below ground surface.

The moisture profiles for both the rectangular and kinematic cases must know S_{ei} and z_f for the wetting event. Because i (1.0 cm/hr) is less than K_e (1.3 cm/hr), S_{ei} is given by equation 13.55 as 0.891. The initial depth of the wetting front z_{fi} is calculated from equation 13.56 as 11.1 cm. Values of S_e and z for the rectangular profile are given by equations 13.60 and 13.62, respectively. For the kinematic profiles, the first step is to determine the time and depth

where the plateau disappears, to check to see which equations apply. Using equation 13.71, t_{dp} is calculated as 0.56 hrs, and using equation 13.72, z_{fdp} is calculated as 12.62 cm; therefore, for times of 8, 48, and 240 hours, the plateau has disappeared. Thus, the depth of the wetting front z_f at various times is calculated using equation 13.71, and S_e for each of the z_f values is calculated using equation 13.66. After establishing the depth and effective saturation of the kinematic profile at the wetting front for the three times, values of S_e behind the wetting front are calculated using equation 13.66. Figure 13.9 presents the results for a sandy loam soil for both the rectangular and kinematic profiles.

The moisture flux rate (Darcian velocity) for the sandy loam at a depth of 30 cm below the ground surface, is calculated for the rectangular profile using equation 13.61, and for the kinematic profile using equation 13.67. First, the time to reach the 30-cm depth (as well as the effective saturation at that depth) is calculated for both profiles. For the rectangular profile, the time to reach 30 cm is calculated using equation 13.62 and S_e at 30 cm is calculated from $z_f = I/[S_e(\theta_m - \theta_r)]$. For the kinematic profile, the time to reach the 30-cm depth is calculated using equation 13.71 and S_e is calculated using equation 13.66. Figure 13.10 shows the flux rates at the 30-cm depth for the sandy loam soil.

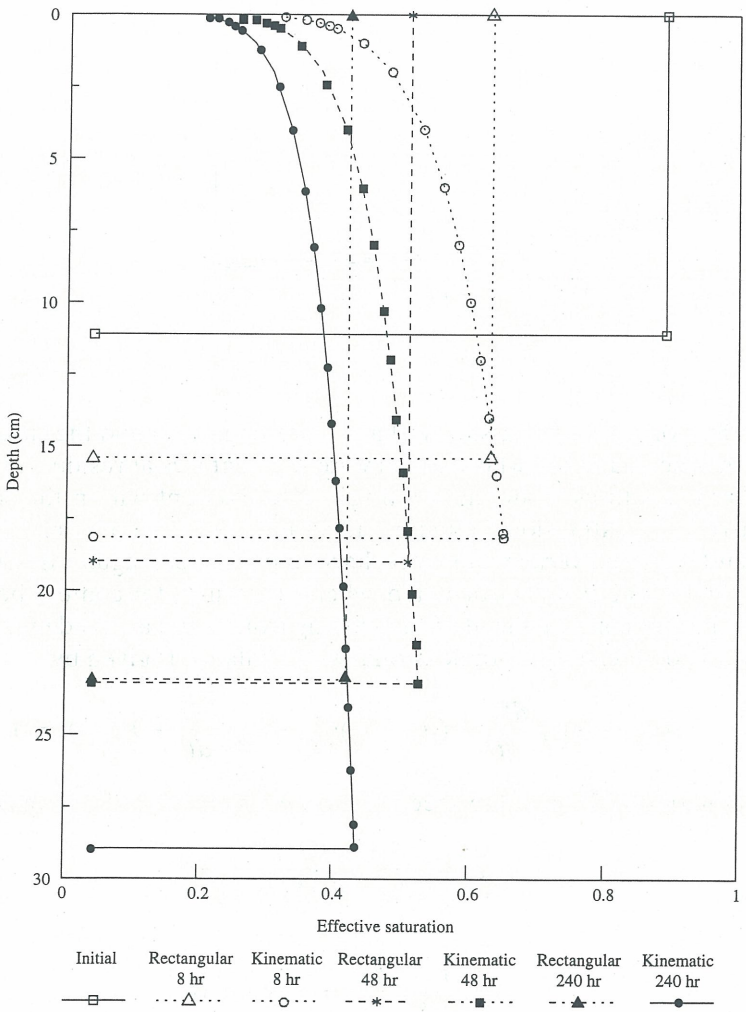

Figure 13.9 Example of rectangular and kinematic moisture profiles

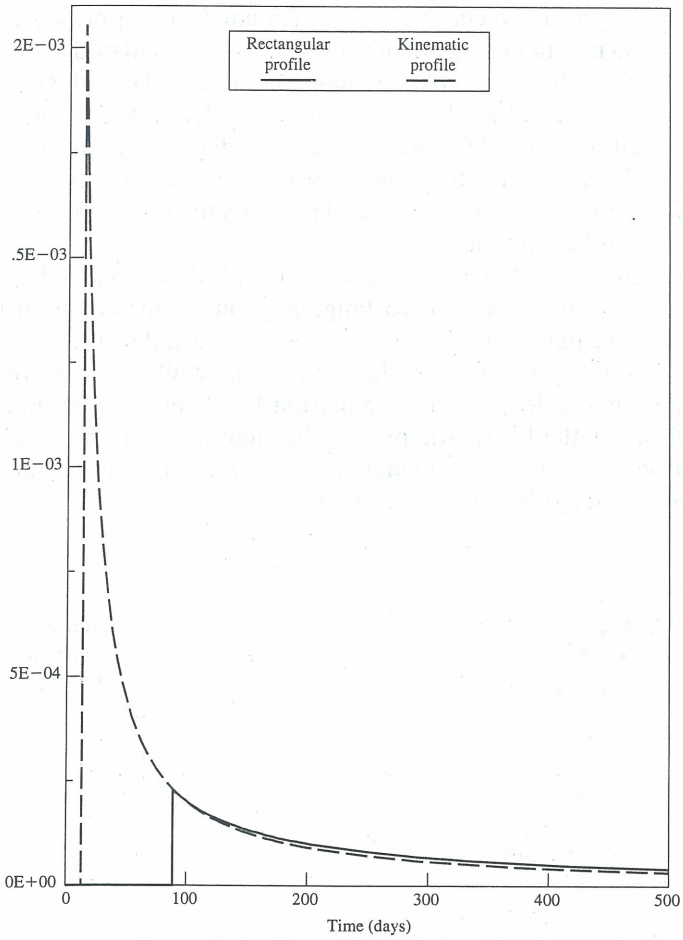

Figure 13.10 Flux rates at 30-cm depth for rectangular and kinematic profiles with an initial water content at residual saturation

Up to this point, we have assumed that the wetting event and the subsequent moisture redistribution occurred in soil whose initial water content was at residual saturation. A more realistic approach is to estimate an initial soil-water content within the soil profile that is higher than residual saturation. Equation 13.53 provides an estimate of antecedent soil-water content based on average annual recharge. For the rectangular model, the water balance across the wetting front is calculated, where the soil-water content behind the wetting front is S_e, and water content ahead of the wetting front is the antecedent moisture given by S_{ea}. In a control volume, the one-dimensional water balance is given by

$$(\theta_m - \theta_r)z_f \frac{dS_e}{dt} + (\theta_m - \theta_r)(S_e - S_{ea}) \frac{dz_f}{dt} + K(S_{ea}) = 0 \tag{13.74}$$

Combining equation 13.74 with the speed of the wetting front and noting that

$$z_f = \frac{I}{(\theta_m - \theta_r)(S_e - S_{ea})} \tag{13.75}$$

gives

$$\frac{I}{S_e - S_{ea}} \frac{dS_e}{dt} = K(S_e) = 0 \tag{13.76}$$

While equation 13.76 looks similar to equation 13.59, it is no longer possible to determine a general analytical solution in terms of simple functions. Using separation of variables, S_e is written as a function of t, such that

$$\frac{K_s}{I}t = \int_{S_e}^{S_{ei}} \frac{dx}{(x - S_{ea})x^n} \tag{13.77}$$

Equation 13.77 is easily evaluated numerically, by assuming a reasonably small value of dx (say 0.001 or 0.0001) and letting x take on values slightly larger than S_{ea} to S_{ei}, and presenting the results in a table. The value of the initial time at S_e is obtained by looking up the value of the integral in the table and then solving for t. After S_e is known, the flux rate q is calculated from equation 13.49 [$q = K_s(S_e)^n$].

For the kinematic profile, the wetting front initially follows a straight path at the base-characteristic plane, with drainage characteristics given by equation 13.65. One approach to solving the kinematic problem with antecedent moisture is to write the water-balance equation in the vicinity of the wetting front as

$$\frac{dW}{dt} + q(z_f, t) = 0 \tag{13.78}$$

where W is the water-storage depth within the profile given by equation 13.68. Recognizing that the water content remains constant at depth z_f up to time t, equation 13.78 is integrated at its antecedent water content to give

$$W(z_f, t) - W(z_f, 0) + Q_a = 0 \tag{13.79}$$

where Q_a is the cumulative drainage depth from the profile at time t, with the soil-water content constant at its antecedent value:

$$Q_a = K_s(S_{ea})^n t \tag{13.80}$$

The water content (within the kinematic profile to depth z_f at the beginning of the redistribution process) consists of the moisture present at its antecedent value, plus the moisture added through infiltration. Thus, equations 13.79 and 13.80 become

$$(\theta_m - \theta_r)S_{ea}z_f + I = W(z_f, t) + K_s(S_{ea})^n t \tag{13.81}$$

Equation 13.81 states that the sum of the drainable water at the antecedent water content (down to depth z_f) plus the infiltration added to the profile, is equal to the drainable water depth above the wetting front at time t, plus the amount of soil-water that has drained (from the profile above z_f) during the time period since the end of the infiltration event. Combining equations 13.66, 13.68, and 13.81 gives

$$(\theta_m - \theta_r)S_{ea}z_f + I = \frac{(n-1)z_f(\theta_m - \theta_r)}{n}\left(\frac{z_f(\theta_m - \theta_r)}{nK_s t}\right)^{1/n-1} + K_s(S_{ea})^n t. \tag{13.82}$$

Equation 13.82 provides the kinematic wetting-front depth as a function of time for the antecedent water content case, and is valid once the plateau has disappeared from the profile.

As an application of the above equations for antecedent-moisture conditions, consider the same sandy loam as above, with a cumulative infiltration of 4 cm over a period of 4 hours. We want to find the time-history of water flux at a depth of 150 cm if the average annual recharge is 40 cm, using both the rectangular- and kinematic-profile assumptions. From equation 13.53, S_{ea} is calculated to be 0.465. For the rectangular profile, equation 13.75 shows that

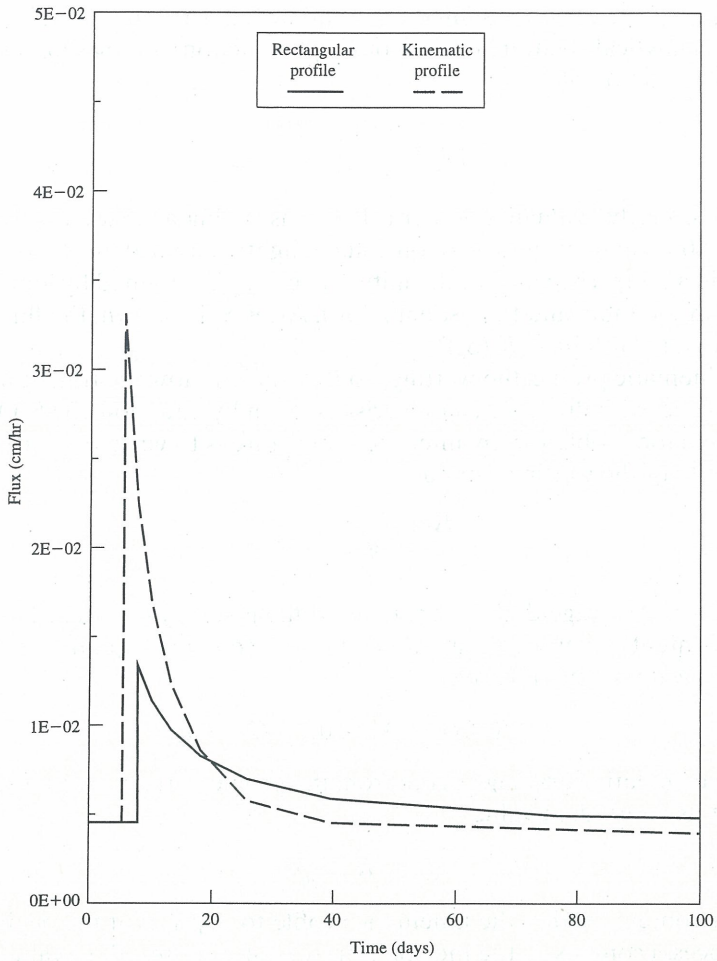

Figure 13.11 Flux rates at 150-cm depth for rectangular and kinematic profiles with an antecedent water content caused by average annual recharge

the wetting front reaches $z_{zt} = 150$ cm with a water content $S_e = S_{ea}I/(\theta_m - \theta_r)z_{zt} = 0.530$. With $S_e = 0.530$ in equation 13.77, the corresponding time for the wetting front to reach 150 cm is 188 hours or 7.8 days. The flux rate is found from $q = K_s(S_e)^n$, and the maximum flux is 0.0134 cm/hr. Figure 13.11 shows the flux rate as a function of time for the rectangular profile.

The corresponding results for the kinematic profile are also shown in figure 13.11. According to equation 13.82, the wetting front reaches the 150-cm depth at 133 hours or 5.5 days, and the maximum flux rate is, according to equation 13.67, 0.0331 cm/hr. Figure 13.11 indicates that most of the drainage occurs earlier for the kinematic model than for the rectangular model.

Other analytical models Other analytical and semi-analytical models are also available for use in the unsaturated zone. These models are summarized in table 13.1, along with the model source and reference. The analytical solutions presented in the models given in table 13.1 solve problems generally similar to the one-dimensional solutions presented above. As with most analytical solutions, the models assume that the input-flux term q is constant over the time of interest in the solution. A description of many of the one-dimensional analytical models presented in table 13.1 can be found in van der Heijde (1994), who compiled a description of over 90 unsaturated-flow models. The reader is referred to the individual reference for details on a particular analytical model.

TABLE 13.1 Other Analytical and Semianalytical Liquid-Flow Models

Model name	Source
FLO	National Hydrology Research Institute, Inland Waters Directorate, Ottawa, Ontario, Canada—Vandenberg (1985)
SOILMOP	Colorado State University, Department of Civil Engineering—Ross and Morel-Seytoux (1982), Morel-Seytoux (1979)
HSSWDS (Hydraulic Simulation of Solid Waste Disposal Sites)	EPA—Perrier and Gibson (1982)
HELP (Hydrologic Evaluation of Landfill Performance)	EPA—Schroeder and others (1994a, b)
B&W analytical solution	Broadbridge and White (1988)
McWhorter analytical solution	McWhorter and Sunada (1990), McWhorter and Kueper (undated)
Warrick analytical solution	Warrick et al. (1971; 1990; 1991)
Fokas analytical solution	Fokas and Yortsos (1982)

Numerical Models

In numerical models, a discrete solution is obtained in both space and time by using numerical approximations of the governing partial differential equations. Because the numerical solutions are only approximations, the conservation of mass and accuracy in prediction are not always assured. Therefore, numerical models need to be verified by either field measurements or comparison to analytical solutions. Because the unsaturated-zone solutions involve nonlinear equations, sophisticated solution techniques are often required.

The primary solution techniques used for approximating the spatial components of the governing flow equations in the unsaturated zone are: **(1)** finite-difference methods (FDM); **(2)** integral finite-difference methods (IFDM); and **(3)** finite-element methods (FEM). In most models, time is approximated by finite-difference techniques resulting in explicit, implicit, or fully implicit solution schemes. In the FDM, the solution is obtained by approximating the derivatives of the differential equations. In the FEM approach, integral equations are formulated first, followed by numerical evaluation of the integrals over the flow domain.

There are many considerations in selecting a numerical simulation model for the unsaturated zone. Simulating flow in nearly saturated-soil systems requires expression of Richards' equation in terms of hydraulic head, matric-potential head, or suction head, especially when parts of the modeled system become fully saturated. This application of Richards' equation causes significant convergence problems when simulating an infiltration front in soil where the initial soil-water content is at residual saturation. Also, significant mass balance problems can occur when site-specific conditions result in highly nonlinear model relations. Other issues that should be addressed in selecting an unsaturated-zone model for flow simulation are: possible needs for double-precision versus single-precision variables; the time-stepping approach; the definition of intercell conductance; and the method in which steady-state simulation is achieved.

The International Ground Water Modeling Center (IGWMC) has identified, compiled, and published a description of over 90 unsaturated-zone models (van der Heijde 1994). The compilation includes models for: flow only; flow and solute transport; solute transport requiring a given head distribution; flow and heat transport; and flow, solute and heat transport in the unsaturated zone. Table 13.2 summarizes the numerical flow-only models documented by the IGWMC (van der Heijde 1994), along with the model source and reference.

TABLE 13.2 Numerical Liquid-Flow Models

Model name	Source
UNSAT2	Department of Hydrology and Water Resources, University of Arizona, Tucson, Arizona—Davis and Neuman (1983)
TRUST	Lawrence Berkeley Laboratory, Earth Sciences Division, University of California, Berkeley, California—Reisenauer et al. (1982)
FLUMP	Lawrence Berkeley Laboratory, Earth Sciences Division, University of California, Berkeley, California—Narasimhan, Neuman, and Witherspoon (1978)
MUST (Model for Unsaturated flow above a Shallow water Table)	International Institute for Hydraulic and Environmental Engineering, Delft, The Netherlands de Laat (1985)
UNSAT1D	Battelle Pacific Northwest Laboratory, Richland, Washington—Bond, Cole, and Gutknech (1984)
SWACROP (Soil WAter and CROP production model)	Winand Staring Centre, Department of Agrohydrology, Wageningen, The Netherlands—Wesseling et al. (1989)
SEEPV	Water, Waste and Land, Inc., Fort Collins, Colorado—Davis (1980)
The One-Dimensional Princeton Unsaturated Code	Princeton University, Princeton, New Jersey—Celia, Bouloutas, and Zarba (1990)
FEMWATER/FECWATER	Pennsylvania State University, University Park, Pennsylvania—Yeh and Ward (1980), Yeh and Strand (1982)
UNSAT-1*	USDA Salinity Laboratory, University of California at Riverside, Riverside, California—van Genuchten (1978)
INFIL*	Institute de Mecanique de Grenoble, St. Martin D'Heres, France—El-Kadi (1983)
GRWATER	Department of Civil Engineering, Colorado State University, Fort Collins, Colorado—Kashkuli (1981)
UNSAT-H	Battelle Pacific Northwest Laboratory, Richland, Washington—Fayer and Gee (1985)
INFGR	Oak Ridge National Laboratory, Environmental Sciences Division, Oak Ridge, Tennessee—Craig and Davis (1985)
FLOWVEC	Simons, Li and Associates, Newport Beach, California—Li, Eggert, and Zachman (1983)
LANDFIL	Department of Civil and Environmental Engineering, Rutgers University, New Brunswick, New Jersey—Korfiatis (1984)
WATERFLO	Soil Science Department, University of Florida, Gainesville, Florida—Nofziger (1985)
SEEP/W (PC-SEEP)	Geo-Slope Programming, Ltd, Calgary Alberta, Canada—Krahn, et al. (1989)
SIMGRO (SIMulation of GROundwater flow and surface water levels)	Institute for Land and Water Management Research, Wageningen, The Netherlands—Querner (1986)
UNSAT	New Mexico Institute of Mining and Technology, Socorro, New Mexico—Khaleel and Yeh (1985)

Source: Summarized from van der Heijde (1994).
*Code and documentation available from the IGWMC, Colorado School of Mines, Golden, Colorado 80401

13.2 THREE-DIMENSIONAL DETERMINISTIC LIQUID- AND VAPOR-FLOW MODELS

Analytical Models

Three-dimensional analytical solution for liquid-water content from a point source leak: Linearization technique As we have seen in section 13.2, the governing equation for liquid-moisture flow in the vadose zone derives from Richards' (1931) equation. Among other parameters, Richards' equation includes matric potential, volumetric water content, and unsaturated hydraulic conductivity as a function of water content. Matric potential (or capillary pressure) is related to volumetric water content through the moisture-characteristic curve. Due to interrelation between matric potential and volumetric water content, as well as hydraulic conductivity as a function of water content, obtaining solutions to Richards' equation is not easy, even with the help of numerical methods. Because of these difficulties, flow in the unsaturated zone is not well understood by practicing engineers and soil and environmental scientists. McKee and Bumb (1988) and Bumb et al. (1988) describe a computer model that uses an analytical solution to Richards' equation, applying an exponential function to describe the moisture-characteristic curve as shown in equation 13.10. This type of exponential function, along with other empirical forms for relating matric potential and volumetric water content are described here. Bumb, Murphy, and Everett (1992) compare three of the functional forms for representing moisture-characteristic curves and recommend use of a particular functional form.

A typical plot relating matric potential and volumetric water content is presented in figure 13.12. The two variables θ_m and θ_r are approximately established, as shown in the

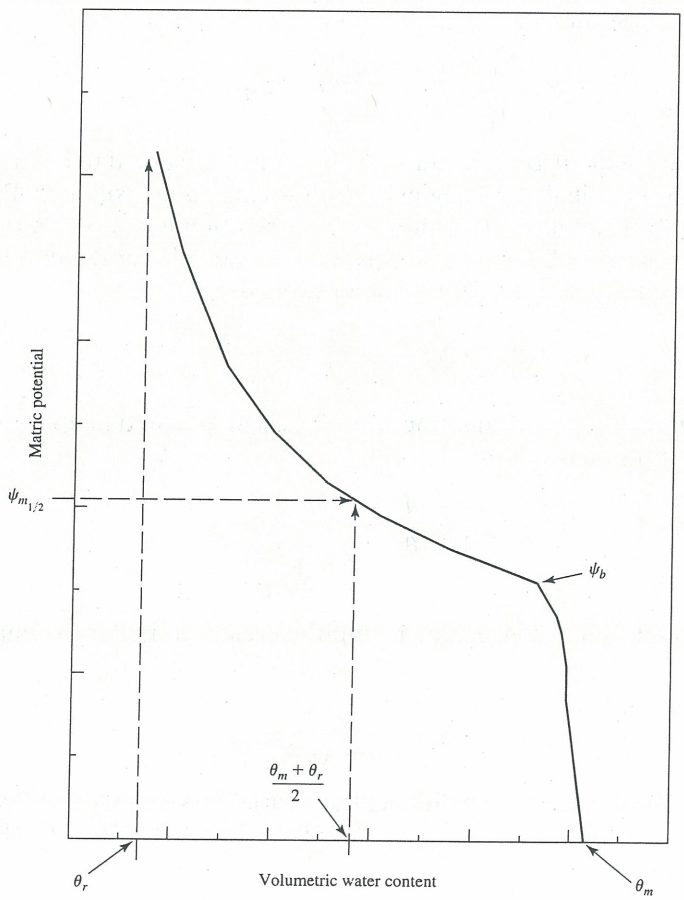

Figure 13.12 Typical soil moisture-characteristic curve

figure. The residual water content θ_r specifies the maximum amount of water in the soil that will *not* contribute to liquid flow, due to blockage from the flow paths or strong adsorption to the solid phase. Mathematically, θ_r is defined as the soil-water content at which both $d\theta/d\psi_m$ and K go to zero when ψ_m becomes large. Therefore, the residual-water content is an extrapolated (or fit) value, and does not necessarily represent the smallest possible water content in a soil. This is especially true for arid regions, where vapor-phase transport can dry the soil to water contents well below θ_r. The maximum-water content θ_m denotes the maximum volumetric water content of a soil. This maximum water content is not equated to the porosity of the soil θ_s for field conditions, because maximum field-water contents are generally 5 to 10 percent smaller than the porosity, due to entrapped air. Therefore, according to Van Genuchten, Leij, and Yates (1991), θ_r and θ_m are viewed as essentially empirical constants in soil moisture-characteristic curves, and hence, without much physical meaning.

Several expressions have been proposed to relate matric potential ψ_m to volumetric-water content θ or more commonly, effective saturation S_e, as given by

$$S_e = \frac{\theta - \theta_r}{\theta_m - \theta_r} \tag{13.83}$$

where θ is the volumetric water content, θ_m is the maximum volumetric water content, and θ_r is the residual volumetric water content. The maximum water content θ_m is generally less than 1.0 due to entrapped air, but can be nearly 1.0 at high-overburden pressures (Way et al. 1985). Fourteen closed-form expressions for water-retention data are presented by Leij, Rossell, and Lesch (1997).

Brooks and Corey (1964) plot S_e versus ψ_m on log–log paper and suggest a relation as given by equation 13.50, or

$$S_e = \frac{\theta - \theta_r}{\theta_m - \theta_r} = \left(\frac{\psi_b}{\psi_m}\right)^{\lambda}, \quad \text{for} \quad \psi_m > \psi_b \tag{13.84}$$

where ψ_m is matric potential, ψ_b is the air-entry pressure—assumed to be the matric potential at which the largest pore in the soil begins to drain—and λ is an exponent. Brooks and Corey (1964) show that the exponent λ (the pore-size distribution index) often has a typical value in soils of approximately 2. Equation 13.84 is best for use only for the drainage cycle; for the wetting cycle, Su and Brooks (1975) suggest an expression given by

$$\psi_m = \psi_b\left(\frac{\theta - \theta_r}{c}\right)^{-m}\left(\frac{1 - \theta}{d}\right)^{dm/c} \tag{13.85}$$

where c, d, and m are constants. Equation 13.85 is designed to fit data for $\psi_m > 0$. When $c = d$, equation 13.85 simplifies to

$$\frac{\theta - \theta_r}{1 - \theta_r} = \frac{1}{1 + \left(\frac{\psi_m}{\psi_b}\right)^{1/m}} \tag{13.86}$$

Van Genuchten (1980) suggested an empirical relation similar to equation 13.86, given by

$$S_e = \frac{1}{[1 + (\alpha\psi_m)^n]^m} \tag{13.87}$$

where α, n, and m are constants. Van Genuchten's variable n is related to Brooks and Corey's variable λ by $n = \lambda + 1$. The variable m is related to λ by $m = \lambda/(1 + \lambda)$. (Rawls et al. 1993).

Laliberte (1969) points out that equation 13.84 overestimates S_e for ψ_m near ψ_b, and suggests another expression of the form

$$S_e = 0.5(1 + \text{erf}\ \xi) \tag{13.88}$$

where erf is the error function (for which a series expansion is given in appendix 3) and ξ is given by

$$\xi = \frac{a}{(\psi_m + b)} - c \tag{13.89}$$

where a, b, and c are properties of the soil. Equation 13.89 is valid for $\psi_m > -b$, where $|b| < \psi_b$. For Laliberte's expression (equation 13.88), we need only one equation to fit data over the entire range of S_e. This is also true for Van Genuchten's relation (equation 13.87), and for the expression of Su and Brooks (equation 13.85).

McKee, Bumb, and Deshler (1983) and McKee and Bumb (1984) suggest an exponential form for the relation between effective saturation and matric potential, referred to as the "Boltzmann distribution" (see equation 13.10), given by

$$S_e = \exp\left(-\frac{\psi_m - \psi_1}{\beta}\right) \tag{13.90}$$

where β and ψ_1 are adjustable variables. This expression is very successful in matching data for $\psi_m > \psi_b$, but like the Brooks–Corey relation (equation 13.84), it is not meant to be used for $\psi_m < \psi_b$. For data that closely follow the trend of the curve in figure 13.9, ψ_1 is roughly equivalent to the air-entry (bubbling) pressure. As ψ_1 changes, the whole curve shifts up or down. The β fitting parameter generally gets smaller as the pore-size distribution becomes more uniform and the moisture-characteristic curve becomes flatter in the middle.

The Brooks–Corey relation and Boltzmann distribution are valid for matric potentials greater than the air-entry pressure, but are not valid near maximum moisture contents or under fully saturated conditions that occur in the capillary-fringe region. McKee and Bumb (1987) and Bumb (1987) suggest a new distribution, called the "Fermi distribution"—so-named due to its functional similarity to the energy relation among electrons. The Fermi distribution relates water content to matric potential over the complete range of saturations, given by

$$S_e = \frac{1}{1 + \exp\left(\dfrac{\psi_m - \psi_{m_{1/2}}}{\beta}\right)} \tag{13.91}$$

The Fermi distribution achieves a fit using only two curve-fitting parameters, $\psi_{m_{1/2}}$ and β. As shown in figure 13.12, the first parameter, $\psi_{m_{1/2}}$, is the matric potential when the effective saturation is halfway between the maximum and residual saturations. As with ψ_1 in the Boltzmann distribution, changes in $\psi_{m_{1/2}}$ shift the Fermi distribution up or down. The second parameter β is related to the pore-size distribution. The smaller β is, the more uniform the pore sizes, and the moisture-characteristic curve becomes flatter in the middle section.

Most of the equations above do not result in linear differential equations when substituted into Richards' equation. These include the power equation of Brooks and Corey, as well as the equations of Su and Brooks, Van Genuchten, and Laliberte. The Boltzmann distribution results in an analytical solution to Richards' equation using the Kirchhoff transform of equations 13.4 and 13.5. The Fermi distribution can also be integrated using the Kirchhoff transform under many conditions that cover most practical cases (Way et al. 1985).

Bumb, Murphy, and Everett (1992) compare the Brooks–Corey, Boltzmann, and Fermi relations for moisture-characteristic data assembled by Rawls, Brakensiek, and Saxton 1982. Way et al. (1985) fit the Fermi distribution to data found in Brooks and Corey (1964) as well as Laliberte, Corey, and Brooks (1966). McKee and Bumb (1988) fit the Brooks and Corey relation, and Bumb et al. (1988) fit the Boltzmann distribution to data from Brooks and Corey (1964). Bumb, Murphy, and Everett (1992) used least-squares, relative least-squares, minimization of absolute error, and minimization of relative error curve-fitting techniques to match the Brooks–Corey, Boltzmann, and Fermi relations to data. For implementing the least-squares method (the most commonly used fitting technique), the Brooks–Corey, Boltzmann, and Fermi equations were rearranged to provide linear equations:

Brooks–Corey:

$$\frac{1}{\lambda} \ln S_e = \ln \psi_b - \ln \psi_m \tag{13.92}$$

Boltzmann distribution:

$$\beta \ln S_e = -\psi_m + \psi_1 \tag{13.93}$$

Fermi distribution:

$$\beta \ln \left[\frac{(1 - S_e)}{S_e} \right] = \psi_m - \psi_{m_{1/2}} \tag{13.94}$$

These equations are suitable for standard least-squares analysis and can be plotted on log–log or semi-log graph paper for visual analyses as well. Generally, a plot is produced for one or more of these methods and a final selection is made manually, to determine which of the methods results in the best visual fit to the data (Bumb, Murphy, and Everett 1992). Because the Brooks–Corey power relation results in no analytical solution, it is used only for comparison purposes. Bumb, Murphy, and Everett (1992) conclude that, in general, the Boltzmann distribution and the Brooks–Corey relation produced equally good fits to the data. The Fermi distribution, while providing excellent matches to data in several cases, did not achieve the high rate of success that the Brooks and Corey equation or the Boltzmann distribution attained (Bumb, Murphy, and Everett 1992).

Because equations 13.92 through 13.94 are linear in λ or ψ and S_e, the optimum values of the fit variables are obtained. Before least-squares curve-fitting techniques are utilized, saturation data has to be converted to effective saturation using equation 13.83. This can be done using volumetric water content θ or degree of saturation S, related to volumetric-water content by $S = \theta/\phi$, where ϕ is the porosity. Values of S_r and S_m are selected using, the extreme points of the capillary pressure versus saturation data, in most cases. In some cases, data for high values of ψ_m—where S is near S_r—were ignored because these data seemed to be unduly controlling the shape of the curve. It is believed that this does not represent a serious error, because most of the flow takes place at volumetric water contents somewhat removed from S_r. Figure 13.13 shows the linearized least-squares best-fit for equations 13.92 through 13.94 to data for a Touchet silt loam from Brooks and Corey (1964). Note that the fits are done using degree of saturation S rather than volumetric water content. In some cases, the values of S_r were increased (or decreased) slightly to force the curves to turn upward sooner than would have been the case otherwise; this is especially true for the Fermi-distribution fit. This is necessary for the distributions that are quite flat, to begin to show a gradual increase of ψ_m with decreasing saturation. By adjusting S_r, the curve is made to bisect this region of the data. Brooks and Corey (1964) and Corey (1977) also use an interpolative procedure to adjust the value of S_r so that the functional form fits the data well. For the Fermi

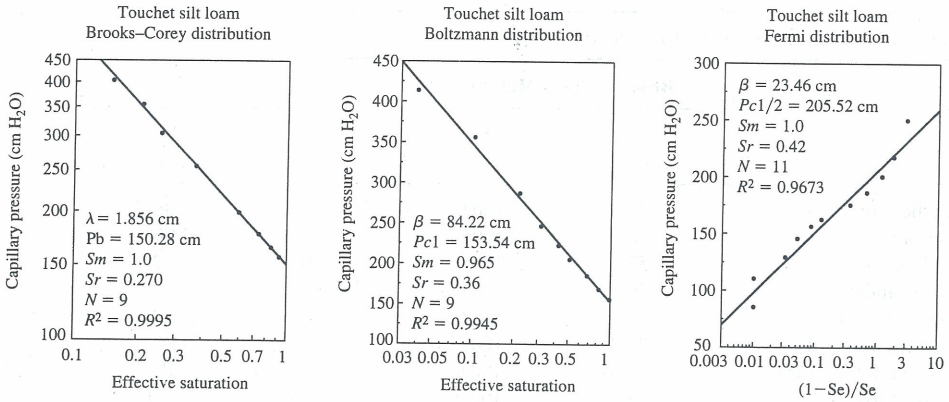

Figure 13.13 Linearized least-squares fit to various distributions to data from Brooks and Corey (1964). (Data converted to an equivalent water–air system using Brooks and Corey's equation 17)

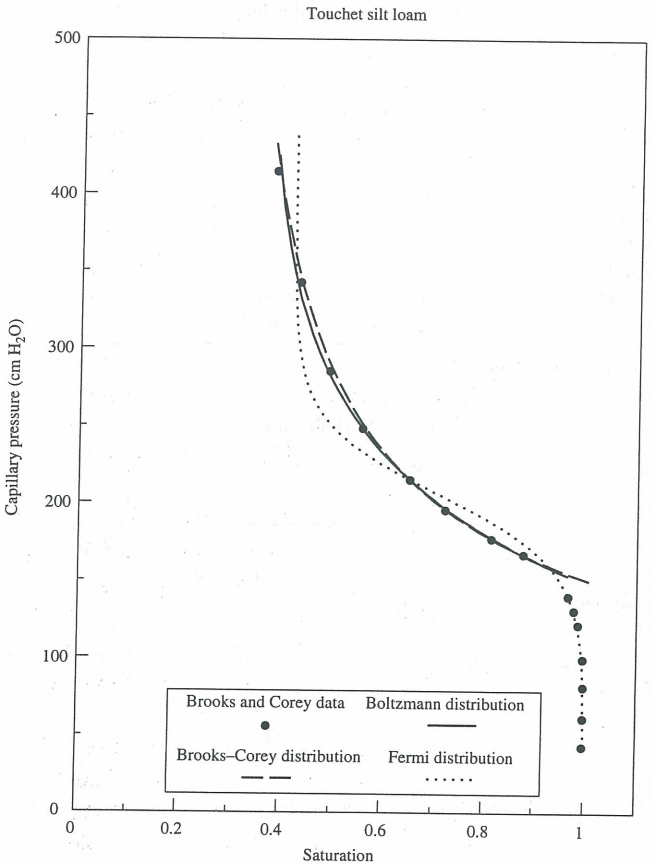

Figure 13.14 Brooks–Corey, Boltzmann, and Fermi distribution matches to capillary pressure versus saturation data for touchet silt loam

distribution, only the interior points ($S_r < S < S_m$) are used to obtain values of the variables $\psi_{m_{1/2}}$ and ψ, because the ln $(1 - S_e)/S_e$ is undefined at $S_e = 0$ and $S_e = 1$. Figure 13.14 shows the moisture-characteristic curve matches. Table 13.3 summarizes the variables of various soil types and textures, for fits by the Brooks–Corey relation, Boltzmann distribution, and Fermi distribution. Bumb, Murphy, and Everett (1992) present fitted variables for the Brooks–Corey relation as well as the Boltzmann and Fermi distributions to 12 soil-texture

TABLE 13.3 Fitted Variables[1] for Selected Media

Brooks–Corey Relation

Sample	S_r (%)	S_m (%)	ψ_b (cm)	λ (cm)
Touchet-silt loam	27.0	100.0	150.3	1.86
Fine sand	16.7	100.0	82.0	3.70
Hygiene sandstone	57.7	100.0	108.0	4.17
Berea sandstone	29.9	100.0	86.0	3.69
Volcanic sand	15.7	100.0	32.0	2.29
Fragmented sandstone	30.0	100.0	20.6	1.92
Fragmented mixture	27.6	100.0	34.4	2.89
Glass beads	8.5	100.0	58.0	7.30

Source: Data from Brooks and Corey (1964)

Boltzmann Distribution

Sample	S_r (%)	S_m (%)	ψ_1 (cm)	β (cm)
Touchet-silt loam	36.0	96.5	153.5	84.2
Fine sand	17.4	94.5	75.0	33.7
Hygiene sandstone	58.0	97.5	107.2	33.2
Berea sandstone	31.0	96.0	86.1	27.9
Volcanic sand	15.5	98.0	31.0	22.2
Fragmented sandstone	33.0	97.0	16.9	17.3
Fragmented mixture	30.0	96.0	33.2	14.9
Glass beads	9.5	97.0	57.1	9.2

Source: Data from McKee and Bumb (1988)

Fermi Distribution

Sample	S_r (%)	S_m (%)	$\psi_{m_{1/2}}$ (cm)	β (cm)
Touchet-silt loam	42.0	100.0	205.5	23.5
Fine sand	19.0	99.5	104.4	14.8
Hygiene sandstone	62.0	100.0	129.5	10.2
Berea sandstone	32.0	100.0	107.5	10.4
Volcanic sand	16.0	100.0	47.0	5.19
Fragmented sandstone	33.0	100.0	34.2	6.39
Fragmented mixture	32.0	99.0	48.7	6.06
Glass beads	9.7	100.0	65.2	6.85

Source: Data from Way et al. (1985)

[1]Converted to an equivalent water–air system using Equation 17 of Brooks and Corey (1964)

types obtained from Rawls, Brakensiek, and Saxton (1982) for 1,323 soils from about 5,380 horizons in 32 states of the United States.

Three-dimensional analytical solution Bumb et al. (1988) and McKee and Bumb (1988) propose a three-dimensional analytical solution to Richards' equation. McKee and Bumb (1988) detail both an exact steady-state solution as well as an approximate time-dependent solution. Steady-state solutions for constant-rate infiltration from a point source is presented by Philip (1969), Raats (1972), and Lomen and Warrick (1978). All of these solutions assume that the unsaturated hydraulic conductivity K decreases as an exponential function of the matric potential ψ, or as a power function of the effective saturation S_e. The

resulting solution to Richard's equation becomes linear in the matric-flux potential H. This was shown in section 13.2 by equation 13.8, for the exponential case, and equation 13.12 for the power-equation case. Additionally, McKee and Bumb (1988) show that if a Boltzmann distribution is fit to the moisture-characteristic curve data, a linear relation for matrix flux potential results, of the form of equation 13.12.

For the three-dimensional LaPlace equation with z taken as positive downward, McKee and Bumb (1988) write the equation for matric flux potential for an isotropic medium:

$$\frac{\partial^2 H}{\partial x^2} + \frac{\partial^2 H}{\partial y^2} + \frac{\partial^2 H}{\partial z^2} - \alpha \frac{\partial H}{\partial z} = \frac{1}{D} \frac{\partial H}{\partial t} \tag{13.95}$$

where H is the matric flux potential defined by equation 13.12 for a Boltzmann-distribution fit to the moisture-characteristic curve data as $(\beta/n)K$, with K being the unsaturated hydraulic conductivity in the x, y, and z directions. The constant α is defined as n/β, and is the same α defined by López-Bakovic and Nieber (1989) in Section 13.2. D is defined as the diffusivity and is (McKee and Bumb, 1988)

$$D = \frac{\beta K_s}{(\theta_m - \theta_r)} S_e^{n-1} \tag{13.96}$$

Equation 13.96 is still nonlinear in D for all $n \neq 1$. However, for $n = 1$, D simplifies to

$$D = \frac{\beta K_s}{(\theta_m - \theta_r)} \tag{13.97}$$

If we assume that the anisotropy is in the x and y directions, and that each z-layer is isotropic over its thickness, then transformations are needed for changing the results from an isotropic to an anisotropic system. The change involves scaling the x, y, and z axes using the following transformations

$$x^* = x\left[\frac{K_y}{K_x}\right]^{1/4} \tag{13.98}$$

$$y^* = y\left[\frac{K_x}{K_y}\right]^{1/4} \tag{13.99}$$

$$z^* = z\frac{[K_x K_y]^{1/4}}{[K_z]^{1/2}} \tag{13.100}$$

and

$$\alpha^* = \frac{n}{\beta}\frac{[K_z]^{1/2}}{[K_x K_y]^{1/4}} \tag{13.101}$$

where x, y, z are the untransformed coordinates, and x^*, y^*, z^* are the actual coordinates of the anisotropic media, and coincide with the principal axes of the hydraulic-conductivity tensor.

The *time-dependent solution* to equation 13.95 is available only for the value of $n = 1$, and is analogous to the problem of heat flow from a point source of constant strength moving through a uniform, infinite medium (McKee and Bumb 1988). The solution for a source at the origin of a Cartesian-coordinate system is (Carslaw and Jaeger 1959)

$$\Delta H = H - H_0 = \frac{Q}{8\pi\sqrt{\pi D}} \int_0^t \frac{\exp\left\{-\dfrac{[z/\alpha D(t-t')]^2 + x^2 + y^2}{4D(t-t')}\right\}}{(t-t')^{3/2}} dt' \tag{13.102}$$

where H_0 is the value of H at the initial saturation, and ΔH is the change in H. If the initial saturation is near residual saturation, then H_0 is small compared to H, and ΔH can be approximated by H. Evaluating the integral for a constant-strength point-source infiltration rate Q located at coordinates x', y', and z' in an infinite soil gives (McKee and Bumb 1988)

$$H - H_0 = \frac{Qe^{\alpha(z-z')/2}}{8\pi R}\left(e^{\alpha R/2}\,\mathrm{erfc}\left[\frac{R}{2\sqrt{Dt}} + \frac{\alpha\sqrt{Dt}}{2}\right] + e^{-\alpha R/2}\,\mathrm{erfc}\left[\frac{R}{2\sqrt{Dt}} - \frac{\alpha\sqrt{Dt}}{2}\right]\right) \tag{13.103}$$

where $R = \sqrt{(x-x')^2 + (y-y')^2 + (z-z')^2}$ and x, y, and z are coordinates of any point in space.

The above solution is for a point source only. An areal source—such as leakage from a pond or land treatment facility—is obtained by superposition of a large number of points. This superposition is used to sum any number of solutions of the form of equation 13.103, because the solution is linear when $n = 1$ or in the steady-state case presented following. The effective saturation as a function of space and time is obtained after calculation of the matric flux potential H, by using the inverse transform from equations 13.9, 13.10, and 13.12 to obtain

$$S_e = \left(\frac{nH}{\beta K_s}\right)^{1/n} \tag{13.104}$$

The nonlinearity in equation 13.95 occurs only in the diffusivity D because of the S_e term. McKee and Bumb (1988) suggest that a conservative estimate of the time-dependent solution is possible for $n \neq 1$ by substituting a value of 1 for S_e in equation 13.96, but by doing so, both D and spreading of the moisture are overestimated. McKee and Bumb (1988) point out that for large times, the time-dependent solution is the same as the steady-state solution, indicating some confidence in this approximation.

The *steady-state solution* does not depend on diffusivity, because the right-hand side of equation 13.95 is zero. Therefore, equation 13.95 is linear for all values of n at steady-state. The boundary and initial conditions for the solution of equation 13.95 are obtained by recognizing that: **(1)** the soil is initially assumed to be at a constant volumetric-water content; **(2)** at a large distance from the point source, the soil is unaffected; and **(3)** the point source is of constant strength. Carslaw and Jaeger (1959) and Philip (1969) presented a steady-state solution in an infinite soil, with a point source Q located at x', y', and z' as

$$\begin{aligned}\Delta H_\infty = H_\infty - H_0 &= \Delta H_\infty[r, (z-z')] \\ &= \frac{Q}{4\pi\sqrt{r^2 + (z-z')^2}} \exp\left\{\frac{\alpha}{2}\left[(z-z') - \sqrt{r^2 + (z-z')^2}\right]\right\}\end{aligned} \tag{13.105}$$

where $r = \sqrt{(x-x')^2 + (y-y')^2}$. The subscript ∞ indicates that the solution is for a column of soil of infinite x, y, and z.

The previous time-dependent and steady-state solutions were for an infinite depth and areal extent of unsaturated soil. Raats (1972) gives a solution for the steady-state case when no flow is allowed through the soil surface. This upper boundary is common under a lined pond, where the lining forms an impermeable boundary. In general, solutions for impermeable boundaries can be developed using superposition techniques, by imposing image sources across the impermeable boundary and then superimposing the solutions to obtain the solution with the boundary. In this analysis, only one image is used for impermeable boundaries, and therefore, the solutions are approximate but adequate for most practical problems.

Raats' (1972) solution for an impermeable boundary at a distance d above the source (see figure 13.15) is given by

$$\Delta H = \Delta H_\infty[r, z - d] + e^{-\alpha d}\Delta H_\infty[r, z + d] - \frac{Q\alpha}{4\pi} e^{\alpha d} E_i\left[\frac{\alpha}{2}\left(z + d + \sqrt{r^2 + (z + d)^2}\right)\right] \tag{13.106}$$

where E_i is the exponential integral function; the exponential integral function is closely approximated by the series expansion given in appendix 3. Equation 13.106 is the superposition of an image source a distance d above the impermeable boundary, where the notation $\Delta H_\infty[r, z - d]$ and $\Delta H_\infty[r, z + d]$ are for the infinite cases defined by equation 13.105. In this case the value of z' is replaced by d. Equation 13.106 is applicable to any impermeable boundary a distance d above the point source, as shown in figure 13.15 (McKee and Bumb 1988).

For a horizontal impermeable boundary a distance $z = a$ beneath the surface and also the real source (see figure 13.16), McKee and Bumb (1988) show that the no-flux condition is represented by

$$q = -K\frac{\partial}{\partial z}\left(\psi_m + \frac{g \cdot \hat{e}_z z}{|g|}\right) = 0, \quad \text{at } z = a \tag{13.107}$$

where q is the flux, g is the acceleration due to gravity and $\hat{e}_z$ is the unit vector in the positive z direction (downward). This condition, represented in terms of matric flux potential H is

$$q = \left.\frac{\partial H}{\partial z}\right|_{z=a} - \left.\frac{g \cdot \hat{e}_z}{|g|} K\right|_{z=a} = 0 \tag{13.108}$$

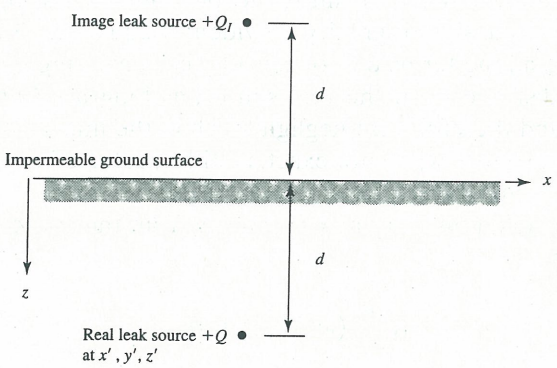

Figure 13.15 Schematic of real and image sources used to model an impermeable surface above the real source

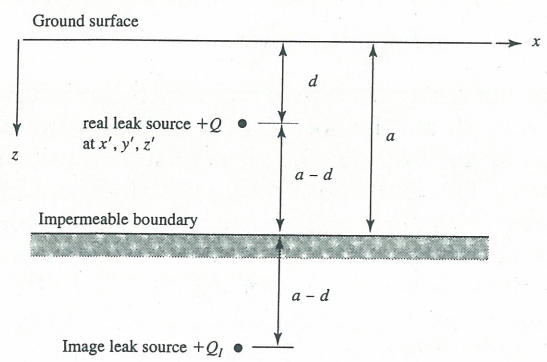

Figure 13.16 Schematic of real and image sources used to model a horizontal impermeable boundary beneath the real source

The theory of images, shown schematically in figures 13.15 and 13.16, has been used extensively in hydrology to model impermeable and constant-head boundaries, and has also been used in heat flow in solids by Carslaw and Jaeger (1959). For these applications, H represents the potential, and the no-flow boundary condition is given by $\nabla \cdot H = 0$ at the boundary. In that case, the exact method of images results in $H = H_R + H_I$, where H_R is the solution for the real source and H_I is the solution for the image source. In the saturated case ($\alpha = 0$), the real and image solutions have the same mathematical form but for unsaturated flow, the presence of gravity causes an asymmetry between them. McKee and Bumb (1988) present a modified method of images with the same form as the classical method, or

$$\Delta H = \Delta H_R + \Delta H_I^h \tag{13.109}$$

In equation 13.109, ΔH_R is the solution for a real point source at x', y', z' in an infinite porous medium, which may either time-dependent (equation 13.103) or steady-state (equation 13.105), and ΔH_I^h is the solution for an image point source for a horizontal impermeable boundary at $x', y', 2a - z'$ in an infinite porous medium with the gravitational force acting upward, or for the time-dependent solution

$$H_I^h - H_0 =$$

$$\frac{Qe^{\alpha(z-2a+z')/2}}{8\pi R_I}\left(e^{\alpha R_I/2}\operatorname{erfc}\left[\frac{R_I}{2\sqrt{Dt}} + \frac{\alpha\sqrt{Dt}}{2}\right] + e^{-\alpha R_I/2}\operatorname{erfc}\left[\frac{R_I}{2\sqrt{Dt}} + \frac{\alpha\sqrt{Dt}}{2}\right]\right) \tag{13.110}$$

where $R_I = \sqrt{(x - x')^2 + (y - y')^2 + (z - 2a + z')^2}$.

The steady-state image solution is obtained by changing the sign of $z - z'$ in equation 13.105 and replacing R with R_I. In this case, the real solution H_R is downward (gravity pulling water downward), whereas the image solution H_I^h is upward (the direction of gravity is reversed). However, the total net flux at the impermeable boundary is approximately zero. The error caused by reversing the sign of gravity is evident if equation 13.109 is substituted into equation 13.95, because all the terms do not cancel. The remaining terms are shown to vanish exponentially with distance from the real source, as long as R and z are positive (McKee and Bumb 1988), and therefore are negligible. Thus, the image solution for a horizontal boundary beneath the source, while not exact, is still a preferred approximation to an otherwise very complex problem.

For a vertical impermeable boundary at $x = b$ away from the source, as shown in figure 13.17, the flux is given by

$$q = -K\frac{\partial}{\partial x}(\psi_m + z) = 0 \tag{13.111}$$

or equivalently by $\nabla \cdot H = 0$. This is easily satisfied (with no change in the sign of gravity) by

$$\Delta H = \Delta H_R + \Delta H_I^v \tag{13.112}$$

where ΔH_R is the solution for the real point source and ΔH_I^v is the solution for the image-point source located at $2b - x', y', z'$. The solution for ΔH_I^v is obtained by substituting $2b - x'$ for x' in the equations for the time-dependent or steady-state cases.

To demonstrate the use of the above equations, a steady-state leak of 500 liters of water per day into a homogeneous and isotropic Touchet silt loam is modeled using equations 13.104 and 13.105. In this example, the leak is located 5 m below ground surface. The Touchet silt loam soil has the properties shown in table 13.1 for the Boltzmann distribution. In addition, the soil has a saturated hydraulic conductivity of 0.35 m/day, a porosity of 50.1 percent, a maximum saturation of 96.5 percent, and an irreducible saturation of 36.0 percent.

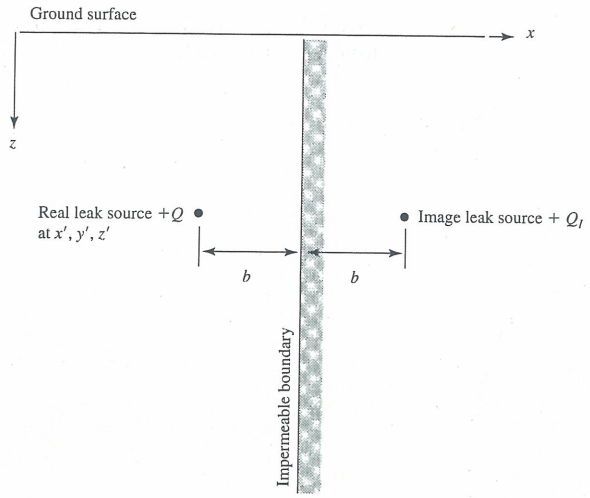

Figure 13.17 Schematic of real and image sources used to model a vertical impermeable boundary

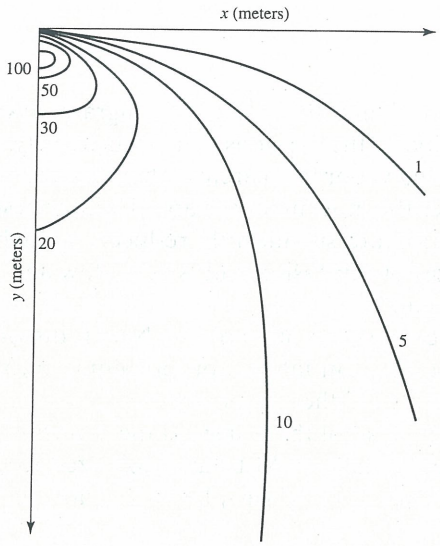

Figure 13.18 Steady-state effective water saturations (S_e=%) from a point-source leak into a Touchet silt loam

The solution is to find the steady-state water-content distribution as a result of the point-source leak.

The steady-state effective saturations S_e and actual saturations S are shown in figures 13.18 and 13.19, respectively. The highest saturations are directly below the leak, with measurable saturations spreading away from the leak laterally, a distance of over 20 m. Such an analysis is used to assess the locations of monitoring devices or to assess the relative location of conservative contaminants.

Three-dimensional semianalytical solution for vapor diffusion from an initial contaminant distribution in the vadose zone During the early stages of liquid-phase releases to the subsurface, liquid advection occurs. The above section presented an analytical solution for the advective transport of this liquid downward under gravity for a point source. This solution can also be extended to a plane source by using superposition. If the liquid phase can volatilize—such as is the case with most non-aqueous phase liquids (NAPLs)—downward migration of the gaseous-phase continues by gravity-driven density gradients, if the vapor

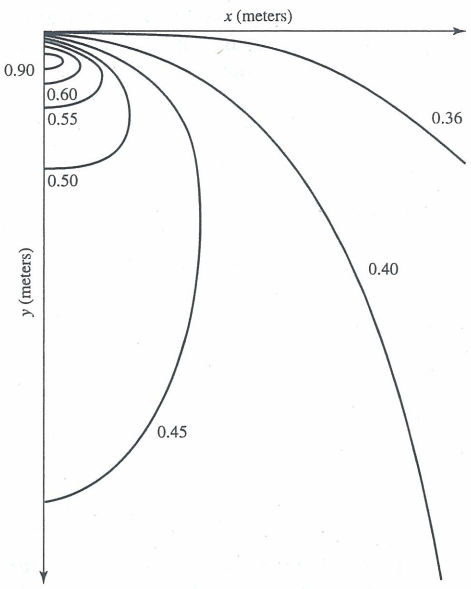

Figure 13.19 Steady-state actual saturations (S= decimal) from a point-source leak into a Touchet silt loam

density is heavier than air. If the vapor is lighter than air, it will migrate upward. This process is highly dependent on the concentration of the vapor as well as its density.

Gaseous diffusion occurs by moving vapor from areas of high concentration to areas of low concentration. This process involves the movement of vapor by intermolecular collisions. Gaseous diffusion and gaseous advection are significantly reduced by high soil-water content. Aqueous diffusion is similar to gaseous diffusion, but is very slow and is assumed to be negligible, compared to gaseous diffusion.

Aqueous advection is the passive transport of a volatile NAPL dissolved in the aqueous phase. Aqueous fluxes typically occur from infiltration of rainfall into the unsaturated zone; this transport mechanism dominates if the fluxes are high. Volatile NAPLs migrate through the unsaturated zone by one or more of the transport mechanisms described above, until the capillary fringe is encountered. Volatile NAPLs are mobilized to the ground water from the capillary fringe by advection, aqueous- and gas-phase diffusion, or flucuations in the water table.

The governing equation for transport of a single NAPL in the unsaturated zone is (LLNL 1990)

$$\begin{aligned}\frac{\partial}{\partial t}(\phi S_l C_l + \phi S_g C_g + C_s) = &-\nabla \cdot |C_g q_g| - \nabla \cdot |C_l q_l| \\ &+\nabla \cdot |\rho_g \phi S_g \tau_g D_g \nabla(C_g/\rho_g)| \\ &+\nabla \cdot |\rho_l \phi S_l \tau_l D_l \nabla(C_l/\rho_l)| \\ &-\lambda_l \phi S_l C_l - \lambda_g \phi S_g C_g \\ &-\lambda_g \phi \rho_B K_d C_l + q_{src}\end{aligned} \tag{13.113}$$

where t is time; C is volatile NAPL concentration (mass/volume); ϕ is effective porosity; S is saturation; l is the subscript for the aqueous phase; g is the subscript for the gaseous phase; s is the subscript for sorption onto the solid phase; src is the subscript for a source term; τ is a tortuosity factor; ρ_b is bulk density; D is the diffusion coefficient of the NAPL; λ is the decay constant for NAPL degradation; q is mass flux; ρ is density; $\nabla\cdot$ is the divergence operator, and ∇ is the gradient operator.

The three terms in parentheses on the left-hand side of equation 13.113 are the changes in accumulated mass of volatile NAPL in the aqueous, gaseous, and liquid phases, respectively. The first two terms in brackets on the right-hand side are the advective fluxes in the gaseous and aqueous phases; the next two terms in brackets are the diffusive fluxes in the gaseous and aqueous phases; the next three terms are the chemical or biological degradation in the three phases; and the last term is the source term.

In the absence of free product, liquid advection is nonexistent and the total concentration of contaminant is given by the total-concentration equation, which represents partitioning among the solid, aqueous (pore water), and gaseous phases in the soil. This total contaminant concentration C_T is $C_s + C_l + C_g$, where C_s is the concentration of the solids, C_l is the concentration of the liquid, and C_g is the concentration of the gas for a given contaminant. Equilibrium partitioning between the solid and aqueous phases is described by a linear isotherm given by

$$C_s = \rho_b K_d C_l \tag{13.114}$$

where ρ_b is the soil bulk density, and K_d is the partitioning coefficient between the aqueous phase and solid phase. Henry's law is used to partition between the gaseous phase and the aqueous phase for a contaminant, or

$$C_g = K_H C_l \tag{13.115}$$

where K_H is Henry's law constant for an individual contaminant.

Gaseous diffusion occurs by the movement of vapors from areas of high concentration to areas of low concentration in the vadose zone, due to intermolecular collisions. Both gaseous advection and gaseous diffusion are significantly reduced by increases in water content in the vadose zone. If the relative humidity of the vadose zone is high, then vapor-to-solid sorption is assumed to be negligible. Laboratory studies (LLNL 1990) indicate that soils with less than 90 percent relative humidity have a very high sorptive capacity due to the direct sorption of the vapor into the soil phase. Under these conditions, the upper layers of the soil retard vapor flux diffusing to the surface.

The boundary of the ground surface often acts as a sink to gaseous diffusion, because the concentration at the surface is often approximately zero due to dispersion into the atmosphere by wind currents. An exception occurs when sufficient vegetative cover creates a stagnant boundary layer, resulting in a buffer zone between the air in motion above the surface and the upper boundary of the vadose zone (Jury 1986); transport across this zone is primarily by diffusion. If the surface is paved, an additional buffer zone exists that has a diffusion coefficient specific to the paving material. If the paving material is completely impervious, a no-flow boundary applies instead of the diffusion sink.

When gaseous- or aqueous-flow velocities are low (such as in the vadose zone), diffusion is the important contributor to dispersion and transport, and the dispersion equals the diffusion coefficient ($D_L = D^*$). The decision, as to the relative significance of aqueous advection or gaseous diffusion in the vadose zone, can be made using the Peclet number which provides a quantitative estimate of the dominant mode of transport. The Peclet number $\mathcal{P}$ is given as (Freeze and Cherry 1979)

$$\mathcal{P} = \frac{vL}{D^*} \tag{13.116}$$

where v is the linear velocity of water percolating through the vadose zone, L is the characteristic length (or distance traveled) of the aqueous front, and D^* is the apparent diffusion coefficient for the gaseous contaminant. The linear velocity v, is determined by dividing the recharge rate by the product of effective porosity and the degree of saturation S_l of the soil

of interest. For a recharge rate q of water percolating through the vadose zone, the advective mass flux, q_a, is given by

$$q_a = \frac{C_g q}{K_H R} \tag{13.117}$$

where R is defined as the unsaturated retardation coefficient, given by

$$R = S_l + S_g K_H + \frac{\rho_b K_d}{\phi} \tag{13.118}$$

where S_l and S_g, respectively, are the degree of saturation of water and air in the soil ($S_l + S_g = 1$); ρ_b is the bulk density of the soil; K_H is Henry's law constant; K_d is the partitioning coefficient between the aqueous and solid phases; and ϕ is the porosity of the soil. The apparent gaseous-diffusion coefficient is given by

$$D^* = \frac{S_g \phi \tau D_g}{R} \tag{13.119}$$

where D_g is the actual gaseous-diffusion coefficient for the contaminant of interest, and τ is the tortuosity factor to account for reduced cross-sectional areas and increased path length in the soil for the gaseous transport around the water-filled pores (see chapter 7). The tortuosity is determined empirically by Millington and Quirk (1961) as

$$\tau = S_g^{7/3} \phi^{1/3} \tag{13.120}$$

The Peclet number provides a quantitative estimate of the relative importance of aqueous advection (compared to gaseous diffusion) as the dominant mode to transport, and is given by

$$\mathcal{P} = \frac{qL}{S_g \phi \tau D_g K_H} \tag{13.121}$$

Peclet numbers must be greater than 10 for advection to become important (Dragun 1988) and for Peclet numbers less than 1, chemical exchange is completely independent of flow velocities. Peclet numbers between 1 and 10 indicate that chemical exchange is essentially diffusion controlled. For most unsaturated soil, chemical exchange should be diffusion controlled (Dragun 1988). Additionally, if the diffusion rate of one contaminant is known, the diffusion rate D of a structurally similar chemical is estimated using Graham's law of diffusion (Dragun 1988)

$$\frac{D_1}{D_2} = \left(\frac{\rho_2}{\rho_1}\right)^{0.5} = \left(\frac{M_2}{M_1}\right)^{0.5} \tag{13.122}$$

where ρ is the density and M is the molecular weight of the contaminants of interest.

The characteristic length L is the distance the aqueous front moves through the vadose zone during a recharge event, and is equal to

$$L = \frac{q\,\Delta T}{\phi R} \tag{13.123}$$

It is likely that temporal variations in volumetric and mass flux in the vadose zone are highly attenuated by the time infiltrating water reaches a depth where contaminants are located, and an almost constant flux exists down to the water table. In this case, the characteristic length becomes the distance from the center of the contaminant plume down to the water

table. Therefore, the Peclet number is calculated based on the average annual recharge rate and the distance to the water table. While this Peclet number may be larger than that calculated using equations 13.121 and 13.123, it still results in a Peclet number less than 10.

Another way to compare advective versus diffusive transport modes is to note the movement of aqueous fronts based on average annual water balances, including both precipitation and evapotranspiration. Often in arid and semiarid environments, this movement is only a few centimeters per year. This should be compared to the order-of-magnitude movement of the diffusive-contaminant front computed by

$$L = \sqrt{(S_g \tau D_g K_H) \times 1 \text{ year}/R} \tag{13.124}$$

which gives a distance greater than the aqueous-front movement.

The Peclet number can also be used to assess the relative importance of gaseous advection through density gradients, compared to gaseous diffusion. If a vapor is denser than air, it sinks toward the ground water in the gaseous phase; otherwise it rises to the ground surface. For example, consider a denser-than-air vapor. The density gradients in the gaseous phase that drive the vapor toward the ground water are significant during the early and intermediate stages of the release, because of elevated concentrations. However, in time the concentrations in the vadose zone are diluted by gaseous diffusion, and the transport of the contaminant by gravity-driven density gradients is unimportant compared to gaseous diffusion (Falta et al. 1989).

Falta et al. (1989) use an approximate expression for the maximum, nonretarded-Darcian flux q_g under vapor-density gradients as

$$q_g = K_g \frac{M_g - M_a}{M_g}\left(\frac{C_g}{\rho_g}\right) \tag{13.125}$$

where K_g is the vapor conductivity, M_g is the molecular weight of the vapor, M_a is the molecular weight of air, and C_g is the vapor concentration (mass/volume). This approximation is accurate to within ±20 percent (LLNL 1990). The Peclet number for the gaseous case is now given by

$$\mathcal{P} = \frac{q_g L}{S_g \phi \tau D_g} \tag{13.126}$$

The maximum Peclet number occurs at the maximum concentration of the vapor. Again, if the Peclet number is less than 10, then gaseous diffusion is assumed to be the dominant mode of transport.

To solve for transport in the vadose zone under gaseous diffusion, LLNL (1990) proposes a semi-analytical solution of the diffusion equation with the initial mass distribution approximated by a three-dimensional, radially symmetric Gaussian function. If there is no degradation, the soil concentrations C_s satisfy the diffusion equation given by

$$D^*\left(\frac{\partial^2 C_s}{\partial x^2} + \frac{\partial^2 C_s}{\partial y^2} + \frac{\partial^2 C_s}{\partial z^2}\right) = \frac{\partial C_s}{\partial t} \tag{13.127}$$

where D^* is the apparent gaseous-diffusion coefficient given by equation 13.119. C_s is used because the primary process is gaseous diffusion from the soil. LLNL (1990) assumed radial symmetry so that the concentration distribution was a function in cylindrical coordinates, r and z, as well as a function of time. The initial soil-contaminant distribution was approximately equal to the product of Gaussian functions in the vertical z, and horizontal r, directions as shown schematically in figure 13.20. The equation for the initial distribution is

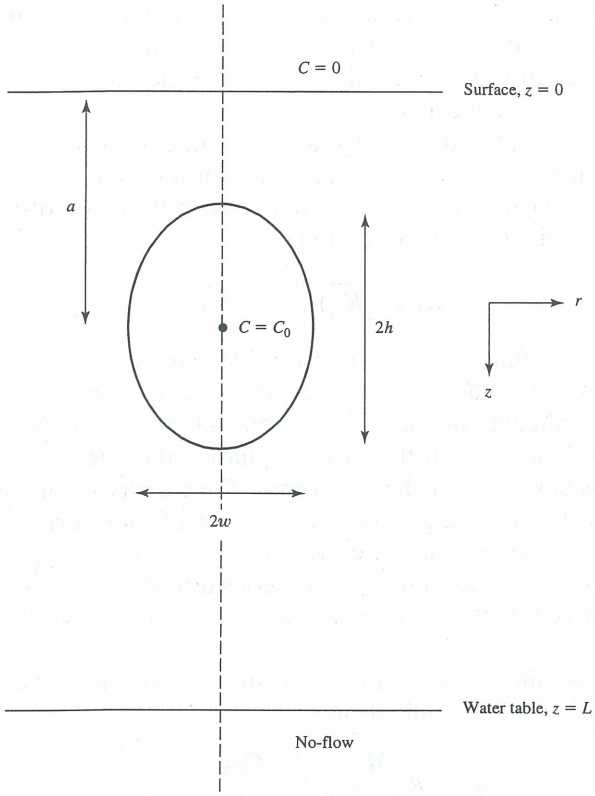

Figure 13.20 Initial gaseous-diffusion contaminant distribution variables

given as

$$C_s(r, z, t = 0) = C_0 \exp\left(-\frac{(z - a)^2}{2h^2}\right) \exp\left(-\frac{r^2}{2w^2}\right) \tag{13.128}$$

where h is the standard deviation half-width of the initial release in the vertical direction, w is the half width in the horizontal direction, and a is the distance from the center of the contaminant mass from the ground surface (figure 13.20). The constant C_0 represents the peak soil concentration at the center of the contaminant distribution.

The boundary condition at the ground surface is zero concentration while the top of the ground water can be approximated as a no-flow boundary. Therefore,

$$C_s(r, z = 0, t) = 0 \tag{13.129}$$

and

$$\frac{\partial C_s(r, z = L, t)}{\partial z} = 0 \tag{13.130}$$

are applied to the top ($z = 0$) and bottom ($z = L$) of the vadose zone. By making the variable substitution $z = z/L$, $r = r/L$, and $t = t/\sqrt{L^2/D^*}$, the diffusion equation 13.127, becomes

$$\frac{\partial^2 C_s}{\partial x^2} + \frac{\partial^2 C_s}{\partial y^2} + \frac{\partial^2 C_s}{\partial z^2} = \frac{\partial C_s}{\partial t} \tag{13.131}$$

Substituting $C_s(r, z, t) = R(r, t)Z(z, t)$ gives

$$\frac{1}{r}\frac{\partial R}{\partial r} + \frac{\partial^2 R}{\partial r^2} = \frac{\partial R}{\partial t} \tag{13.132}$$

and

$$\frac{\partial^2 Z}{\partial z^2} = \frac{\partial Z}{\partial t} \tag{13.133}$$

Solutions that are Gaussian at time zero are given by

$$R(r, t) = \frac{1}{t + \frac{w^2}{2}} \exp -\left\{\frac{r^2}{4\left(t + \frac{w^2}{2}\right)}\right\} \tag{13.134}$$

and

$$Z(r, t) = \frac{1}{\sqrt{t + \frac{h^2}{2}}} \exp -\left\{\frac{z^2}{4\left(t + \frac{h^2}{2}\right)}\right\} \tag{13.135}$$

To satisfy the boundary conditions, periodic image solutions are superimposed to obtain the final solution of

$$C_s(r, z, t) = R(r, t) \sum_{n=-\infty}^{\infty} \{(-1)^n Z(z - [2n + a], t) + (-1)^{n+1} Z(z - [2n - a], t\} \tag{13.136}$$

This solution is adjusted to give the correct peak concentration at the center of the release, by using a multiplication factor. Because of the superposition, the variables a, h, and w do not correspond exactly to their definitions (as above), and need to be readjusted to match the shape of the initial distribution. For all practical purposes, the solution using equation 13.136 is approximated by using only one image for the soil surface and one image for the no-flow boundary at the water table.

The solution given by equation 13.136 is applicable when there is no degradation. Therefore, the solution obtained using equation 13.136 must be multiplied by the appropriate exponential time-decay factor, to provide the solution for first-order contaminant decay. The first-order decay factor λ is given by

$$\lambda = 2^{(-t/T)} \tag{13.137}$$

where t is time and T is the decay half-life of the contaminant of interest. Equation 13.136 is multiplied by the factor λ to obtain a solution when there is degradation. Table 13.4 presents values for relative vapor density, Henry's constant K_H, molecular weight M, degradation half-life T, and vapor-diffusion coefficient for selected constituents.

An example of the use of the above vapor-diffusion equations is given for trichloroethylene (TCE) contamination at a site. The original concentrations of TCE are observed by laboratory testing of soil-vapor samples. Both the age and amount of the TCE releases are unknown; however, the maximum measured soil TCE concentration is far below the free-phase concentration. Free-phase advection is terminated well above the water table, and the highest DNAPL concentrations are at approximately 6.1 m below ground surface. Equation 13.128 is used by trial and error to estimate the values of w and h, by assuming that the initial TCE concentration that occurred at a depth of 6.10 m below ground surface was 6,000 ppb.

TABLE 13.4 Properties for Selected Constituents

Constituent	Relative vapor density* (g/m^3)	Henry's law constant ($atm\text{-}m^3/mole$)	Molecular weight (g/mole)	Degradation half-life (yrs)	Vapor diffusion coefficient (cm^2/sec)
Acetone	1.30	3.7E–05	58.08	0.06	—
Ammonia	0.79	—	17.03	—	0.28†
Benzene	1.21	0.0054	78.12	0.19–0.30	0.088†
Carbon Tetrachloride	1.51	0.023	153.8	0.5–1.0	0.080†
Chlorobenzene	1.05	0.0036	112.6	0.10	0.075‡
Chloroform	1.62	0.0028	119.4	0.27	0.099†
Chlorine	—	—	70.91	—	—
Gasoline	1.10	—	114.2	—	0.060†
n-Hexane	1.31	1.85	86.18	—	0.084†
Isopropyl Alcohol	1.06	0.0000081	60.09	0.01	0.137‡
Mercury	—	—	200.6	—	—
Nitrobenzene	1.00	0.000024	123.1	0.03–0.53	0.072‡
Methylene Chloride	2.10	0.0027	84.94	0.02–0.08	0.102‡
Phenol	1.00	0.00000040	94.11	0.25	0.085†
Tetrachloroethylene (PCE)	1.09	0.0149	165.8	0.82	0.078†
Toluene	1.08	0.0059	92.15	0.10	0.049†
Trichloroethylene (TCE)	1.27	0.0103	131.5	0.82	0.081†
Xylene	1.02	0.0051	106.2	0.088	0.071†
Air	1.00	—	29.0	—	—
Water	0.99	0.000001	18.01	—	0.256†

Note: Additional selected data on DNAPLs can be found in Cohen, Mercer, and Matthews 1993
* Relative to dry air at 20°C and 760 mm Hg
† At 25°C
‡ At 30°C

The final initial-Gaussian TCE distribution is shown in figure 13.21. The half-width of the Gaussian distribution in the horizontal direction is $w = 6.31$, and in the vertical direction is $h = 4.11$ (see figure 13.21). These values are obtained from the field data as follows: **(1)** the variable a is chosen so that the peak of the Gaussian distribution (actually the sum of Gaussian distributions chosen to satisfy the boundary conditions) matched the peak concentration of the measured field distribution; **(2)** the variable h is adjusted until the depth of the 1-ppm concentration closest to the water table matched the field data; and **(3)** the variable w is adjusted to match the volume of the region estimated to exceed 1 ppm in concentration.

Equation 13.136 was solved for TCE migration into the future at 50 and 100 years as shown in figures 13.22 and 13.23, respectively, and the peak concentration is adjusted at the center of the release by using a multiplication factor determined by solving equation 13.136 for $t = 0$ years. First-order decay is used (equation 13.137) with the half-life of TCE assumed to be 50 years for this particular case, even though table 13.4 shows a half-life of 0.82 years. Other parameter values used: bulk dry density $\rho_b = 1.8$ g/cm^3; effective porosity $\phi = 0.30$; solid sorption, $\rho_b K_d/\phi = 5.0$; Henry's law constant $K_H = 0.39$; and liquid saturation of the soil $S_l = 0.50$.

Other analytical models Other fate and transport analytical solutions are often used to assess cleanup levels in the unsaturated zone, in order to minimize exposure to the underlying ground water or overlying air. Because these models rely on the quantification of relations between specific variables to simulate the effects of natural processes, a close match between the natural processes and those of the selected models has to exist if the modeling

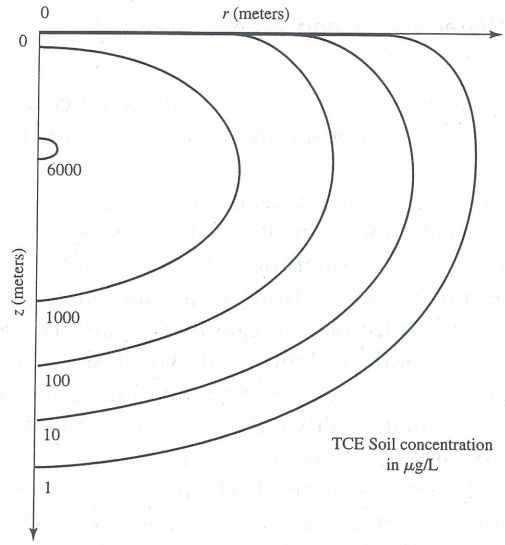

Figure 13.21 Cross-section showing initial TCE soil concentration

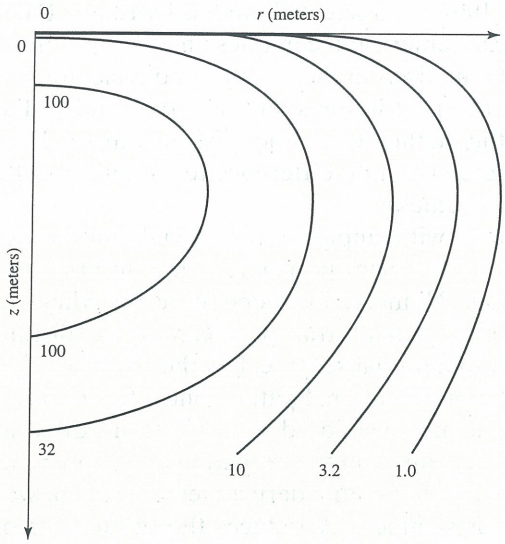

Figure 13.22 Cross-section of predicted TCE soil concentration at the end of fifty years

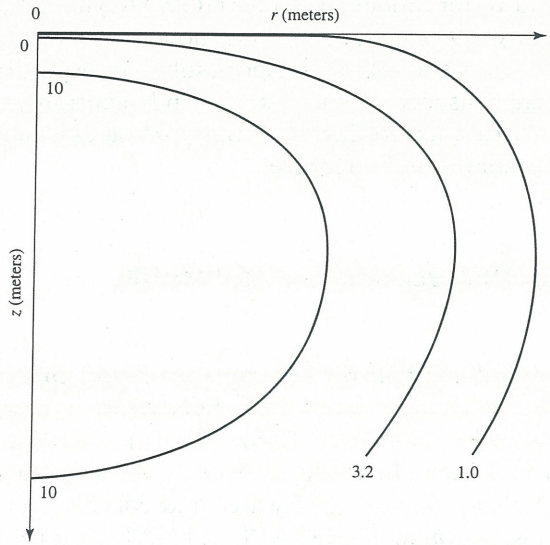

Figure 13.23 Cross-section of predicted TCE soil concentration at the end of hundred years

is to provide satisfactory results. For example, a model that does not consider attenuation of chemicals in the unsaturated zone is not appropriate for a site where the depth to ground water is considerable.

Transport processes strongly depend on chemical speciation. The simplest approach to estimating the concentration of a hazardous constituent is to assume it behaves conservatively. Rigorous models generally include consideration of transformation, transport, and speciation. In this approach, the rate constant for first-order attenuation in the unsaturated zone and the partition coefficient between solid, liquid, and gas phases has to be considered. The inclusion of degradative processes (e.g., biodegradation and hydrolysis) increases the chemical and environmental data required to model the fate of a compound considerably and consequently, the evaluation of hazard to human health and the environment. Where such degradative processes are suspected, a more-refined assessment is necessary.

Several additional analytical models—some of which are presented elsewhere in this text—account for one or more of these processes. These models include: simple Fruendlich isotherms (U.S. EPA 1989); the SUMMERS model (Summers, Gherini, and Chen 1980); the CHAIN model (van der Heijde 1994); and selected models by ES&T-IGWMC (1992).

Numerical Models Typical numerical techniques encountered in solving the convective–dispersive solute-transport equations in the unsaturated zone are comparable to those employed in simulating solute transport in the saturated zone, and include various FDMs, IFDMs, FEMs, and variants of the method of characteristics (van der Heijde 1994). As with flow, time is generally approximated by finite-difference techniques resulting in explicit, implicit and fully implicit solution schemes.

Typical problems associated with applying traditional finite-difference and finite-element techniques to simulate contaminant transport in the unsaturated zone include numerical dispersion and oscillations. Numerical dispersion occurs when the actual physical-dispersion mechanism of the contaminant transport cannot be distinguished from the front-smearing effects of the computational scheme. For the FDM, this problem is reduced by using the central difference approximation. Spatial-concentration oscillations can occur near a sharp concentration front in an advection-dominated transport system. Remedies for these problems are found (to some extent) in the reduction of grid increments (or time-step size), or by using upstream weighting for spatial derivatives. The use of weighted differences or the selection of other methods significantly reduces the occurrence of these numerical problems.

The International Ground Water Modeling Center (IGWMC) has identified, compiled, and published a description of over 90 unsaturated-zone models (van der Heijde 1994). The compilation includes models for flow and solute transport; solute transport requiring a given-head distribution; flow and heat transport; and flow, solute, and heat transport in the unsaturated zone. Table 13.5 summarizes selected flow and transport models documented by the IGWMC, along with the model source and reference.

13.3 THREE-DIMENSIONAL DETERMINISTIC IMMISCIBLE LIQUID-FLOW MODEL

Analytical Model

Three-dimensional analytical solution for non-aqueous liquid content from a point-source leak If the liquid being transported is not water but a dense non-aqueous phase liquid (DNAPL) or a light non-aqueous phase liquid (LNAPL), a modification to the analytical solutions in sections 13.2 and 13.3 has to be made. Previously, it was assumed that only two phases were present: a liquid phase consisting of water and constituents dissolved in the water; and air that can contain water vapor. If a DNAPL or LNAPL is introduced to the two-

TABLE 13.5 Selected Numerical Unsaturated-Zone Flow and Transport Models

Model name source	Fate and transport processes
VIP (Vadose Zone Interactive Processes)/U.S. Environmental Protection Agency, Stevens, Grenney, and Yan (1991)	Conservative transport (advection, dispersion, isotropic, diffusion); first-order chemical/microbial decay
NMODEL/University of Florida	Conservative transport (advection, dispersion, isotropic, anisotropic, diffusion); solid/liquid-phase transfers; first-order radioactive decay; single mother/daughter decay; first-order chemical/microbial decay
PMODEL/Louisiana State University	Conservative transport (advection, dispersion, isotropic, anisotropic, diffusion); solid/liquid-phase transfers; ion exchange; reduction/oxidation reactions; first-order chemical/microbial decay; plant uptake
SATURN (Saturated-Unsaturated Flow and Radionuclide Transport)/Geotrans, Inc.	Conservative transport (advection, dispersion, isotropic, anisotropic, diffusion); solid/liquid-phase transfers; first-order radioactive decay; single mother/daughter decay; first-order chemical/microbial decay
MMT/DPRW/Pacific Northwest Laboratory, Ahlstrom and Baca (1974)	Conservative transport (advection, dispersion, isotropic, anisotropic, diffusion); solid/liquid-phase transfers; first-order radioactive decay; single mother/daughter decay; first-order chemical/microbial decay
GS3/U.S. Nuclear Regulatory Commission, Davis and Segol (1985)	Conservative transport (advection, dispersion, isotropic, anisotropic, diffusion)
GS2/U.S. Nuclear Regulatory Commission, Davis and Segol (1985)	Conservative transport (advection, dispersion, isotropic, anisotropic, diffusion); solid/liquid-phase transfers; reduction/oxidation reactions; first-order radioactive decay; single mother/daughter decay; first-order chemical/microbial decay
VADOSE/Analytic & Computational Research, Inc.	Conservative transport (advection, dispersion, isotropic, anisotropic, diffusion); reduction/oxidation reactions; first-order radioactive decay; single mother/daughter decay; first-order chemical/microbial decay
CADIL (Chemical Adsorption and Degradation In Land)/AGTEHM/Oak Ridge National Laboratory, Emerson, Thomas, and Luxmoore (1984)	Conservative transport (advection, dispersion, diffusion); reduction/oxidation reactions; first-order radioactive decay; single mother/daughter decay; first-order chemical/microbial decay
FLOTRA/Analytic & Computational Research, Inc.	Conservative transport (advection, dispersion, isotropic, diffusion); solid/liquid phase transfers; first-order radioactive decay; single mother/daughter decay; first-order chemical/microbial decay, zero-order production
CXTFIT/U.S. Salinity Lab, ARS, Riverside, California (1995)	Conservative transport (advection, dispersion, isotropic, diffusion); solid/liquid–liquid/solid-phase transfers; ion exchange; reduction/oxidation reactions; first-order radioactive decay; single mother/daughter decay; first-order chemical decay
DISPEQ/DISPER/PISTON, Fluhler and Jury (1983)	Conservative transport (advection); solid/liquid/gas-phase transfers; reduction/oxidation reactions; first-order chemical/microbial decay; plant uptake
CREAMS/U.S. Department of Agriculture (1984)	Conservative transport (advection, dispersion, isotropic, anisotropic, diffusion); solid/liquid-phase transfers; first-order radioactive decay; single mother/daughter decay; first-order chemical/microbial decay; plant uptake
SUTRA*/U.S. Geological Survey, Voss (1984)	Conservative transport (advection, dispersion, isotropic, anisotropic, diffusion); solid/liquid-phase transfers; reduction/oxidation reactions; first-order radioactive decay; single mother/daughter decay; first-order chemical/microbial decay
TRACER3D/Los Alamos National Laboratory, Travis (1984)	Conservative transport (advection, diffusion); solid/liquid-phase transfers; first-order chemical/microbial decay
FEMTRAN/Sandia National Laboratory, Martinez (1985)	Conservative transport (advection, dispersion, isotropic, anisotropic, diffusion); solid/liquid-phase transfers; first-order radioactive decay; single mother/daughter decay
SBIR/Simons, Li and Associates, U.S. Bureau of Reclamation (1984)	Conservative transport (advection, dispersion, isotropic, anisotropic, diffusion)
GASOLINE/U.S. Geological Survey	Conservative transport (advection, dispersion, isotropic, diffusion); solid/liquid/gas-phase transfers; reduction/oxidation reactions; first-order chemical/microbial decay

(*continued*)

TABLE 13.5 Selected Numerical Unsaturated-Zone Flow and Transport Models (*continued*)

Model name source	Fate and transport processes
MOTIF (Model of Transport In Fractured/Porous Media)/Atomic Energy of Canada, Ltd.	Conservative transport (advection, dispersion, isotropic, anisotropic, diffusion); solid/liquid phase-transfers; ion exchange; reduction/oxidation reactions; first-order radioactive decay; single mother/daughter decay; first-order chemical/microbial decay
VS2D/VS2DT*/U.S. Geological Survey	Conservative transport (advection, dispersion, isotropic, anisotropic, diffusion); solid/liquid-phase transfers; ion exchange; first-order radioactive decay; single mother/daughter decay; first-order chemical/microbial decay; plant uptake
NITROSIM/University of Florida	Conservative transport (advection, dispersion, isotropic, diffusion); solid/liquid phase-transfers; ion exchange; reduction/oxidation reactions; first-order chemical/microbial decay; plant uptake
FEMWASTE/FECWASTE/Oak Ridge National Laboratory	Conservative transport (advection, dispersion, isotropic, anisotropic, diffusion); solid/liquid-phase transfers; ion exchange; first-order radioactive decay; single mother/daughter decay; first-order chemical/microbial decay
FLAMINCO/Geotrans, Inc., Huyakorn and Wadsworth (1985)	Conservative transport (advection, dispersion, isotropic, anisotropic, diffusion); solid/liquid-phase transfers; ion exchange; first-order radioactive decay; single mother/daughter decay; first-order chemical/microbial decay
SESOIL* (Seasonal Soil Compartment Model)/U.S. Environmental Protection Agency	Conservative transport (advection, dispersion, isotropic, diffusion); solid/liquid-phase transfers; ion exchange; substitution/hydrolysis; reduction/oxidation reactions; acid/base reactions; complexation; first-order chemical/microbial decay; plant uptake
CTSPAC/University of Oregon, Lindstrom, Garfield, and Boersma (1988)	Conservative transport (advection, dispersion, isotropic, diffusion); solid/liquid-phase transfers; plant uptake
DOSTOMAN (Dose to Man)/Savannah River Laboratory	Conservative transport (advection); solid/liquid phase transfers; first-order radioactive decay; single mother/daughter decay; first-order chemical/microbial decay
VAM2D (Variably Saturated Analysis Model in 2 Dimensions)/HydroGeologic, Inc.	Conservative transport (advection, dispersion, isotropic, anisotropic, diffusion); solid/liquid phase transfers; first-order radioactive decay; single mother/daughter decay; first-order chemical/microbial decay
PRZM (Pesticide Root Zone Model)/U.S. Environmental Protection Agency	Conservative transport (advection); solid/liquid/gas-phase transfers; first-order chemical/microbial decay; plant uptake
RITZ (Regulatory and Investigative Treatment Zone Model)/U.S. Environmental Protection Agency	Conservative transport (advection); solid/liquid/gas-phase transfers; first-order chemical decay
CHEMRANK/University of Florida	Conservative transport (advection); solid/liquid/gas-phase transfers; first-order chemical decay.
ICE-1/International Ground Water Modeling Center	Conservative transport (advection)
PATHRAE/Clemson University	Conservative transport (advection, dispersion, isotropic, diffusion); first-order radioactive decay; single mother/daughter decay; first-order chemical/microbial decay
BIOSOIL/Occidental Chemical Corporation	Conservative transport (advection, dispersion, isotropic); solid/liquid-phase transfers; first-order radioactive decay; single mother/daughter decay; first-order chemical/microbial decay; biotransformation; aerobic/anaerobic
CMIS (Chemical Movement in Soils)/University of Florida	Conservative transport (advection); solid/liquid-phase transfers; ion exchange; first-order chemical/microbial decay
CMLS (Chemical Movement in Layered Soils)/University of Florida	Conservative transport (advection); solid/liquid phase-transfers; ion exchange; first-order chemical decay
GLEAMS (Groundwater Loading Effects on Agricultural Management Systems)/U.S. Department of Agriculture (ARS)	Conservative transport (advection, diffusion); solid/liquid-phase transfers; first-order chemical/microbial decay
CHEMFLO/U.S. Environmental Protection Agency	Conservative transport (advection, dispersion, isotropic, diffusion); solid/liquid-phase transfers; first-order chemical/microbial decay

(*continued*)

TABLE 13.5 Selected Numerical Unsaturated-Zone Flow and Transport Models (*concluded*)

Model name source	Fate and transport processes
MOUSE (Method of Underground Solute Evaluation)/Cornell University	Conservative transport (advection, dispersion, isotropic, diffusion); solid/liquid-phase transfers; first-order chemical/microbial decay
PESTAN* (Pesticide Analytical Model)/U.S. Environmental Protection Agency	Conservative transport (advection, dispersion, isotropic, diffusion); solid/liquid-phase transfers; first-order chemical/microbial decay
LEACHMP (Leaching Estimation and Chemistry Model-Pesticides)	Conservative transport (advection, dispersion, isotropic, diffusion); solid/liquid-phase transfers; first-order chemical/microbial decay; plant uptake
MLSOIL/DFSOIL (Multi-Layer Soil Model)/Oak Ridge National Laboratory	Conservative transport (advection); first-order radioactive decay; single mother/daughter decay; chain decay.
MOFAT/Environmental Systems & Technologies, Inc.	Conservative transport (advection, dispersion, isotropic, anisotropic, diffusion); solid/liquid/gas phase transfers; first-order chemical/microbial decay.
PORFLOW-3D/Analytic & Computational Research, Inc.	Conservative transport (advection, dispersion, isotropic, anisotropic, diffusion); solid/liquid-phase transfers; first-order radioactive decay; single mother/daughter decay; first-order chemical/microbial decay
VENTING/Environmental Systems & Technologies, Inc.	Conservative transport (advection); solid/liquid/gas-phase transfers; first-order chemical/microbial decay
VADOFT/HydroGeologic, Inc.	Conservative transport (advection, dispersion, isotropic, diffusion); solid/liquid phase transfers; first-order radioactive decay; single mother/daughter decay; first-order chemical/microbial decay.
MOTRANS/Environmental Systems & Technologies, Inc.	Conservative transport (advection, dispersion, isotropic, anisotropic, diffusion); solid/liquid/gas phase transfers; first-order chemical/microbial decay.
NITRO/Environmental Systems & Technologies, Inc.	Conservative transport (advection, dispersion, isotropic, anisotropic, diffusion); solid/liquid/gas-phase transfers; first-order chemical/microbial decay
TDFD1O/Slotta Engineering Associates, Inc.	Conservative transport (advection, dispersion, isotropic, anisotropic, diffusion); solid/liquid-phase transfers; first-order radioactive decay; single mother/daughter decay; first-order chemical/microbial decay
VSAFT2 (Variable Saturated Flow and Transport in 2 Dimensions)/University of Arizona	Conservative transport (advection, dispersion, isotropic, anisotropic, diffusion)
RUSTIC/U.S. Environmental Protection Agency	Coupled-root-zone (PRZM), unsaturated-zone (VADOFT) and saturated-zone (SAFTMOD) modeling package

Source: Summarized from van der Heijde (1994).
*Code and documentation available from the IGWMC, Colorado School of Mines, Golden, Colorado 80401

phase air–water system, a three-phase system is created that can consist of water, the NAPL, and a vapor phase containing both water and NAPL vapors. Parker, Lenhard, and Kuppusamy (1987) proposed a method to scale the air–water, moisture-characteristic curve to obtain a two-phase air–NAPL or water–NAPL system, if one of the three phases is assumed to be at residual saturation. This scaling technique is valid for monotonic wetting-phase drainage from near saturation (Parker, Lenhard, and Kuppusamy 1987). Before continuing with the presentation of a scaling methodology, an understanding of the concepts of surface tension and wetting are needed.

Whether or not a fluid is wetting or nonwetting depends on its ability to adsorb to solid particles, as well as its ability to adsorb to other fluids. Liquid fluids (e.g., water) are often wetting fluids, and gaseous fluids (e.g., air) are often nonwetting fluids. NAPLS can be either wetting or nonwetting, and generally fall into an intermediate category between air and water. Figure 13.24 shows a schematic of a soil with two fluid phases, where one phase is a wetting (w) phase and the other a nonwetting (a) phase. Figure 13.25 shows a schematic of a soil with three fluid phases, where one is a wetting (w) phase, another is a nonwetting (a) phase, and the third is an intermediate (o) phase.

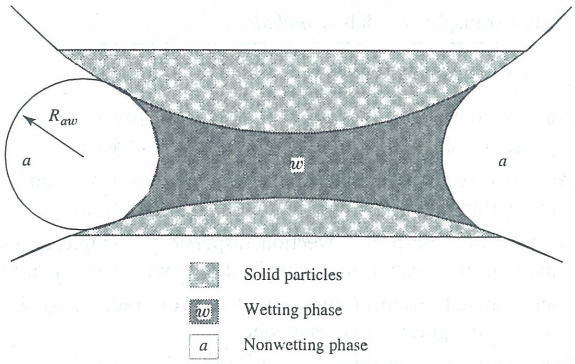

Figure 13.24 Schematic of soil with two fluid phases

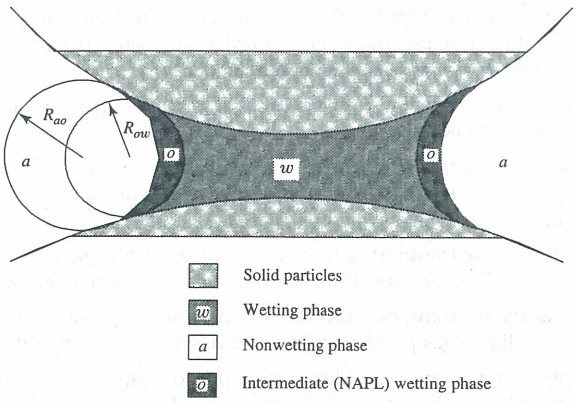

Figure 13.25 Schematic of soil with three fluid phases

Scaling an air–water system to a two-phase Air–NAPL system Parker, Lenhard, and Kuppusamy (1987) propose that for a given soil, the saturation/matric potential (capillary pressure) function or moisture-characteristic curve, is written in a generalized form. This generalized form is presented as the effective saturation/matric potential ($\overline{S}/\psi_m$) function, where S is the effective saturation as defined by equation 13.83. The generalized function of the saturation/matric potential curve is written by Murphy, Bumb, and McKee (1987) as

$$\overline{S}^*(\psi_m^*) = \overline{S}^*(\eta_{ij}\psi_{mij}) = \overline{S}_j^{ij}(\psi_{mij}) \tag{13.138}$$

where $\overline{S}^*(\psi_m^*)$ is the generalized function and $\overline{S}_j^{ij}(\psi_{mij})$ is the specific function for a two-phase system in which i is the nonwetting phase and j is the wetting phase. In this case, η_{ij} is a scaling factor, and a function of the interfacial tension between the two phases, which relates the specific to the generalized function for one of the phases. If we assume that the nonwetting phase is air, then we can let $i = a$. If the wetting phase is water $j = w$, or if it is NAPL, $j = o$. Generally, it is convenient to let $\eta_{aw} = 1$ Then,

$$\overline{S}^*(\psi_m^*) = \overline{S}^*(\psi_{maw}) = \overline{S}_w^{aw}(\psi_{maw}) \tag{13.139}$$

Thus, if the air–water characteristic curve for a given soil is known, then that same curve is scaled to define the saturation/matric potential curve for any other two-phase system. For example, an air–NAPL system is described as

$$\overline{S}_o^{ao}(\psi_{mao}) = \overline{S}^*(\eta_{ao}\psi_{mao}) = \overline{S}_w^{aw}(\eta_{ao}\psi_{mao}) \tag{13.140}$$

and a NAPL–water system as

$$\overline{S}_w^{ow}(\psi_{mow}) = \overline{S}^*(\eta_{ow}\psi_{mow}) = \overline{S}_w^{aw}(\eta_{ow}\psi_{mow}) \tag{13.141}$$

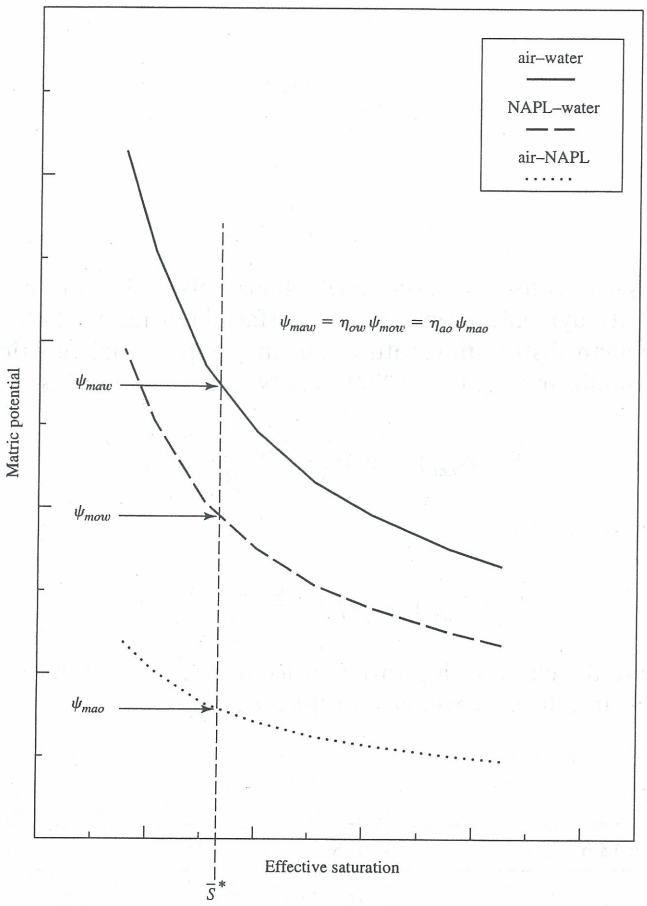

Figure 13.26 Schematic of scaling of saturation/matric potential functions

Figure 13.26 illustrates of the effects of scaling. At a given effective saturation, the corresponding matric potential on the NAPL–air characteristic curve is ψ_{mao}, while the corresponding potential on the water–air characteristic curve is ψ_{maw}, and they are related by

$$\psi_{maw} = \eta_{ao}\psi_{mao} \tag{13.142}$$

If η_{ao} is constant for any arbitrary values of $\bar{S}(\psi_{mao})$, then the NAPL–air characteristic curve is scaled to the water–air characteristic curve through the scaling factor η_{ao}.

Lenhard and Parker (1986) show that the values of η depend on the interfacial tensions σ_{ij}. They also point out that at a given effective saturation, it is evident that $\psi_{maw} = \eta_{ao}\psi_{mao} = \eta_{ow}\psi_{mow}$, and the capillary-rise equation can be applied to give

$$\frac{\sigma_{aw}}{R_{aw}} = \frac{\eta_{ao}\sigma_{ao}}{R_{ao}} = \frac{\eta_{ow}\sigma_{ow}}{R_{ow}} \tag{13.143}$$

where R is the radius of curvature of the fluid interfaces, as defined in figures 13.24 and 13.25. Lenhard and Parker (1986) also note that for idealized monotonic drainage paths in a soil, the fluid interfaces have the same geometry for any two-phase system if the solid surfaces are completely wet by the wetting fluid, such that the contact angle with the surface is zero. Thus, assuming that $R_{aw} = R_{ao} = R_{ow}$ at a fixed-wetting phase, saturation yields

$$\sigma_{aw} = \eta_{ao}\sigma_{ao} = \eta_{ow}\sigma_{ow} \tag{13.144}$$

Thus,

$$\eta_{ao} = \frac{\sigma_{aw}}{\sigma_{ao}} \tag{13.145}$$

and

$$\eta_{ow} = \frac{\sigma_{aw}}{\sigma_{ow}} \tag{13.146}$$

Table 13.6 gives physical constants for selected fluids; this table can be used to obtain selected values of density, dynamic viscosity, and interfacial tension for two-phase systems.

For the Boltzmann distribution saturation- matric-potential function, scaling is presented by Murphy, Bumb, and McKee (1987) for a NAPL–air system as

$$\overline{S}_o^{ao}(\psi_{mao}) = \exp\left(-\frac{\psi_{mao} - \psi_{1ao}}{\beta_{ao}}\right) \tag{13.147}$$

and for an air–water system as

$$\overline{S}_w^{aw}(\psi_{maw}) = \exp\left(-\frac{\psi_{caw} - \psi_{1aw}}{\beta_{aw}}\right) \tag{13.148}$$

where ψ_{1ao} and β_{ao} are the curve-fitting variables for the NAPL–air characteristic curve, and ψ_{1aw} and β_{aw} are the curve-fitting variables for the air–water characteristic curve. Combining

TABLE 13.6 Physical Constants for Selected Liquids

Liquid*	Interfacial tension (dynes/cm)	Viscosity (cp)	Density (g/mL)
Acetone	23.7†‡	0.33	0.79
Ammonia	20†	0.2	—
Benzene	29†‡	0.65	0.88
Carbon Tetrachloride	27†‡	0.97	1.59
Chlorobenzene	34‡	0.80	0.96
Chloroform	27†	0.58	1.49
Chlorine	19†	0.3	—
Gasoline	21†	0.48	0.73
n-Hexane	18.4†	0.33	0.66
Isopropyl Alcohol	21.7†‡	2.5	0.8
Mercury	471†	1.87	13.6
Nitrobenzene	43.9†‡	2.03	1.2
Methylene Chloride	26.5†	0.43	1.33
Phenol	40.9†‡	10	1.06
Tetrachloroethylene (PCE)	31.7‡	0.9	1.62
Toluene	27.7‡	0.59	0.87
Trichloroethylene (TCE)	29.3‡	0.57	1.46
Xylene	30.1†	—	0.86
	28.9‡		
Water	73†	1.01	1.00

Note: Additional selected data on DNAPLs can be found in Cohen, Mercer, and Matthews (1993).

*At 20°C.

†In contact with air.

‡In contact with vapor.

equations 13.142 and 13.148 gives

$$\bar{S}_w^{aw}(\psi_{maw}) = \bar{S}_w^{aw}(\eta_{ao}\psi_{mao}) = \exp\left(-\frac{\eta_{ao}\psi_{mao} - \psi_{1aw}}{\beta_{aw}}\right) \tag{13.149}$$

or

$$\bar{S}_w^{aw}(\eta_{ao}\psi_{mao}) = \exp\left(\frac{\psi_{mao} - \frac{\psi_{1aw}}{\eta_{ao}}}{\frac{\beta_{aw}}{\eta_{ao}}}\right) \tag{13.150}$$

Equating equation 13.147 and equation 13.150, gives

$$\exp\left(-\frac{\psi_{mao} - \psi_{1ao}}{\beta_{ao}}\right) = \exp\left(-\frac{\psi_{mao} - \frac{\psi_{1aw}}{\eta_{ao}}}{\frac{\beta_{aw}}{\eta_{ao}}}\right) \tag{13.151}$$

or

$$\psi_{1ao} = \frac{\psi_{1aw}}{\eta_{ao}} \tag{13.152}$$

and

$$\beta_{ao} = \frac{\beta_{aw}}{\eta_{ao}} \tag{13.153}$$

where η_{ao} is given by equation 13.145. Equations 13.152 and 13.153 permit the calculation of a characteristic curve for an NAPL–air system, given the curve-fitting variables for the water–air characteristic curve for the same soil. Figures 13.27 and 13.28 show the characteristic curves for a water–air and TCE–air, and a water–air and gasoline–air system, respectively, for a Touchet–silt loam soil. These curves are calculated using the water–air characteristic curve and equations 13.152 and 13.153.

Relating a two-phase system to a three-phase system After scaling NAPL–air and NAPL–water systems to the reference water–air system, Parker, Lenhard, and Kuppusamy (1987) and Murphy, Bumb, and McKee (1987) applied commonly accepted (Leverett 1941) correspondences of three-phase interfaces to two-phase systems, to reduce the three-phase problem to sets of two-phase problems. Figure 13.29 shows a soil with a three-phase fluid system, and provides an illustration for the correspondence theorem as well. The S/ψ_m function characterizing the behavior of water in the three-phase system (see figure 13.25) depends only on the radius of curvature at the water–NAPL interface R_{ow}. The corresponding water saturation is S_w^{III}, and is a function of the matric potential across the water–NAPL interface ψ_{mow}. According to the correspondence theorem, $S_w^{III}(\psi_{mow})$ the functional relation is identical to that for water saturation in the two-phase system, or

$$S_w^{III}(\psi_{mow}) = S_w^{ow}(\psi_{mow}) \tag{13.154}$$

since this function also depends solely on the radius-of-curvature of the water–NAPL interface.

The S/ψ_m function characterizing the behavior of air in the three-phase system (see figure 13.25) depends only on the radius of curvature at the air–NAPL interface R_{ao}. The corresponding air saturation is S_a^{III}, and is a function of the matric potential across the air–NAPL interface ψ_{mao}. According to the correspondence theorem, the $S_a^{III}(\psi_{mao})$ functional relation is identical to that for the air saturation in the two-phase system, or

$$S_a^{III}(\psi_{mao}) = S_a^{ao}(\psi_{mao}) \tag{13.155}$$

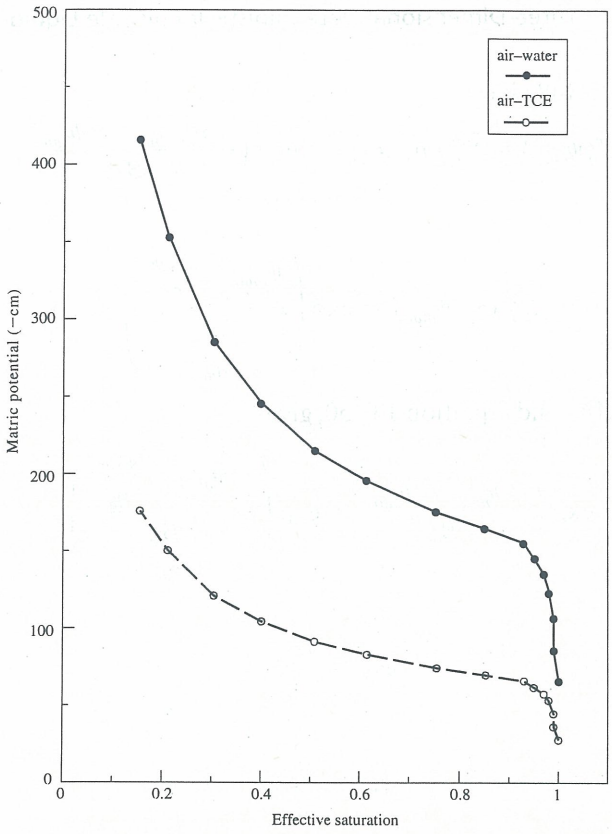

Figure 13.27 Moisture-characteristic curves for water and TCE

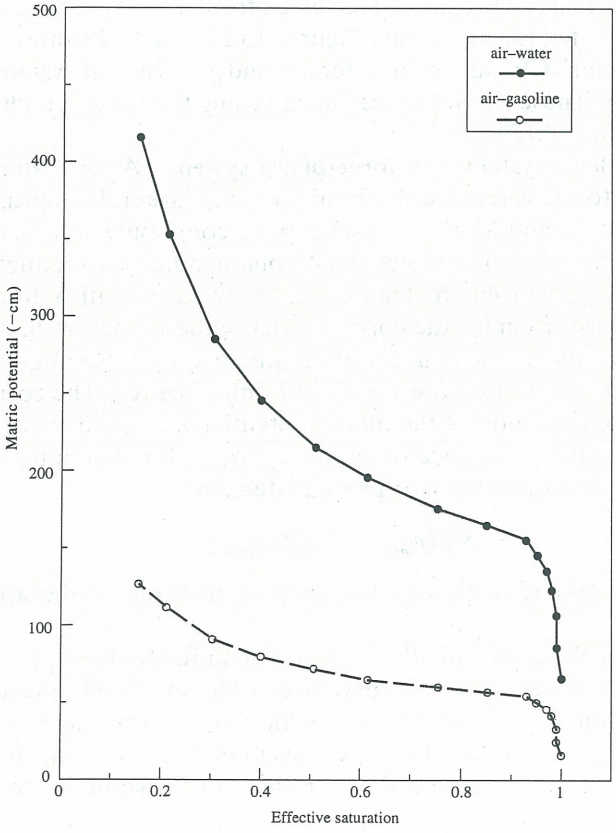

Figure 13.28 Moisture-characteristic curves for water and gasoline

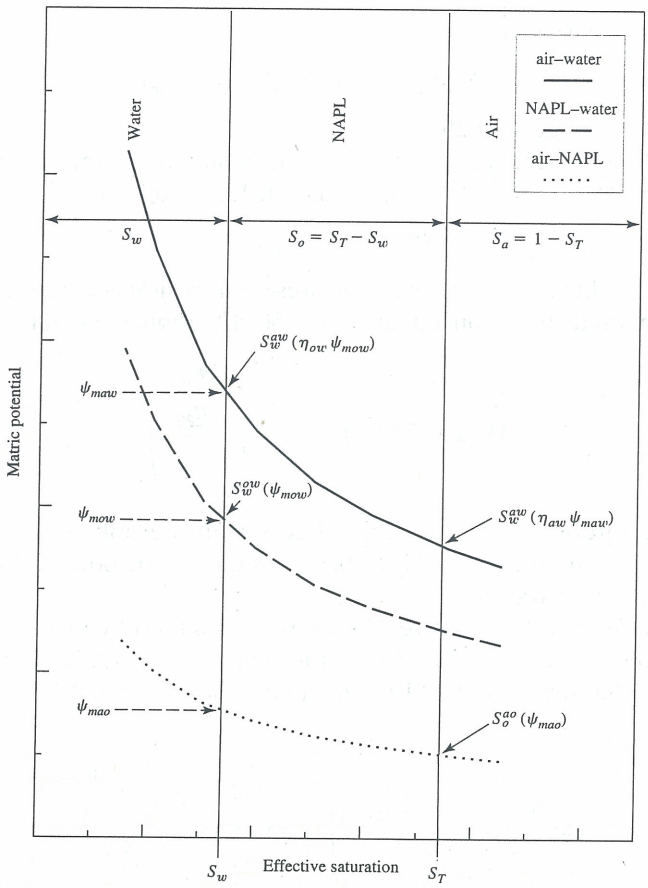

Figure 13.29 Correspondence of three-phase and scaled two-phase system

because this function also depends solely on the radius of curvature of the air–NAPL interface. However, in the two-phase system $S_a = 1 - S_o$, where S is the effective saturation of air or NAPL, while in the three-phase system, $S_a^{III} = 1 - S_T^{III}$, and $S_T^{III} = S_w^{III} + S_o^{III}$, where S_T is the total liquid saturation, the sum of the water saturation and NAPL saturation.

Both air and water (the nonwetting and wetting fluid phases of the three-phase system) behave as they would in a two-phase system. The NAPL, however, is of intermediate wettability and has two fluid interfaces affecting its S/ψ_m characteristic curve in the three-phase system. One of these two interfaces in the water–NAPL interface and the other is the air–NAPL interface (see figure 13.25). The small radius is established by the water saturation and the water–NAPL interface. The larger radius is established by the total liquid saturation (water plus NAPL) and the air–NAPL interface. Thus, the NAPL S/ψ_m characteristic curve in the three-phase system corresponds to both the water–NAPL and the air–NAPL systems as expressed by (Murphy, Bumb, and McKee 1987)

$$S_o^{III} = S_T^{III}(\psi_{mao}) - S_w^{III}(\psi_{mow}) \tag{13.156}$$

For effective saturations, this corresponds (functionally) to two-phase systems (Murphy, Bumb, and McKee 1987) as

$$\bar{S}_o^{III} = \bar{S}_o^{ao}(\psi_{mao}) - \bar{S}_w^{ow}(\psi_{mow}) \tag{13.157}$$

Scaling equation 13.157 in accordance with equations 13.140 and 13.141, we see that the difference is analytically equivalent to the difference between two points on the air–water

reference characteristic curve, or

$$\bar{S}_o^{III} = \bar{S}_w^{aw}(\eta_{ao}\psi_{mao}) - \bar{S}_w^{aw}(\eta_{ow}\psi_{mow}) \tag{13.158}$$

as shown schematically in figure 13.29.

For the special case where water is present at its residual saturation, the effective saturation of water is zero ($\bar{S}_w^{ow} = \bar{S}_w^{III} = 0$), and equation 13.158 becomes

$$\bar{S}_{or}^{III} = \bar{S}_o^{ao}(\psi_{mao}) \tag{13.159}$$

where the subscript *r* indicates that the water is present at residual saturation.

For the Boltzmann distribution, equation 13.150 still applies, so that

$$\bar{S}_{or}^{ao}(\psi_{mao}) = \exp\left(-\frac{\psi_{mao} - \frac{\psi_{1aw}}{\eta_{ao}}}{\frac{\beta_{aw}}{\eta_{ao}}}\right) \tag{13.160}$$

which shows NAPL saturation in the three-phase system described in terms of a single, scaled-two-phase equation. In equation 13.160, ψ_{mao} is the matric potential at the air–NAPL interface in the three-phase system.

If water is present at other than residual saturation, the effective water saturation is greater than zero, thus the NAPL saturation is not so easily defined. In such a case, equation 13.158 still holds and the corresponding Boltzmann distribution equation is (Murphy, Bumb, and McKee 1987)

$$\bar{S}_o^{III} = \exp\left(-\frac{\psi_{mao} - \frac{\psi_{1aw}}{\eta_{ao}}}{\frac{\beta_{aw}}{\eta_{ao}}}\right) - \exp\left(-\frac{\psi_{mow} - \frac{\psi_{1aw}}{\eta_{ow}}}{\frac{\beta_{aw}}{\eta_{ow}}}\right) \tag{13.161}$$

In equations 13.160 and 13.161, ψ_{mao} refers to the matric potential at the interface between the air and NAPL phases for the three-phase system, and ψ_{mow} refers to the matric potential at the interface between water and NAPL for the three-phase system.

Murphy, Bumb, and McKee (1987) have shown that the unsaturated hydraulic conductivity *K* for a three-phase system—where the water is at residual saturation—also follows a power expression of the same form as equation 13.9. Because the saturated hydraulic conductivity K_s used in the power expression varies directly with fluid density and inversely with fluid viscosity, its value must be revised for the NAPL of interest. Thus,

$$K_{so} = K_{sw}\left(\frac{\rho_o}{\rho_w}\right)\left(\frac{\mu_w}{\mu_o}\right) \tag{13.162}$$

where ρ is density and μ is viscosity (throughout text we use η for viscosity, but use μ here to avoid confusion), and o and w are subscripts referring to the NAPL and water phases, respectively. Values of density and viscosity for selected liquids also are presented in table 13.6.

To demonstrate the use of the above equations, a steady-state leak of 500 liters of gasoline per day into a homogeneous and isotropic Touchet silt loam is modeled using equations 13.104 and 13.105. In this example, the leak is located 5 m below ground surface. The Touchet silt loam soil has the properties shown in table 13.3 for the Boltzmann distribution, but these properties have been scaled to gasoline by equation 13.153, using the ratio of the interfacial tension of water to gasoline. The saturated hydraulic conductivity for the loam soil is scaled to gasoline using equation 13.162. The soil has a saturated hydraulic conductivity to gasoline of 0.54 m/day (scaled using equation 13.162, a porosity of 50.1 percent, a maximum satura-

tion of 96.5 percent, and an irreducible saturation of 36.0 percent. The solution consists of finding the steady-state gasoline-content distribution as a result of the point-source leak.

The steady-state effective saturations and actual saturations are shown in figures 13.30 and 13.31, respectively. The highest saturations are directly below the leak, with measurable saturations spreading away from the leak laterally, a distance of approximately 12 m. The gasoline spreading is much less than for water (see figures 13.18 and 13.19) and extends deeper, because of the interfacial tension and higher saturated hydraulic conductivity of the gasoline. Such an analysis can be used to assess the locations of monitoring devices, or to assess the relative location of conservative contaminants.

Numerical Models

Selected additional numerical models for transport of NAPLs are presented in table 13.5 and in van der Heijde (1994).

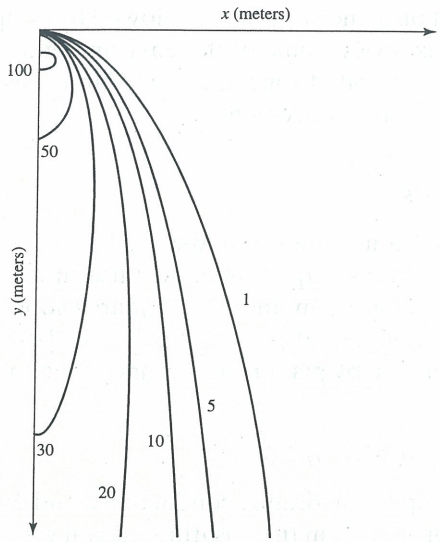

Figure 13.30 Steady-state effective gasoline saturations (S_e= %) from a point-source leak into a Touchet silt loam

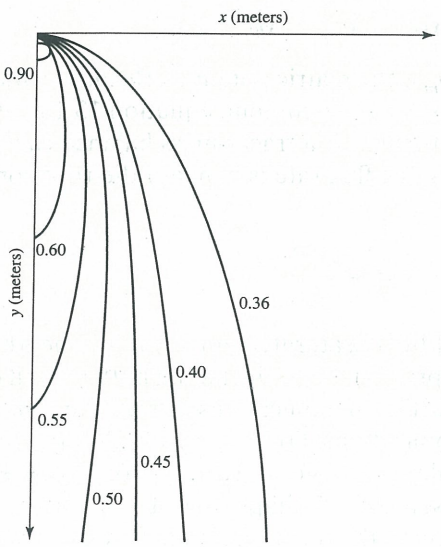

Figure 13.31 Steady-state actual gasoline saturations (S= decimal) from a point-source leak into a Touchet silt loam

13.4 USE OF TRACERS IN UNSATURATED SOIL STUDIES

Environmental and applied tracers have been used to measure water and contaminant movement in the unsaturated zone (Phillips 1994). This is especially true in arid and semiarid areas, where the diffuse downward flux (recharge) is typically very small compared to either annual precipitation or annual evapotranspiration. Because at low volumetric water content both matric potential and unsaturated hydraulic conductivity vary by several orders of magnitude with changes in water content, tracers are often used in place of traditional water-balance techniques to calculate the small fluxes associated with annual recharge. Environmental and applied tracers allow direct measurement of the displacement of water and/or solutes, thus eliminating the need for indirect calculations using uncertain variables, as is required in the water-balance technique. Tracers can also be the method of choice for assessing the impacts of preferential flow paths in the unsaturated zone.

Environmental tracers include both naturally occurring tracers as well as contaminants added to the environment as a result of human intervention. Applied tracers, in contrast to environmental tracers, are those input on a one-time basis, followed by sampling of the tracer pulse with time. The following sections review some of the environmental and applied tracers used for various purposes in the unsaturated zone; the single largest use of tracers in the unsaturated zone has been to measure water movement.

Theory of Unsaturated Liquid Movement Using Tracers

Many studies have reported attempts to use unsaturated-zone hydraulic characteristics K and ψ, to solve either Darcy's law or Richards' equation in the unsaturated zone, and to estimate soil-flux rates for time periods ranging from months to years (Sophocleous and Perry 1985; Stephens and Knowlton 1986). If the liquid (water) flux is calculated at a point below the root zone—where no further extraction by plant roots occurs—then the flux rate is equal to the ground water recharge, or

$$q = K(\theta)\,\Delta\psi_h \tag{13.163}$$

where q is the flux rate, K is the unsaturated hydraulic conductivity, and $\Delta\psi_h$ is the hydraulic potential gradient. If the concentration of salts in the unsaturated-soil water is sufficiently dilute so that osmotic potential is considered negligible, then

$$\Delta\psi_h = \Delta\psi_g + \Delta\psi_m \tag{13.164}$$

where ψ_g is the gravity potential and ψ_m is the matric potential. Because values of K and ψ are often difficult to measure with decreasing water content, equation 13.163 often leads to substantial errors in flux and recharge estimates. If a tracer-mass balance can be undertaken in the unsaturated zone—again assuming the flux rate is beneath the root zone—then the flux rate is given by

$$q = \frac{c_P P}{c_r} \tag{13.165}$$

where c_r is the tracer concentration of the unsaturated-zone water beneath the root zone, c_P is the average tracer concentration in precipitation—including both wetfall (rain) and dryfall (dust)—and P is the precipitation. If artificial applications of water are made, then P and c_P are defined for the artificial water applications. For tracers, obtaining reliable estimates of wetfall and dryfall over long time scales is a large source of error (Cook et al. 1994). Some studies (Peck, Johnston, and Williamson 1981; Phillips et al. 1988; Walker et al. 1992) have used a mass-balance approach to estimate the mean-drainage flux $\overline{q}$ to some depth z within

the plant-root zone, or conversely, to estimate the age of water at a given depth within the root zone. In this case, the mean flux rate becomes

$$\bar{q}(z) = \frac{c_P P}{\bar{c}(z)} \tag{13.166}$$

where $\bar{c}(z)$ is the mean tracer concentration to depth z, given by the total tracer to depth z divided by the total water content. Cook et al. (1994) point out that such an approach is valid only if steady-state piston flow occurs in the unsaturated zone. If infiltration flows along preferential flow pathways, then equation 13.166 is not valid. If the flux rate is transient, then the tracer concentration is higher than that given by equation 13.165. Under these circumstances, the displacement of a tracer can be used to estimate the flux rate, defined by the tracer front z_{cf} (Walker et al. 1992) as

$$\int_0^{z_{cf}} \theta(z)\, dz = \int_0^{z_b} \theta(z) \frac{c_b - c(z)}{c_b - c_n}\, dz \tag{13.167}$$

where $\theta(z)$ is the volumetric water content; c_b is the equilibrium tracer concentration at a previous time; c_n is the new equilibrium tracer concentration (given by equation 13.165, above); and z_b is the depth below which $c = c_b$. The amount of water that has drained below the plant-root zone z_r since some previous time, is given by

$$Q_d = \int_{z_{cf}^o}^{z_{cf}^n} \theta(z)\, dz + \int_{z^r}^{z_{cf}^o} \delta\theta(z)\, dz + \left[\int_0^{z_r} \delta\theta(z)\, dz\right] \frac{c_n}{c_b} \tag{13.168}$$

where z_{cf}^n and z_{cf}^o are the depths to the tracer front under the new and previous times, respectively, and $\delta\theta$ is the change in water content (from the previous to the new time). This formulation is for changes in land use where infiltration and recharge increase as a result of this change, and tracer stored in the unsaturated zone is moved downward. The drainage rate can be approximated by

$$q = \frac{Q_d}{t} \tag{13.169}$$

where t is the time since the change in land use. Note that the tracer from z_{cf}^n is analogous to the center of mass c_c of an applied tracer introduced at depth z_{cf}^o at the time of a change in land use. The water flux is then given by the velocity of the tracer front, with a correction for changes in water content within the root zone.

The position of the tracer in the soil profile is described by using the center of mass z_c (median depth), or by the position of the peak concentration. The velocity of the soil water is inferred from the movement of either the center of mass or the peak concentration. The center of mass z_c is defined (Cook et al. 1994) by

$$\int_0^{z_c} \theta(z)c(z)\, dz = \frac{1}{2}\int_0^{\infty} \theta(z)c(z)\, dz \tag{13.170}$$

where $\theta(z)$ and $c(z)$ are the volumetric water content and the solute-concentration profiles, respectively. In practice, the volume of water in the soil profile above the center of mass (or peak concentration) is usually assumed equal to the total-water flux over the relevant time period. This flux is divided by the number of years that have elapsed since the center of mass of the wetfall and dryfall, or the year of highest fallout. If water movement in the unsaturated zone is by piston flow only, then using either the center of mass or peak concentration accurately measures the movement of the water (Cook et al. 1994). If water movement is via preferential flow, then the center-of-mass technique is preferred.

For the special case of tritium (^{3}H), which can be evapotranspired and decays, the mass balance is written as

$$q = \frac{\int_0^\infty \theta(z)c(z)\,dz}{\sum_{i=1}^{\infty} \omega_i c_i e^{-t\lambda}} \tag{13.171}$$

where q is the mean water flux below the soil surface, $c(z)$ is the tritium concentration of the soil water at depth z, $c_i e^{-t\lambda}$ is the tritium concentration in precipitation i years before the present (corrected for decay), and ω_i is a weighting function that takes into account year-to-year variations in drainage ($\omega_i = q_i/\bar{q}$). Different researchers have used different functions to assign the relative contribution of each year's precipitation to the total tritium in the soil profile. Most authors weight according to the mean annual precipitation, or $\omega_i = P_i/\bar{P}$, whereas others have used weighted fluctuations in ground water levels.

Environmental Tracers

Because of atmospheric nuclear testing in the late 1950s and early 1960s, significant increases in the concentrations of tritium (^{3}H) and chlorine-36 (^{36}Cl) occurred, and then decreased to lower levels. The ^{3}H and ^{36}Cl fallout is different for different locations on the earth's surface. Figure 13.32 shows tritium concentrations and chlorine-36 fallout distributions from the early 1950s until the late 1980s (Cook et al. 1994) at Adelaide, South Australia. Both tritium and chorine-36 have been used extensively for unsaturated-zone tracers and recharge studies (Zimmerman, Ehhalt, and Munnich 1967; Gvirtzman and Margaritz 1986; Phillips et al. 1988; Cook et al. 1994). Tritium has a half-life of approximately 12.3 years, whereas ^{36}Cl has a half-life of approximately 301,000 years. Another-often-used environmental tracer is ^{14}C, which has a half-life of approximately 5,700 years. The concentrations of these three radioactive tracers have changed dramatically over the last 30 years. Other naturally-occurring, nonradioactive tracers commonly used in unsaturated-zone studies include ^{15}N, ^{18}O, ^{2}H (deuterium), ^{13}C, and Cl. Input concentrations of these isotopes have also changed over time but

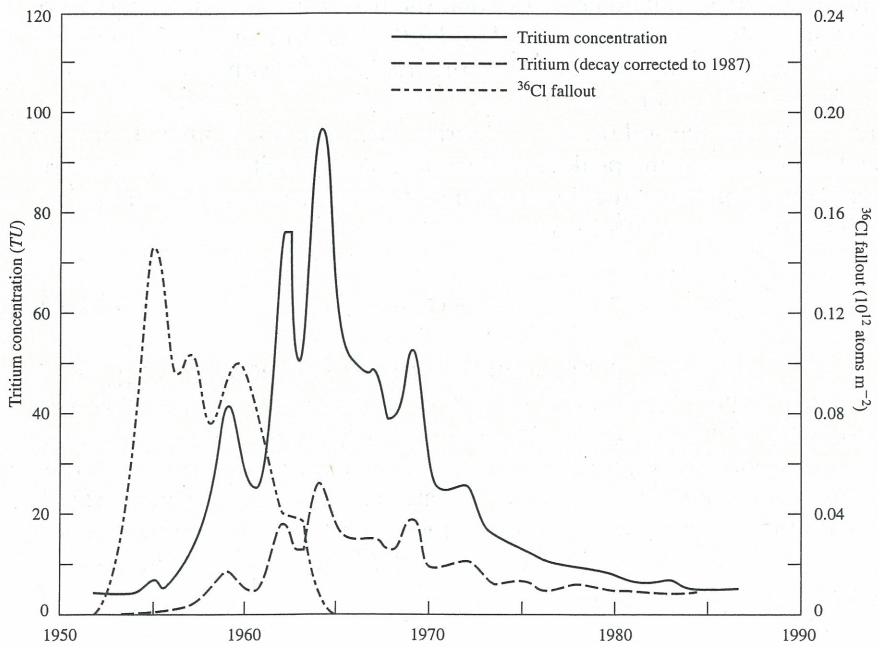

Figure 13.32 Fallout distributions for ^{3}H and ^{36}Cl at Adelaide, South Australia. Reproduced from Cook et al. 1994, copyright by the American Geophysical Union

on a much longer time scale, primarily due to changes in global climatic patterns (Allison, Gee, and Tyler 1994). Recently, Cl has been used extensively as a natural tracer, even though little is known of the temporal changes in the fallout of Cl.

Of the tracers mentioned above ^{3}H, ^{2}H, and ^{18}O probably simulate the movement of water in unsaturated soil most accurately, because they form part of the water molecule. In most unsaturated soils, ^{36}Cl and Cl also move with the water; however, in some clayey soils, anion exclusion can cause these tracers to move more rapidly than the water being traced (Allison, Gee, and Tyler 1994). While steady-state, piston flow is often capable of explaining the behavior of tracers in the field, there is mounting evidence that water movement along preferential pathways is the rule, rather than the exception. Thus, nonpiston flow has to be assessed in any unsaturated-zone tracer analysis. Unsaturated-zone flow in preferential pathways has been found to occur in both humid and arid sites (Gish and Shirmohammadi 1991).

Tritium Studies using tritium have made use of the fact that the peak of ^{3}H in precipitation has been preserved in the unsaturated zone. As indicated in section 13.5, the position of ^{3}H in the unsaturated zone is best described using the center-of-mass technique. Many studies on the estimation of recharge using natural ^{3}H in the unsaturated zone are given in the literature (Allison, Gee, and Tyler 1994; Cook et al. 1994). To estimate recharge from ^{3}H profiles, the ^{3}H concentration of the effective input to the unsaturated-zone water system has to be known. It is noted that, in the northern hemisphere, mean annual concentrations of ^{3}H reached several hundred times the natural levels. In the southern hemisphere, mean annual ^{3}H concentrations exceeded 5 to 10 times the natural levels in the early 1960s, but have since decayed to near-natural fallout levels (see figure 13.32) (Cook et al. 1994). The techniques for measuring ^{3}H are not valid in areas where the root zone is deep, and interpretation of data can become difficult if flow regimes are not reasonably uniform. It has also been suggested that in arid areas, where soils are sandy and have a low water content, it is possible for water vapor with high ^{3}H concentrations to diffuse into unsaturated-zone water or ground-water systems. Estimates of recharge made using ^{3}H in arid areas, therefore, are high. This is especially true for recharge rates less than 1 mm/yr. Careful consideration should be given to this possibility when interpreting data in arid areas.

Chlorine-36 Bomb-pulse ^{36}Cl has been used in a number of studies (Allison, Gee, and Tyler 1994; Cook et al. 1994). Concentrations of ^{36}Cl were over 1,000 times greater than natural fallout levels between 1952 and 1965 (Bentley, Phillips, and Davis 1986). In studies in arid and semiarid areas, the ^{36}Cl profile appeared to match that of the input signal; however, the pulse was still very near the soil surface, often within the root zone. Thus, the bomb peak of ^{36}Cl, like ^{3}H, is not an ideal tracer in areas of low recharge or in areas of changing land use, because its root-zone movement can be affected by water uptake. Chlorine-36 is probably best-suited for regions where the local recharge is expected to be higher than 30 to 50 mm/yr, but this depends on the water-holding capacity of the soil and the root-zone depth. Other difficulties in using ^{36}Cl is analyzing near-background concentrations, and/or the cost of analyses. Per-sample costs for ^{36}Cl range from a few hundred to a few thousand dollars, depending on the concentration.

Chloride Input of Cl occurs at the soil surface both as precipitation and as dryfall. The Cl can be either atmospheric or terrestrial in origin. Several researchers have found that Cl of oceanic origin can exist several hundred miles inland. Because most plant species do not take up significant quantities of Cl from unsaturated-zone water, Cl is concentrated in the root zone by evapotranspiration. If we assume that flow of water in the unsaturated zone is by piston flow, the Cl concentration in the soil increases through the root zone, obtaining a constant value beneath the root zone. If the water table is deep or has the same Cl concentration as the unsaturated-zone water, a profile such as that shown in figure 13.33 results. Under steady-state conditions, the flux of Cl is given by equation 13.163. The Cl mass-balance technique has been used in the unsaturated zone to evaluate recharge in a range of

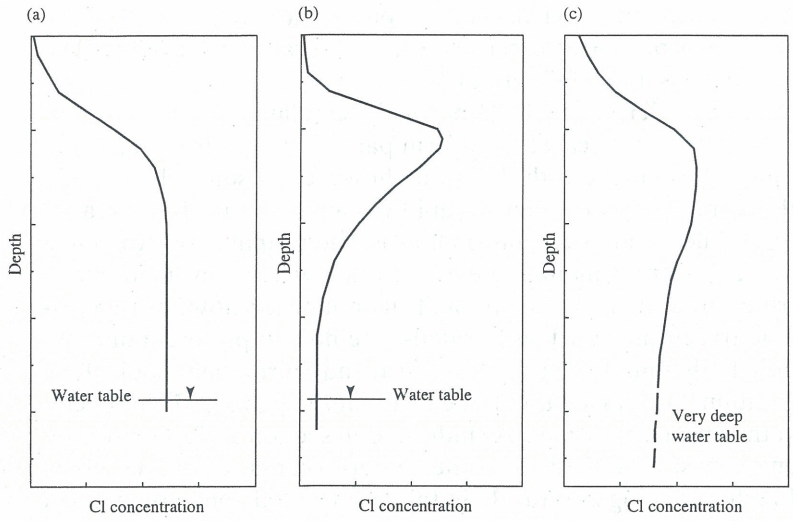

Figure 13.33 Schematic of Cl concentration depth profiles of soil water (data from Allison, Gee, and Tyler 1994)

environments successfully (Allison, Gee, and Tyler 1994). Many of the depth profiles of Cl concentration in soil water show a more complex shape than that of figure 13.33a. Some idealized examples of these more-complex shapes are given for comparison, in figures 13.33b and 13.33c. While figure 13.33a is an example of steady-state piston flow with extraction of water by plant roots, figure 13.33b is an indication of extraction of water by roots, but also either by preferred-pathway flow of water through and below the root zone, or diffusive loss of Cl to the water table. Figure 13.33c is a possible profile reflecting paleo-recharge conditions (Allison, Gee, and Tyler 1994).

Oxygen-18 and deuterium The stable isotopes ^{18}O and ^{2}H have been used successfully in determining the origin of ground water. Variations of isotopic composition with rainfall intensity, as well as the changes that occur following evaporation, have led to a determination of the possible sources of ground water in arid areas. However, relatively few studies using these stable isotopes have been done in the unsaturated zone. The studies using ^{18}O and ^{2}H in unsaturated zone have been carried out in temperate areas where recharge was on the order of 200 mm/yr or more. In more arid areas, strongly positive values of the displacement of either ^{18}O or ^{2}H concentration from the concentration found in precipitation can occur near the surface due to evaporation through the soil surface, leading to the possibility of identifying an annual marker in unsaturated-zone water. Barnes and Allison (1988) developed detailed models for the movement of stable isotopes in both the liquid and vapor phases in unsaturated soil.

Nitrate Nitrate (NO_3) is an involuntary tracer that can be used to give information on the rate of water movement in the unsaturated zone. Because NO_3 has come into increasing agricultural use since the 1950s and some of it has leached below the root zone, the change from higher to lower concentrations of NO_3 in unsaturated-zone water at depth, is an indication of the position in the profile of recharge, originating at the time of increased-use of NO_3. A knowledge of the amount of water stored in the profile enables an estimate of recharge then. In some situations the reverse effect occurs where, once vegetation is cleared, NO_3 associated with the native vegetation can possibly be a marker associated with the time of this clearing.

Applied Tracers

In contrast to the above tracers (input to the unsaturated zone each year in precipitation), applied tracers are a one-time application followed by sampling of the pulse of the tracer

over time and space. Ideally, the applied tracer is applied beneath the root zone to reduce uptake by plants, and a sufficient time allowed to elapse between injection and sampling to allow the depth interval traversed by the tracer peak to be measured accurately (Allison, Gee, and Tyler 1994). In temperate areas, where the root zone is relatively shallow and the annual recharge is high, this method is ideal; in semiarid and arid areas, where root zones are usually deeper and recharge fluxes lower, this technique is less useful if natural precipitation is the only mechanism used to move the tracer downward.

Tracer Flux through the Root Zone

Because root-zone effects of natural environmental and applied conservative tracers are important, the processes that affect the tracer flux are presented here, along with the possible equations to account for tracer flux and extraction within the root zone. The processes that affect environmental and applied conservative tracers in recharge studies are: precipitation; evaporation; transpiration; overland flow; and vapor transport. While many arid systems can have a net upward flux from the water table, this section concerns those systems with a net downward flux. Precipitation falling on the ground surface either runs off or infiltrates the unsaturated-soil profile. Infiltrated water is partitioned within the root zone into evaporation from the wet surface and, just below the wet surface, transpiration by plants and downward flux. If the overland-flow component is assumed to be negligible, the recharge q at the bottom of the root zone is given by equation 13.163. Across the root zone, the net downward flux is also given by equation 13.163, and varies from a maximum at the ground surface to a minimum at the bottom of the root zone. Because of the large ranges of root-zone fluxes encountered in arid and semiarid areas (two to four orders of magnitude between the ground surface and the bottom of the root zone), the velocity of a tracer within the root zone is not constant for most soil profiles. Also of importance is root uptake of water, which strongly affects water movement, mixing, and dispersive processes acting on the tracer. Because recharge velocities are often very small in arid areas, diffusive transport can likely dominate deep in the root zone, while dispersive fluxes can dominate in the upper portion of the root zone, where velocities are usually higher (Tyler and Walker 1994). Therefore, a simple Fickian model probably does not describe the mixing processes in the root zone.

To further complicate the process, plant uptake of water is likely not uniformly distributed with depth in the unsaturated zone. The resulting flow field is strongly controlled by root density and distribution in both horizontal and vertical directions. Therefore, a simple one-dimensional steady-flow approach (or model) can be invalid under these conditions. In contrast, below the root zone, plant uptake is negligible and the flow field is more likely to be one-dimensional and steady-state. While the equations in this section do not account for the complexities of root-zone processes, it is not clear what magnitudes of error are introduced by assuming one-dimensional, steady-state, plug flow. The following equations for a simple model for downward root-zone water flux are taken from Raats (1974), as modified by Tyler and Walker (1994).

Consider a homogeneous soil profile subject to a steady volumetric flux of water P at the soil surface, and a steady-state downward flux q at the bottom of the root zone z_r. Assume that the flux is Darcian, and solely through the soil matrix without any macropore flow. Water is extracted by plant roots throughout the root zone at a rate of $q_{ex}(z)\,dz$. Between the ground surface $z = 0$ and the bottom of the root zone $z = z_r$, the cumulative extraction E is given (Tyler and Walker 1994) by

$$E = \int_0^{z_r} q_{ex}(z)\,dz \equiv P - q \tag{13.172}$$

where $q_{ex}(z)$ is the root extraction of water as a function of depth per unit time. This root-extraction function can be assumed to combine both evaporation and transpiration into a single term, and z represents the depth at which active roots terminate and plant uptake of water ceases. The average downward velocity of water $v(z)$, and of a conservative tracer at any point in the soil profile, is given as

$$\begin{aligned} v(z) &= \frac{P}{\theta(z)} - \frac{1}{\theta(z)} \int_0^z q_{ex}(z)\, dz. \qquad 0 < z \leq z_r \\ v(z) &= \frac{q}{\theta(z)} \qquad z > z_r \end{aligned} \tag{13.173}$$

where $\theta(z)$ is the water content at depth z. Equation 13.173 can be integrated to determine the travel time of a tracer pulse to reach a depth z, provided $q_{ex}(z)$ is known. For a uniform root extraction with depth, the extraction function is given by

$$\begin{aligned} q_{ex}(z) &= \text{constant} = \frac{P - q}{z_r} \qquad 0 < z \leq z_r \\ q_{ex}(z) &= 0 \qquad z > z_r \end{aligned} \tag{13.174}$$

Raats (1974) proposes an exponential root-extraction function, which is probably more realistic compared to a uniform extraction function. This exponential form of the root-extraction function is given by

$$\begin{aligned} q_{ex}(z) &= q_m \exp(-\lambda z/z_r) \qquad 0 < z \leq z_r \\ q_{ex}(z) &= 0 \qquad z > z_r \end{aligned} \tag{13.175}$$

where q_m is the value of the root-extraction function at the ground surface and λ is a constant. From equation 13.172 q_m is given by

$$q_m = \frac{\lambda(P - q)}{z_r(1 - e^{-\lambda})} \tag{13.176}$$

The uniform and exponential root-extraction function models are shown in figure 13.34. The larger the value of λ, the more water extraction that takes place near the ground surface, whereas the smaller values of λ produce an extraction rate approaching the uniform root-extraction rate. Tyler and Walker (1994) suggest that for most arid areas λ is large, accounting for both high density of shallow roots and bare-ground evaporation.

If the water content θ is constant with depth, or $\theta(z) = \theta$, then equation 13.173 can be integrated to obtain the travel time $t(z)$ of a tracer pulse injected at the ground surface (Tyler and Walker 1994)

$$t(z) = \int_0^z \frac{dz}{\left(\frac{P}{\theta}\right) - \left(\frac{1}{\theta}\right) \int_0^z q_{ex}(z)\, dz} \tag{13.177}$$

Equation 13.177 accounts for the variation in water content with depth. Raats (1974) indicates that for most arid conditions, the variation of water content with depth is usually small, except for the upper 5–10 cm that are subject to variations due to evapotranspiration. If the two equations for the uniform root-extraction function (equation 13.174) and the two equations for the exponential root-extraction function (equation 13.175) are inserted into equation 13.177 and integrated, simple expressions for travel time as a function of P and q are obtained. The uniform root-extraction function travel time is

$$t(z) = \frac{z_r \theta}{q - P} \left[\ln\left(1 - \frac{z(P - q)}{P z_r}\right) \right] \tag{13.178}$$

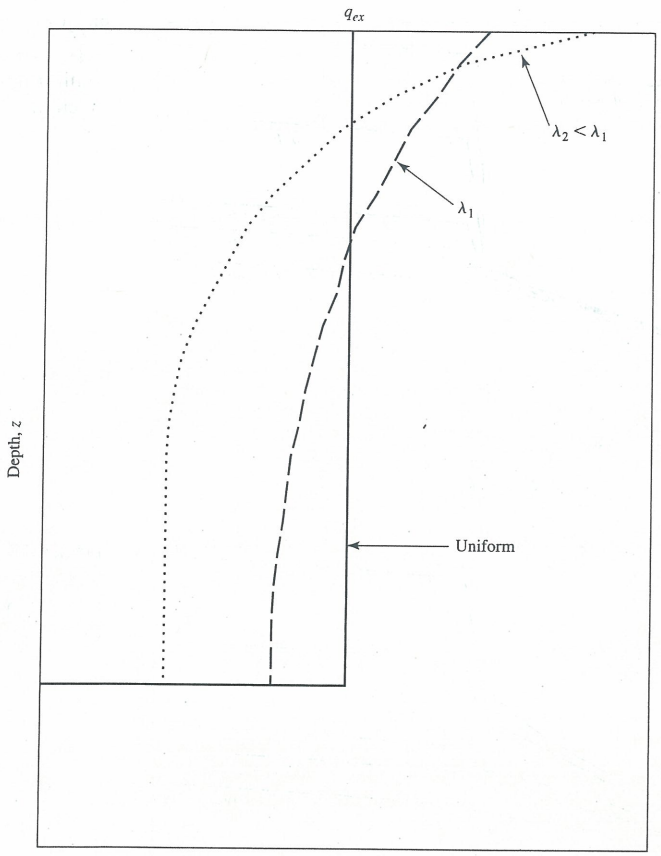

Figure 13.34 Definition of a uniform and exponential root-extraction model

For the exponential root-extraction function, the travel time is

$$t(z) = \frac{z\theta}{P - \dfrac{P-q}{1-e^{-\lambda}}} + \frac{z_r\theta}{\lambda\left(P - \dfrac{P-q}{1-e^{-\lambda}}\right)} \times \left[\ln\left(P - \frac{P-q}{1-e^{-\lambda}} + \frac{P-q}{1-e^{-\lambda}}\exp\left(-\frac{\lambda z}{z_r}\right)\right)\right] - \frac{z_r\theta}{\lambda\left(P - \dfrac{P-q}{1-e^{-\lambda}}\right)}\ln(P) \tag{13.179}$$

Equations 13.178 and 13.179 are applicable for the root zone from ground surface to z_r. For depths below the root zone, the simple constant-velocity model is written in terms of travel time, given by

$$t(z) = \frac{z\theta}{q} \tag{13.180}$$

Figures 13.35 and 13.36 show the travel times for the uniform root-extraction function and a strongly exponential ($\lambda = 5$) root-extraction function, respectively, for selected ratios of recharge flux q to precipitation P, and with $z_r = 100$ cm, $\theta = 0.10$, and average annual P of 25 cm/yr, typical of many arid to semiarid areas. The ratio of recharge to precipitation has little effect on travel times from either root-extraction model in the upper portion of the root

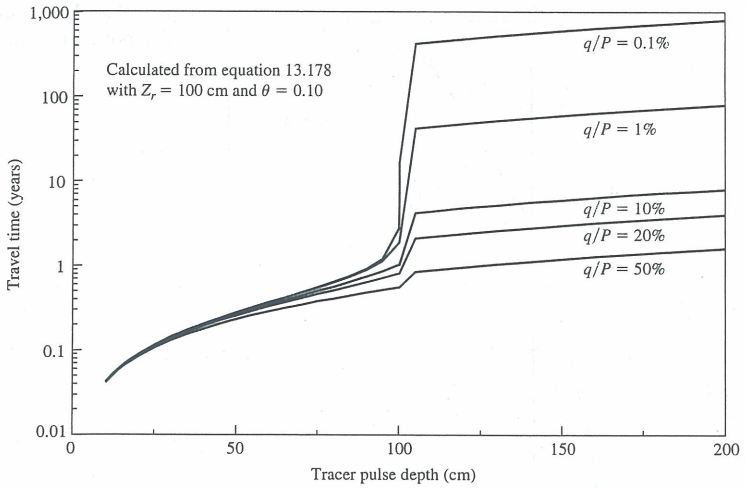

Figure 13.35 Travel time of a tracer through the root zone for a uniform root-extraction function

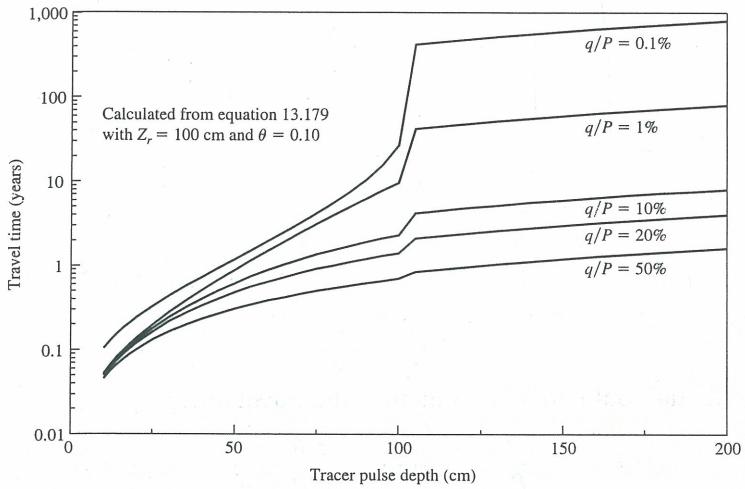

Figure 13.36 Travel time of a tracer through the root zone for an exponential root-extraction function

zone; the difference is apparent as the tracer pulse approaches the bottom of the root zone (z = 100 cm). The choice of root-extraction model is obvious within the root zone, with the uniform model showing the most rapid transport through the root zone. Figure 13.37 shows the comparison of tracer travel times for various root-zone extraction functions for a uniform ratio of recharge to precipitation of 1 percent. For fixed values of q, P, θ and z_r, the travel-times calculation (taking into account plant root uptake of water) is much less than that calculated by the simple steady-state, piston-flow model. If a tracer is injected at the ground surface at t = 0, its velocity through the upper portion of the root zone is much faster than the final recharge velocity. As the tracer moves to the bottom of the root zone, its instantaneous velocity asymptotically approaches the recharge velocity as seen in figures 13.35 and 13.36. Therefore, a constant-velocity estimate of the recharge flux made while the tracer is still in the root zone is erroneous. Only after the tracer has moved below the root zone can the constant-velocity model estimate of recharge begin to approach that of the actual recharge.

Tyler and Walker (1994) investigate the errors associated with the constant-velocity model by calculating the relative errors in travel time between assuming a constant-velocity in the root zone (equation 13.180) versus a root-zone extraction model (equations 13.178 or

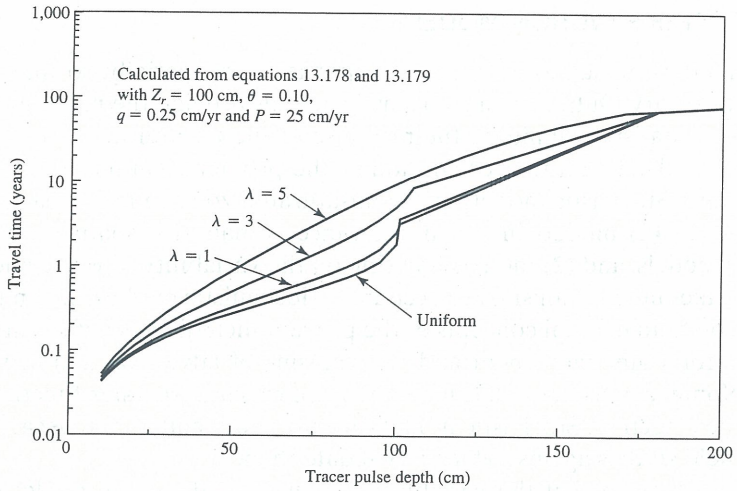

Figure 13.37 Travel time of a Tracer through the root zone for various root-extraction functions, for a 1 percent Recharge-to-precipitation ratio

13.179). The relative error between actual recharge and that calculated by the position of the tracer is given by

$$RE = \frac{z(t)\theta}{t_a q} = \frac{\hat{q}}{q} \tag{13.181}$$

where RE is the relative error between the actual recharge rate and the constant-velocity model recharge rate; $z(t)$ is the position of the tracer pulse at any time t; and depth z; t_a is the actual tracer travel time; q is the actual recharge rate; and $\hat{q}$ is the estimated recharge rate from equation 13.180. Tyler and Walker (1994) show that the relative errors are small for large values of recharge; that is, ratios of q/P are near 50 percent. For recharge ratios approaching those typical of arid areas (between 0.1 and 1 percent), the estimated recharge is two to three orders of magnitude higher than actual recharge through the root zone. Additionally, Tyler and Walker (1994) point out that these errors persist well below the root zone and can still be within a factor of two at twice the root-zone depth. This level of accuracy, however, is well within the estimation errors of other recharge-estimation techniques.

The time for a tracer to reach twice the root zone depth is strongly related to the recharge rate as shown in figures 13.34 and 13.35. Figure 13.34 shows the travel time for a uniform root-extraction function, and indicates that the travel time to twice the root-zone depth (200 cm) ranges from approximately 2 years (when 50 percent of the precipitation is recharged) to over 700 years (when only 0.1 percent of the annual precipitation is recharged). The strongly exponential root-zone functions do not significantly change this conclusion, as shown in figure 13.35. Therefore, it is important to rethink the use of environmental radioactive-tracer pulses, such as ^{36}Cl and ^{3}H, in studies of recharge in arid climates. Because these environmental tracers were introduced through precipitation up to 50 years ago, their applicability to estimate recharge accurately is strongly related to the actual-recharge flux. For typical arid area-recharge variables (P = 25 cm/yr, z_r = 100 cm, and θ = 0.10), the time to reach twice the root-zone depth is 10 years or less when q/P is 10 percent, but approaches 80 years for q/P equal to 1 percent. Tyler and Walker (1994) conclude that radioactive tracers are therefore limited to use in those areas where actual recharge is perhaps 10 percent or more of the actual average-annual precipitation. Local climate and vegetation can, however, combine to produce high-recharge rates that make radioactive (and other) environmental tracers appropriate. Therefore, local conditions have to be investigated prior to the selection of an appropriate tracer.

13.5 STOCHASTIC AND TRANSFER FUNCTION MODELS

Stochastic models presuppose that soil properties vary spatially, so that water and solute movement also vary. Outputs from stochastic models provide the moments (mean, variance, skew, etc.) and statistical limits of the response of the unsaturated-zone system. Stochastic models have evolved with the recognition of the problems caused by variability for deterministic models. Stochastic models in the unsaturated zone can be broadly categorized into two approaches: **(1)** models in which allowance is made for spatial variability in existing mechanistic models; and **(2)** models focusing on the variability of water and solute transport that do not take the mechanism into account. "Mechanistic models" mean that the model incorporates the fundamental concepts of the process, including use of equations derived from Darcy's law for water movement and mechanisms of advection and dispersion for solute transport. Nonmechanistic models have their approach in transfer functions, as we will discuss in the next section. Stochastic models are often difficult to use because of the shortage of suitable field studies against which to validate them.

In general, given that the variables in an unsaturated-zone model vary spatially, the usual approach is to model the resulting flow and transport in terms of: a stochastic representation of those variables; an appropriate simulation of the process; and application of Monte Carlo-techniques (Charbeneau 1989; Addiscott and Wagenet 1985). In this type of modeling, the formulation of the simulation is critical in terms of computational effort. Addiscott and Wagenet (1985), Hill (1986), and Adamson (1976) indicate that the particular model to be randomized can be quite approximate, yet still lead to reasonable results.

Analytical Model

Charbeneau (1989) presents relatively simple stochastic models of soil-water content that can be used in addition to Monte Carlo methods; this simple model is presented below. As a particular example, Charbeneau (1989) considers the water content at a depth z in a soil that was initially at a uniform natural saturation $\widetilde{S}_e$. The simple model formulation assumes that the greatest variability in the field occurs in saturated hydraulic conductivity K_s. Therefore, it was assumed that K_s was the only random variable; additionally, it was assumed that K_s had a log-normal distribution. This is not unreasonable, because many hydrologic variables are shown to be log-normally distributed. Saturated hydraulic conductivity has repeatedly been shown to be log-normally distributed (Paschis, Kunkel, and Keonig 1988). If $y = \ln(K_s)$, then the random variable y has a mean μ_y and a variance σ_y^2. The probability density function of K_s is given by (Benjamin and Cornell 1970)

$$f_{K_s}(y) = \frac{1}{K_s \sigma_y \sqrt{2\pi}} \exp\left\{-\frac{1}{2}\left[\frac{1}{\sigma_y} \ln\left(\frac{K_s}{\overline{m}_y}\right)\right]^2\right\} \tag{13.182}$$

where $f_{K_s}(y)$ is the log-normal probability density function for K_s and $\overline{m}_y$ is the median of K_s. Remembering the kinematic-profile model of Section 13.2, the effective water content S_e at depth z is equal to that given by equation 13.52 if the lowermost-drainage characteristic has not reached a depth L, and is given by equation 13.66 otherwise. The lowermost-drainage characteristic moves downward with a velocity given by equation 13.65. At depths greater than this lowermost-drainage characteristic, the water content is equal to the natural-saturation value, whereas at depths above this characteristic, the water content is equal to its corresponding value on the drainage curve. In terms of the random saturated hydraulic conductivity value, S_e is equal to $\widetilde{S}_e$ (Charbeneau 1989) so long as

$$K_s < \frac{(\theta_m - \theta_r)z}{nt\left(\frac{1}{2}\right)^{n-1/n}} \tag{13.183}$$

otherwise, S_e is given by equation 13.66. Because K_s is considered a random variable, so is S_e. Thus, of interest here is the development of the probability-density function for S_e, or the first two moments of S_e (mean and variance). For this simple problem, the probability density functions for K_s and S_e are related through the general rule for transformation of random variables (Benjamin and Cornell 1970). If two random variables x and y are related such that the function $y = g(x)$ relating the two random variables, is always increasing or decreasing and there is only one value of y for each value of x, then it can be shown (Benjamin and Cornell 1970) that the probability density functions for x and y [$f_X(x)$ and $f_Y(y)$] are related by

$$f_Y(y) = \left|\frac{dx}{dy}\right| f_X(x) = \left|\frac{dg^{-1}(y)}{dy}\right| f_X(g^{-1}(y)). \tag{13.184}$$

For this simple example, $x = K_s$ and $y = S_e$. Because S_e is defined differently over separate ranges of K_s, the resulting probability density function is a mixture of a single-density function defined by $\tilde{S}_e$, and a continuous probability density defined by the drainage wave. The condition defined by equation 13.183 specifies the probability mass associated with the soil moisture when $S_e = \tilde{S}_e$. The continuous part of the probability density function is found from the transformation rule of equation 13.184, applied to equation 13.66 as

$$\left|\frac{dK_s}{dS_e}\right| = \frac{(n-1)(\theta_m - \theta_r)z}{nt(S_e)^n} \tag{13.185}$$

Combining equations 13.182, 13.184 and 13.185 and using equation 13.66 to eliminate K_s gives the continuous part of the probability density function as

$$f_{S_e}(\theta) = \frac{n-1}{\sigma_y \theta \sqrt{2\pi}} \exp\left\{\frac{\left[\ln\left(\frac{(\theta_m - \theta_r)z}{nt\overline{m}_y\,\theta^{n-1}}\right)\right]^2}{2\sigma_y^2}\right\} \tag{13.186}$$

for K_s not satisfied by equation 13.183.

Figure 13.38 shows the continuous probability-density function given by equation 13.186 at times of 100, 1,000, and 10,000 hours for the sandy loam soil example given in section 13.2 at a depth of 30 cm; with $\theta_m = 0.453$; $\theta_r = 0.041$; $\overline{m}_y = 2.59$ cm/hr $n = 8.29$; and $\sigma_y = 1.2$. As indicated in figure 13.38, for small times the probability density function is truncated and most of the mass is associated with the undrained natural-water content. After about 1,000 hours, the singular density no longer contributes to $f_{S_e}(\theta)$.

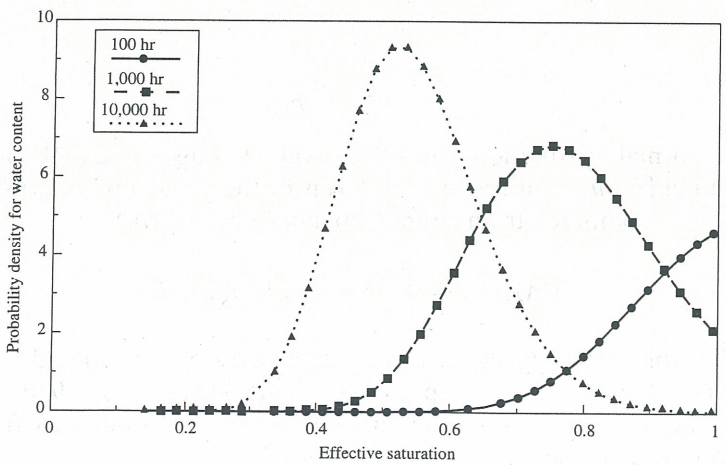

Figure 13.38 Water-content probability density function at times of 100; 1,000; and 10,000 hours for a sandy loam soil

The greatest interest, however, lies in the first two statistical moments, specifically the mean and variance of S_e. The mean (or expected) value of S_e is found from (Benjamin and Cornell 1970)

$$E[S_e] = \int_0^1 \theta f_{S_e}(\theta)\, d\theta \tag{13.187}$$

Charbeneau (1989) shows that with a change in variables ($\alpha = (n-1)\ln\theta$), the integral of equation 13.185 can be simplified to give the expected value of S_e in terms of the standard normal probability distribution, with the final expected value given as

$$E[S_e] = \tilde{S}_e F_K\left\{K_s < \frac{(\theta_m - \theta_r)z}{nt\left(\frac{1}{2}\right)^{(n-1)/n}}\right\} \exp + \left\{\frac{\ln\left[\frac{(\theta_m - \theta_t)z}{nt\overline{m}_y}\right] + \frac{\sigma_y^2}{2(n-1)}}{n-1}\right\} \times N\left\{\ln\left[\frac{nt\overline{m}_y(\tilde{S}_e)^{n-1}}{(\theta_m - \theta_r)z}\right]^{1/\sigma_y} - \frac{\sigma_Y}{n-1}\right\} \tag{13.188}$$

where $F_K\{\}$ is the cumulative normal frequency distribution for K_s and $N\{\}$ is the cumulative normal frequency distribution for the terms in braces.

There is no simple expression for the above cumulative normal distribution, but it has been evaluated numerically and tabulated for the standardized random variable. For the general case of the cumulative normal distribution for K_s

$$\begin{aligned} F_K(x) = P[X \le x] &= P\left[U \le \frac{x - m_X}{\sigma_X}\right] \\ &= F_U\left(\frac{x - m_X}{\sigma_X}\right) = F_U(u) \\ &= \frac{1}{\sqrt{2\pi}}\int_{-\infty}^{u} e^{-1/2v^2}\, dv \qquad -\infty \le u \le \infty \end{aligned} \tag{13.189}$$

in which $u = (x - m_X)/\sigma_X$; tables yield values of $F_U(u)$. Because of the symmetry of the probability density function, tables give only half the range of u, usually $u \ge 0$. Because of the case presented here, $y = \ln K_s$, $F_U(u)$ is evaluated from

$$F_U(u) = F_U\left(\frac{\ln(y/\overline{m}_y)}{\sigma_{\ln Y}}\right) \tag{13.190}$$

where

$$u = \frac{1}{\sigma_{\ln Y}} \ln\frac{y}{\overline{m}_Y} \tag{13.191}$$

The cumulative normal distribution can still be evaluated using the table of the cumulative normal distribution $[F_U(u)]$, but now u is in terms of the logarithmic-transformed variable. The variance of S_e is computed from (Benjamin and Cornell 1970)

$$VAR[S_e] = \int_0^1 (\theta - E[S_e])^2 f_{S_e}(\theta)\, d\theta \tag{13.192}$$

Figure 13.39 shows the expected (mean) effective water content and the standard deviation at a depth of 30 cm for the example sandy loam soil. Figure 13.39 also shows the contributions from the singular-density function and the continuous-density function (the first and second terms, respectively, of equation 13.188). It is of interest to note that while the

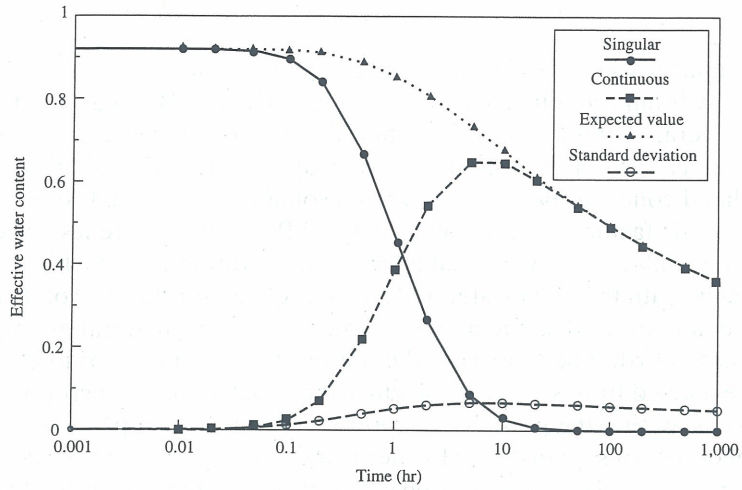

Figure 13.39 Components of stochastic water content at 30-cm depth for a sandy loam soil

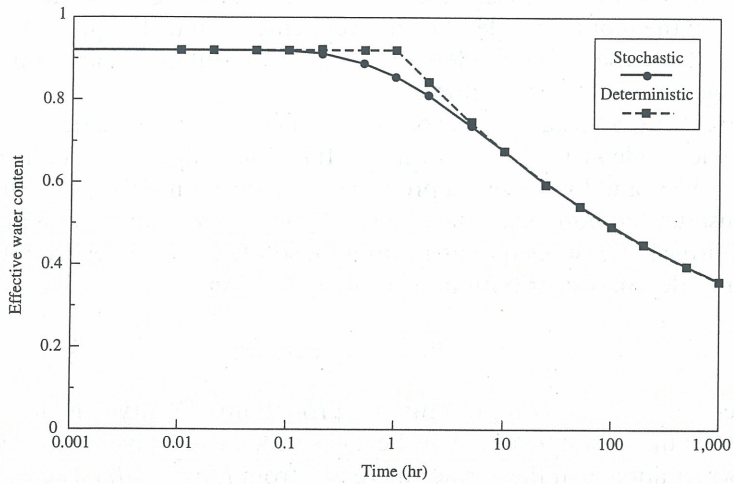

Figure 13.40 Comparison of stochastic and deterministic models at 30-cm depth for a sandy loam soil

standard deviation of S_e is small relative to the mean, this variability is important because both volumetric flux and recharge are related by $(S_e)^n$.

Figure 13.40 presents the water content versus time at the 30-cm depth as predicted by the stochastic model (equation 13.188) and the deterministic model of equation 13.66, with K_s values equal to the mean and median of the distribution. The median value predicts the stochastic mean quite well, as would be expected, because the median value of K_s corresponds to the mean value of $y = \ln K$.

Another stochastic analytical model is VADSAT (ES&T, Inc. and HydroGaia, Inc. 1994). VADSAT is based on coupled analytical solutions of the unsaturated- and saturated-zone flow and transport equations. With appropriate initial and boundary conditions, the model can estimate peak concentrations of contaminant, as well as the time to reach the peak concentration for downgradient receptors in the saturated zone. Uncertainty analyses can be conducted via Monte Carlo simulations to assess effects of soil and waste-property uncertainty on the risk of ground water contamination at land-disposal sites. The model is available as an interactive computer program to simulate the movement of conservative inorganic or reactive organic species. The model considers evaporation of volatile organic contaminants, leaching of soluble contaminants, advective transport, dispersive transport, adsorption, and microbial decay.

Numerical Models

Numerical models also allow for the spatial variation of soil-moisture characteristic curves and relative hydraulic-conductivity curves as input. Bresler, Bielorai, and Laufer (1979) have generated several exemplary cases of chloride movement, representative of the range of moisture-characteristic and unsaturated hydraulic conductivity relations measured in the field. Simulated concentration profiles are reasonably well-related to measured ones when the range of scale factors was used. Wagenet and Rao (1983) were less successful when they attempted to simulate field-measured nitrate concentrations. The fact that they worked on a cropped system with transient water and solute regimes, substantial solute and water extraction by roots, and upward solute and water movement, brought out an important point: the variability in soil hydraulic properties did not produce as much variability in solute concentrations as expected from stochastic-mechanistic simulations of uncropped systems. The apparent conclusion that the presence of roots diminishes the impact of the variability in hydraulic properties—if supported by further work—should prove important.

Numerical models in this class give a conceptual framework for the development of further mechanism-based stochastic models, as well as proving useful in assessing the impact of variability on the input variables. Further refinements in technique can be expected; however, it seems likely that these models will be more useful in research rather than environmental management in the near future.

An interesting alternative approach to numerical mechanistic models (i.e., entirely nonmechanistic models) lies in the transfer functions applied to industrial processes by Dankwaerts (1953) and hydrological processes by Ericksson (1971) and suggested by Raats (1978) for unsaturated porous media. As used by Jury (1982) and Jury and Roth (1990), this stochastic approach measures the distribution of solute travel times from the soil surface to some reference depth. A distribution function of the form

$$P_L(I) = \int_0^I f_L(I)\, dI \tag{13.193}$$

is constructed in which $f_L(I)$ represents the probability density function summarizing the probability (P_L) that a solute added at the soil surface will arrive at a given depth L, as the quantity of water applied at the surface increases from I to $(I + dI)$. The model considers the unsaturated soil composed of twisted capillaries of different lengths, within which water moves by piston flow. An estimate of the travel-time probability density function, $f_L(I)$, is obtained using solution samples of the soil located at depth L at various field locations. In general $f_L(I)$ is log-normally distributed (Biggar and Nielsen 1976; van der Pol, Weirenga, and Neilsen 1977). Calibration of this model using $C(z, I)$ values from one depth, z, provided all the information necessary to predict concentration, C, at deeper depths as well as larger values of I, or values of $C(z)$ at one I. Field comparisons show good agreement between measured and predicted bromide concentrations (Jury, Stolzy, and Shouse 1982), and indicate that these types of models are useful as a stochastically based environmental management model for solute movement. The most important characteristic of transfer-function models is that they attempt to simulate spatially variable field processes with only the minimum of input data. It is not yet known whether such an approach is satisfactory in vertically nonhomogeneous unsaturated soil, or whether such a model can give accurate estimates of flux rate as well as solute concentration.

SUMMARY

In this chapter, we have discussed how variably-saturated-zone mathematical models are useful tools for predicting the extent of subsurface contamination, and conducting pre-monitoring studies for the placement of detection devices in a format understood by both

field-response personnel and regulatory entities. The emphasis of this chapter was on those analytical solutions readily used to solve problems in unsaturated-zone flow. Thus, we discussed analytical models and numerical models in several frameworks: one-dimensional deterministic liquid-flow models; three-dimensional deterministic liquid- and vapor-flow models; and three-dimensional deterministic immiscible-liquid-flow models. Additionally, we described the use of tracers in unsaturated-soil studies and stochastic and transfer-function models. Finally, we have provided several tables listing various models, their developers, and descriptions of the approach the model uses for predictability. For the reader who has little programming language experience, the best approach to understanding modeling may be to understand fully the parameters incorporated within various models, and how changes in these parameters affect predictability; having accomplished this, the reader will understand the physics involved in modeling. Then, once he or she has learned a programming language such as Fortran or C, the principles involved in modeling will be more fully realized.

ADDITIONAL QUESTIONS

13.1. Average characteristics for a sandy loam are $n = 8.29$, $K_s = 18.90$ cm/hr, $\varphi = 0.423$, and residual water content $= 0.048$; $i = 1.5$ cm/hr for 4 hours. Find the soil moisture profiles using **(1)** rectangular profile, and **(2)** kinematic profile at times of 6, 48, and 240 hours. *Hint:* for rectangular profile use equations 13.56–13.60 and 13.62; for kinematic profile you may need to use equations 13.66 and 13.71–13.72

13.2. Use the same soil in question 13.1 and the same value for i; assume average annual infiltration of 40 cm. Find the time history of water flux (drainage) at 1.5 m using rectangular and kinematic profiles. How does the drainage history of the soil differ with the type of profile assumed?

13.3. Brooks and Corey found the following moisture characteristics for a Touchet silt loam soil.

Degree of saturation (decimal)	Matric potential (cm)
1.00	−15.6
1.00	−25.6
1.00	−35.6
1.00	−45.6
0.998	−65.6
0.995	−85.6
0.992	−105.6
0.984	−125.6
0.978	−135.6
0.967	−145.0
0.946	−155.6
0.892	−164.6
0.821	−175.4
0.719	−195.6
0.641	−215.2
0.562	−246.0
0.492	−285.2
0.424	−354.0
0.383	−414.4

For the above data, Brooks and Corey found the porosity to be 0.485. Find fit parameters for the Brooks–Corey relation (λ, S_m, S_r, and ψ_b); the Boltzmann distribution (β, S_m, S_r, and P_{cl}), and the Fermi distribution (β, S_m, S_r, and $P_{cl/2}$). Plot the original Brooks–Corey data along with your fit curves for each of the above three relations.